Politecnico di Torino

Universitat Politècnica De Catalunya

Master's Degree in

Ingegneria Energetica e Nucleare
Sustainable Nuclear Energy

Academic Year 2024/2025
Graduation Session: October 2025

Validation of Forward Propagation of Uncertainties in Thermal Hydraulic Safety Analysis

Supervisors:
Prof. Giuseppe Francesco Nallo
Prof. Jordi Freixa Terradas

Candidate:
Giorgia Chiesa

Abstract

In the past few decades, there has been an increasing interest in the use of Best Estimate Plus Uncertainty (BEPU) methodologies for the safety analyses of nuclear reactors. One of the crucial issues is to quantify and propagate the input uncertainties associated to the physical models in the thermal-hydraulic codes. Such a quantification can be performed by comparison with experimental data, and it is usually referred to as Inverse Uncertainty Quantification (IUQ).

The OECD/NEA project ATRIUM (Application Tests for Realization of Inverse Uncertainty quantification and validation Methodologies in thermal-hydraulics) aims at performing practical IUQ exercises to bring new insights on the applicability of uncertainty quantifications methods in thermal hydraulic safety analysis.

The present work addresses the final Exercise of the project, which involves the propagation of uncertainties in the simulation results of an Intermediate Break Loss-of-Coolant Accident (IBLOCA) in the Hot Leg. The scenario reproduces the conditions of Test 1 conducted at the LSTF facility in Japan, a scaled-down Integral Test Facility (ITF) representing a PWR.

The ultimate objective of this thesis is the validation of a RELAP5 model for the simulation of this specific transient scenario.
Exercise 3 of the ATRIUM project is structured in two main phases: the first phase involves the propagation of uncertainties identified in the previous two exercises—specifically related to choked flow and post-CHF modeling—while the second phase builds upon these results to perform the BEPU analysis also including uncertainties associated with boundary and initial conditions.

The BEPU analysis is conducted according to Wilks' formula, propagating uncertainties across 93 simulation cases in addition to the nominal base case. The input variations are generated using the Monte Carlo method.

The aim is to estimate the 95th percentile of the selected output variables, as required by the Exercise specifications, with a confidence level of 95%, using the RELAP5 code. The post processing has been carried out by employing Python scripts. The chosen Figures of Merit (FoMs) will be presented in the Results section in the form of percentile plots, to demonstrate the accuracy and robustness of the simulation model. Additionally, the time evolution of key system parameters representing relevant physical phenomena will be analyzed.

Contents

List of Tables

List of Figures

Nomenclature

Acc Accumulator. 35, 37, 44

AOOs Anticipated Operational Occurrences. 7

ATRIUM Application Tests for Realization of Inverse Uncertainty quantification and validation Methodologies in thermal-hydraulics. 27, 29, 43, 47, 61, 62, 67

ATWS Anticipated Transients Without Scram. 7, 8, 16

BDBA Beyond Design Basis Accident. 6, 7, 16

BE Best Estimate. 8

BEPU Best Estimation Plus Uncertainties. , 2, 3, 8, 11–15, 17, 29, 44, 47, 56, 67, 71, 73, 78, 79, 83, 84, 91, 98

CCFL Counter-Current Flow Limitation. , 3, 35, 41, 56, 62, 63, 79, 81, 84, 91, 92

CET Combined Effect Test. 27, 38

CHF Critical Heat Flux. , 3, 28, 29, 43–45, 47, 51, 61–63, 67, 71–73, 81–83, 85, 86

CRGT Core-Guide Thimbles. 38, 40, 41

DAA Data Assimilation and Adjustment. 15

DBA Design Basis Accident. 6–8, 45

DEGB Double-Ended Guillotine Break. 34

DiD Defense-in-Depth. 5

DNB Departure from Nucleate Boiling. 7

DoEs Design of Experiments. 14

DSA Deterministic Safety Analysis. 2, 6, 8, 91

ECCS Emergency Core Cooling System. 7, 37, 38

FoM Figure of Merit. , 43, 44, 48, 50, 52

HMC Hamiltonian Monte Carlo. 15

HPSI High Pressure Injection System. 38

IAEA International Atomic Energy Agency. 1

IBLOCA Intermediate-Break Loss of Coolant Accident. , 28, 31, 51, 61, 63, 91

IET Integral Effect Test. 28, 29, 35

INSAG International Nuclear Safety Advisory Group. 29

ITF Integral Test Facility. 34

ITs Integral Tests. 9, 10

IUQ Inverse Uncertainty Quantification. 14, 15, 27–29, 51, 91

LBLOCA Large-Break Loss of Coolant Accident. 16

LOCA Loss of Coolant Accident. 3, 7, 8, 16, 27, 28, 31, 33, 35

LPSI Low Pressure Injection System. , 35, 37, 38, 44, 46, 54, 78, 79, 82, 88, 106

LS Loop Seal. 37, 44, 46, 63, 82

LSTF Large Scale Test Facility. , 3, 9, 33–38

LWR Light Water Reactor. 16

MCMC Markov Chain Monte Carlo. 15

MFW Main Feedwater. 40

MLE Maximum Likelihood Estimation. 15

MSIV Main Steam Isolation Valve. 37

MSLB Main Steam Line Break. 16

NPP Nuclear Power Plant. 5, 8–10, 16

NUTS No-U-Turn Sampler. 15

PCT Peak Cladding Temperature. , 31, 37, 43–45, 54, 63, 67–69, 79, 81–87, 92

pdf Probability Density Function. 47, 52, 59, 97

PSA Probabilistic Safety Assessments. 2, 18, 91

PWR Pressurized Water Reactor. , 19, 33–35, 91

PZR Pressurizer. , 32, 34, 36–38, 64, 66, 103

QoI Quantity of Interest. 29, 43

RCP Reactor Coolant Pump. 7, 32, 37, 38, 40

RCS Reactor Coolant System. 32

RPV Reactor Pressure Vessel. , 32, 37–40

SA Severe Accident. 7

SBLOCA Small-Break Loss of Coolant Accident. 16

SET Separate Effect Test. 9, 10, 27

SG Steam Generator. , 33, 34, 37, 38, 44, 46, 53, 64, 66, 69, 70, 76, 103, 107

SIP Safety Injection Pump. 32

SIS Safety Injection System. 32

SIT Safety Injection Tank. 32

TH Thermal Hydraulic. , 3, 9, 17, 52, 61, 64, 66

UA Uncertainty Analysis. 3, 14, 47

UH Upper Head. 38

UP Upper Plenum. 44

UQ Uncertainty Quantification. 14

Chapter 1

Introduction

> "Safety is not an end in itself but a prerequisite for the purpose of the protection of people in all States and of the environment — now and in the future. The risks associated with ionizing radiation must be assessed and controlled without unduly limiting the contribution of nuclear energy to equitable and sustainable development. Governments, regulatory bodies and operators everywhere must ensure that nuclear material and radiation sources are used beneficially, safely and ethically."[2]

This statement from the International Atomic Energy Agency (IAEA) reflects a key premise of modern nuclear technology: that safety is not merely a regulatory requirement, but a moral imperative, intrinsically tied to the social license under which nuclear energy operates.

Throughout the decades, nuclear safety has evolved into a multidimensional discipline encompassing engineering design, probabilistic risk assessment, human factors, organizational behavior, and emergency preparedness. It is not enough for a reactor to be technically safe; it must also be perceived as such by the public. This is especially true in countries where public skepticism toward nuclear power has historically shaped national policy, often independently of technological progress or international best practices.

In this complex landscape, nuclear safety becomes not only a technical challenge but also a matter of communication, trust, and transparency. For this reason, nuclear safety must be treated as a proactive and continuous effort: one that integrates innovation with conservative design principles, and that seeks to quantify and reduce uncertainties wherever they arise.

A culture of safety requires rigorous methodologies, open data sharing, independent oversight, and a long-term vision that places public interest and environmental protection at its core. As nuclear energy is increasingly reconsidered in the context of decarbonization and energy independence, reaffirming and demonstrating the highest standards of safety remains a non-negotiable foundation upon which its future must rest.

Within this broader context, thermal-hydraulics emerges as a foundational discipline for the technical demonstration of nuclear safety. It serves as the essential interface between the physical behavior of reactor systems and their modeled responses during both normal and accidental conditions. As emphasized by D'Auria [10], thermal-hydraulics encompasses the complex interplay of heat transfer and fluid dynamics that governs the operation of coolant systems, ensuring core cooling, maintaining pressure boundaries, and safeguarding structural integrity under transient scenarios. Its role becomes particularly critical in the assessment of design and beyond-design conditions, where predictive simulations guide the validation of safety functions and the performance of engineered safeguards. Safety analysis methodologies have evolved accordingly, with two principal approaches— Deterministic Safety Analysis (DSA) and Probabilistic Safety Assessments (PSA)—established to address complementary aspects of plant behavior under accidental conditions. While PSA provides a quantitative assessment of risks through statistical modeling of system failures and human actions, DSA is rooted in the in-depth simulation of predefined accident scenarios, typically using conservative or best-estimate assumptions. In this framework, thermal-hydraulic system codes such as RELAP5 enable detailed scenario-specific modeling of complex transients, facilitating verification against regulatory safety limits for critical variables such as peak cladding temperature, system pressure, and coolant inventory. Despite the growing role of PSA in modern risk-informed regulation, DSA remains the cornerstone of nuclear safety demonstration. It is directly aligned with licensing requirements and provides a structured means to evaluate plant behavior under bounding conditions. For this reason, the present work adopts a deterministic methodology, leveraging a best-estimate thermal-hydraulic code to analyze selected transient scenarios. This choice reflects both regulatory compatibility and the ability to generate high-fidelity, traceable results grounded in physical modeling, in accordance with international guidelines and best practices in reactor safety analysis.

This thesis focuses on the solution of Exercise 3 of the ATRIUM project, an international benchmark initiative aimed at the validation and uncertainty quantification of thermal-hydraulic system codes under conditions representative of accident transients in pressurized water reactors. As the core subject of this work, Exercise 3 specifically addresses the application of Best Estimation Plus Uncertainties (BEPU) methodologies using the RELAP5/MOD3.3 system code. BEPU represents the natural evolution of traditional best-estimate analysis by not only seeking to simulate plant behavior as realistically as possible, but also by systematically propagating uncertainties in the input parameters to evaluate their impact on key safety-relevant quantities.

The BEPU analysis carried out in this work builds upon previous phases of the ATRIUM project, which were devoted to inverse uncertainty propagation—a process in which experimental data are used to constrain and calibrate uncertain input parameters through statistical inference. Exercise 3, in contrast, implements a forward propagation of uncertainties, with the objective of quantifying the variability in the system response due to epistemic uncertainties in selected model parameters and boundary conditions.

To manage the computational demands associated with large uncertainty spaces, the analysis employs Wilks' formula, a statistical tool designed to determine the minimum sample size required to estimate tolerance limits at a given confidence level. Specifically, the method allows the analyst to define a one-sided or two-sided bound on an output

variable (e.g., Peak Cladding Temperature) such that a prescribed percentage of the population lies within the bound with a certain confidence—without requiring the full probabilistic distribution.

The ultimate goal of the study is the validation of the RELAP5 code through comparison with experimental data obtained from the ROSA-LSTF (Large Scale Test Facility), an integral test facility designed to simulate the thermal-hydraulic behavior of pressurized water reactors under Loss of Coolant Accident (LOCA) conditions. The uncertainty propagation is structured into three progressive steps, each involving a distinct set of parameters whose uncertainties are propagated. It is expected that increasing the granularity of the uncertainty treatment—by including, for instance, parameters governing Critical Heat Flux (CHF) and Counter-Current Flow Limitation (CCFL)—will lead to improved predictive fidelity and closer alignment with experimental observations.

The structure of the thesis reflects this methodological path. Following the present introductory chapter, a state-of-the-art review is provided, together with a detailed description of the ATRIUM project and the specific analytical tasks addressed in this study. A dedicated methodology chapter outlines the practical steps undertaken to perform the BEPU analysis and associated post-processing, with results organized according to the incremental steps of Exercise 3. Finally, the concluding chapter summarizes the main findings and offers perspectives for methodological refinement and future developments.

Chapter 2

State of the Art

2.1 Deterministic Safety Analysis

Deterministic Safety Analysis (often called Accident Analysis) is a key component in confirming the adequacy and effectiveness of *Defence-in-Depth* provisions in NPPs [3].

The Defense-in-Depth (DiD) principle (Figure 2.1) is a cornerstone of nuclear safety. It involves the implementation of multiple, independent, and redundant layers of protection to prevent accidents and to mitigate their consequences. This structured approach ensures that even if one level fails, others remain in place to protect personnel, the public, and the environment.

The Defence-in-Depth strategy is organized into five safety levels:

Level 1 – **Prevention of Malfunctions:** This level focuses on maintaining high standards of design and operation. It involves applying the principle of "safety first," using robust design practices, conservative safety margins, quality assurance programs, and highly qualified personnel to avoid initiating events.

Level 2 – **Control of Abnormal Operation:** At this level, the goal is to detect and manage deviations from normal operating conditions before they escalate. It includes the use of protection systems and engineered safety features to maintain safe conditions.

Level 3 – **Accident Management:** This level aims to control accidents if they occur, preventing core damage and minimizing radioactive release. It relies on special safety systems and specific accident management procedures.

Level 4 – **Management of Severe Conditions:** When accidents go beyond the design basis, this level ensures additional measures are in place—such as filtered containment venting or core catchers—to maintain the integrity of the containment.

Level 5 – **Emergency Response Planning:** This final level addresses preparedness for off-site emergency response, ensuring public and environmental protection even in the unlikely event of a significant radioactive release.

These levels of protection are supported by three physical barriers that prevent the release of radioactive materials: the fuel matrix and fuel cladding (first barrier), the boundary of the reactor coolant system (second barrier), and the containment building (third barrier). Together, these safety levels and physical barriers create a robust and multilayered defense strategy that ensures the resilience and safety of nuclear power plants.

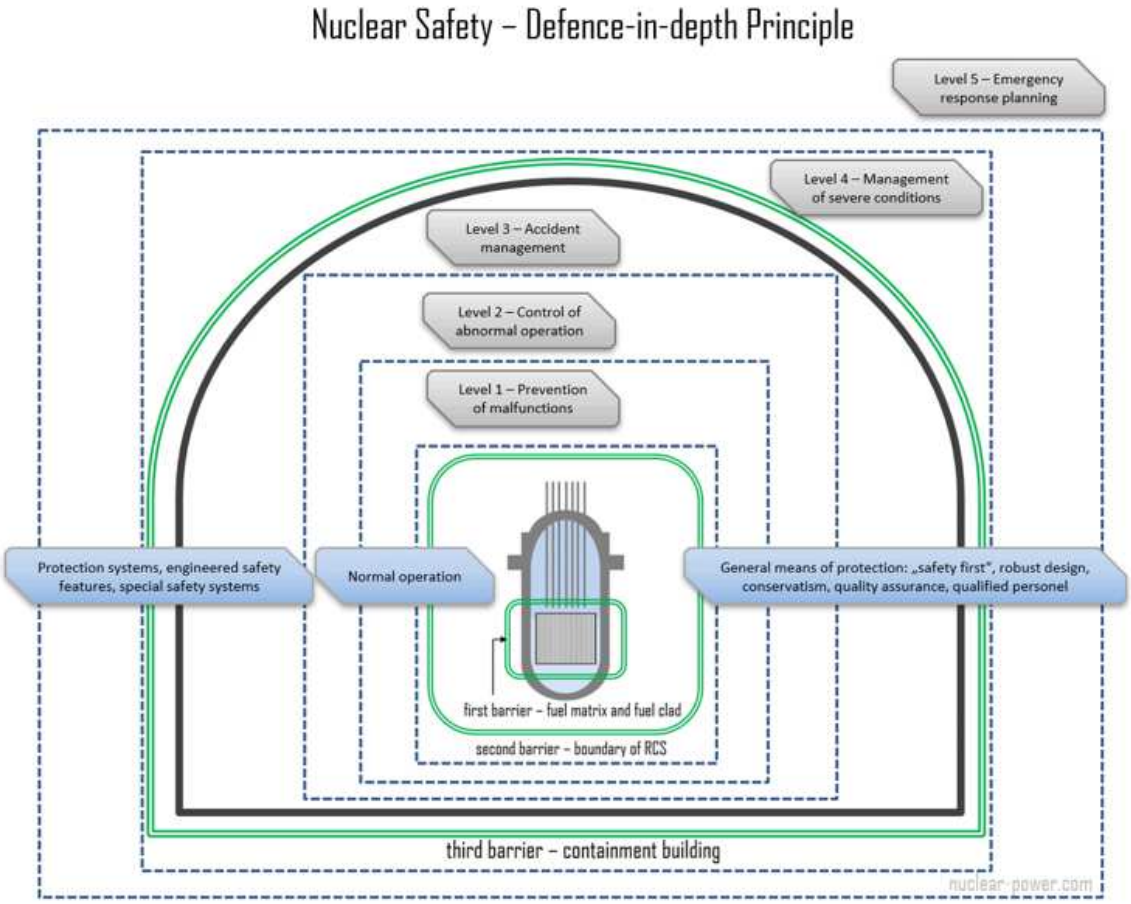

Figure 2.1: Defense-in-Depth: a graphic representation [20].

Typical DSA Workflow

A comprehensive DSA is typically structured in eight steps:

1. Classification of initiating events and selection of acceptance criteria.
2. Definition of the methodological approach.
3. Identification of accident types (Design Basis Accident (DBA)s, Beyond Design Basis Accident (BDBA)s, etc.).
4. Selection of suitable computer codes (RELAP5, TRACE, CATHARE, etc.).
5. Accounting for user effects and modeling uncertainties.

6. Preparation of input data and initial/boundary conditions.
7. Presentation and evaluation of results against criteria.
8. Quality assurance and peer verification.

Initiating Events and Their Categorization

Initiating events are classified by frequency and severity:

- **Anticipated Operational Occurrences (AOOs)** or transients (Ts), expected deviations from normal operation that the plant is designed to handle without significant safety consequences;
- **Accidents**, which subdivide into:
  - **Design Basis Accidents (DBAs)**, postulated accidents that the plant must be specifically designed and equipped to manage safely;
  - **Beyond Design Basis Accidents (BDBAs)**, accidents more severe than DBAs, involving conditions not fully covered by the original design but still considered in safety analyses;
  - **Severe Accidents (SAs)**, extreme events where core damage or significant radioactive releases may occur, exceeding both DBA and BDBA conditions.

A common classification scheme includes:

(a) Reactivity-induced accidents (e.g. control rod ejection);

(b) Loss of coolant flow (e.g. one or more RCP trips);

(c) Inadvertent increase in coolant inventory (e.g. Emergency Core Cooling System (ECCS) actuation);

(d) Steam line breaks (increase in secondary heat removal);

(e) Feedwater line breaks (decrease in secondary heat removal);

(f) Loss of coolant accidents (LOCAs);

(g) Anticipated Transients Without Scram (ATWS)s.

Each category requires distinct acceptance criteria and conservativeness levels in analysis.

Acceptance Criteria

For Transients

To pass, transients must meet:

1. A $\leq$ 5% chance (95% probability, 95% confidence) of Departure from Nucleate Boiling (DNB) anywhere in the core;
2. Reactor coolant and steam system pressures below 110% of design;
3. No evidence of fuel melting.

For DBAs

Beyond the previous criteria, DBAs require demonstration that engineered safety features preserve core and system integrity:

4. Fuel enthalpy below design thresholds to avoid pellet dispersion;
5. Cladding temperature below $1477K$;
6. Melt fraction $\leq$ 0–10%;
7. System pressures below 135% design (ATWS) or 110% (other DBAs);
8. Radioactive dose limits are not exceeded;
9. For LOCA/DBAs, additional coolability criteria include:
    - Local oxidation $\leq$ 17–18%;
    - Hydrogen generation limited $\leq$ 1% of total cladding;
    - Core geometry must permit long-term cooling and control rods movement;
    - Sufficient coolant inventory for long-term cooling.

Initial and Boundary Conditions

Key inputs include:

- Pre-accident NPP state variables;
- Bounding versus realistic values depending on conservative or BEPU approaches;
- Coverage of parameter uncertainty due to tolerances, measurement, or model biases.

Approaches to DSA

Three major methods are used:

Conservative approach: Utilizes pessimistic initial/boundary conditions and degraded system performance (e.g. 20% overpower) to ensure built-in safety margins.

Best Estimate (BE): Uses realistic assumptions and validated code models to match experimental data closely.

Best Estimate Plus Uncertainties (BEPU): Employs best-estimate modeling plus statistical uncertainty propagation, aiming to derive a single worst-case outcome typically at the 95/95 confidence level.

2.2 Verification, Validation and Scaling

The use of Thermal Hydraulic (TH) system codes for the safety analysis of nuclear power plants requires a comprehensive process to ensure that the codes produce trustworthy and physically consistent results. This process consists of three fundamental pillars: **Verification**, **Validation**, and **Consistency with Reality** (commonly abbreviated as V&V&C), along with a careful treatment of **scaling** when extrapolating results from test facilities to full-scale reactors [10].

Verification

Verification addresses the question: *Are we solving the equations right?* It refers to the assessment of the numerical accuracy and correctness of the code implementation. This includes checks on the consistency and convergence of numerical methods, debugging of the software, and assurance that the physical models are implemented as intended.

Validation

Validation answers the question: *Are we solving the right equations?* It is the process of comparing the predictions of a code against physical reality, typically represented by experimental data. The goal is to demonstrate that the code can reproduce the physical behavior of the system within defined uncertainties, for the range of conditions relevant to NPP operation and accidents.

The four categories of test calculations are here listed:

1. **Basic Tests:** These are simple, often academic test cases designed to verify specific portions of the code. They may include analytical solutions or well-known empirical correlations, and although not directly relevant to NPP operation, they are essential for isolating and validating individual physical models.

2. **Separate Effect Test (SET)s:** These focus on specific thermal-hydraulic phenomena (e.g., critical heat flux, two-phase flow, pressure drop) in isolation. Although full-scale SETs are ideal, they are often performed at reduced scale and may require the use of surrogate fluids. SETs help confirm that the code correctly models individual physical processes without interference from system-level feedback.

3. **Integral Tests (ITs):** These involve more complex experimental setups (e.g., Large Scale Test Facility (LSTF)) that reproduce the integrated behavior of multiple components and phenomena of a nuclear plant. While integral tests better reflect the interactions between physical mechanisms, they are typically conducted at reduced pressure, power, and geometric scale.

4. **NPP -level Tests and Operational Transients:** These are conducted on actual nuclear power plants, often during start-up, shutdown, or special test conditions. Combined with operational transient data, they provide a unique opportunity to validate the code against real-scale behavior.

Consistency with Reality

D'Auria [10] proposes that beyond mere verification and validation, a thermal-hydraulic code should demonstrate consistency with reality. This implies the ability to extrapolate predictions beyond the exact conditions of the experiments while preserving physical plausibility and accuracy. This is particularly critical when experimental data do not fully cover the operational envelope of a reactor.

Scaling Considerations

Scaling refers to the process of relating results obtained in scaled-down experimental facilities to the full-scale nuclear reactor. Since it is often unfeasible or unsafe to conduct experiments at reactor scale, integral and separate-effect test facilities are built at reduced size, power, and pressure. However, this introduces challenges due to:

- Differences in non-dimensional parameters (e.g., Reynolds, Richardson, or Bond numbers) that affect flow regime, heat transfer, and phase separation;
- Distorted time or length scales that may lead to altered system response;
- Material and fluid substitutions (e.g., Freon instead of water);
- Limitations in reproducing interactions between components and control systems at real conditions.

To address these challenges, scaling methodologies are applied to ensure that the dominant physical phenomena are preserved across scales. The validation effort must therefore account for both the accuracy of individual models and the limitations introduced by imperfect scaling. The application of a code to both scaled experiments and reactor-scale scenarios is essential to assess its extrapolation capability and to ensure a credible safety analysis.

A qualified system thermal-hydraulic code must:

- Pass verification tests to confirm numerical correctness;
- Be validated through a hierarchy of experimental tests (Basic, SETs, ITs, NPP -level);
- Demonstrate consistency when applied beyond the conditions of direct validation;
- Properly account for scaling effects when using small-scale test data to inform full-scale reactor behavior.

Only by integrating verification, validation, consistency, and scaling can one achieve the level of confidence required for the code's use in licensing, design, and safety analysis.

2.3 The BEPU Method

The Best Estimate Plus Uncertainty (BEPU) methodology has emerged as a powerful alternative to the traditional conservative deterministic approach in the safety analysis of nuclear power plants. It combines realistic physical modeling with systematic uncertainty quantification to ensure safety margins are met under uncertain conditions. In the context of the present thesis, the BEPU methodology has been selected over the conservative approach due to its greater representativeness of the actual behavior of the plant. While the conservative method is based on simplified models and worst-case assumptions—ensuring that safety limits are not exceeded and allowing for easier implementation—it does not accurately reflect the realistic evolution of key plant parameters. In contrast, the BEPU approach employs more sophisticated models and explicitly quantifies the uncertainties associated with input data and model predictions, thereby providing a more accurate and comprehensive depiction of plant performance. An additional advantage of the BEPU methodology is that, by providing a realistic best estimate of system behavior along with its uncertainty bounds, it allows for a wider licensing margin. This increased margin can be used, for instance, to safely justify modifications to plant operating conditions—such as power uprates—while still ensuring compliance with safety limits. However, these benefits come at the cost of significantly increased complexity, both in terms of modeling and computational effort. An illustrative representation of what just stated is presented in Figure 2.2.

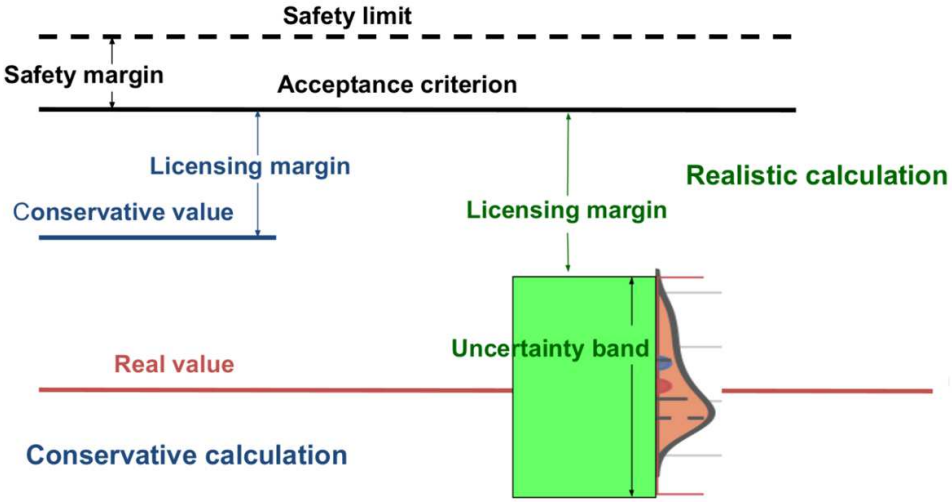

Figure 2.2: Conservative method vs BEPU method [11].

Overview of the BEPU Framework

The BEPU methodology is based on three pillars [10]:

1. Use of **best estimate thermal-hydraulic codes** (e.g., RELAP5, TRACE), which provide realistic representations of physical phenomena;

2. Identification and quantification of **input uncertainties**, typically described by

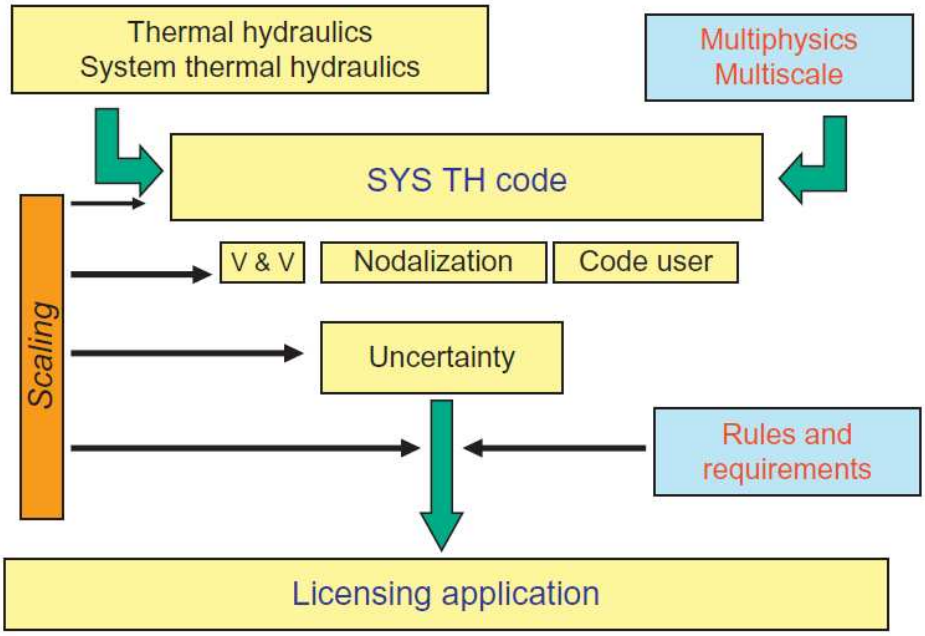

Figure 2.3: Selected key elements for the BEPU approach and interrelations [10].

probability distributions (e.g., uncertainty in initial conditions, boundary conditions, model parameters);

3. **Propagation of these uncertainties** through Monte Carlo simulations to obtain statistical information about key safety-related output variables (e.g., peak cladding temperature, system pressure).

Figure 2.3 [10] schematically illustrates this process: from input parameter distributions, through a set of deterministic code runs, to a final output distribution that match safety requirements. This visualization captures the essence of the uncertainty propagation in BEPU: input uncertainties "flow through" the model, producing a range of output responses.

Monte Carlo Sampling for Uncertainty Propagation

In the framework of this thesis, the propagation of uncertainties in BEPU is carried out using the Monte Carlo method. This involves performing a sufficiently large number of simulations (N) of the best estimate code, each using randomly sampled input parameters from their respective distributions.

Each simulation produces a value of the output quantity of interest (e.g., maximum fuel temperature), and the collection of outputs forms an empirical distribution. This output distribution is then analyzed to assess compliance with safety limits.

However, to confidently draw conclusions from the output distribution, one must also determine how many simulations are required to statistically support a claim, such as "with 95% confidence, the 95th percentile of the true distribution is below the safety limit." This is precisely where Wilks' formula comes into play.

Wilks' formula

Wilks' one-sided tolerance limit method [28] provides a non-parametric approach to determining the required sample size (N) for a given coverage (β) and confidence level (γ), assuming independent and identically distributed outputs and no assumptions on their distribution.

The most commonly used case is the first-order statistic (maximum value), which satisfies:

$$P\left(P\left(X \leq x_{\max}\right) \geq \beta\right) = \gamma$$

This implies that if N simulations are performed, then the maximum observed value $x_{\max}$ can be considered an upper tolerance limit for at least a fraction β of the population, with confidence γ.

For instance, for $\beta = \gamma = 0.95$, Wilks' formula indicates that $N = 59$ simulations are required. This is commonly adopted in safety evaluations to demonstrate that a variable (e.g., cladding temperature) remains below safety limits in 95% of possible cases with 95% confidence.

Table 2.1: Sample Sizes Required for Wilks' First Order Statistic.

Coverage (β)	Confidence (γ)	Required N
0.90	0.95	45
0.95	0.95	59
0.99	0.95	90

In the context of the present thesis, the number of simulations is $N = 93$, that results in an increase of the coverage while maintaining the same confidence level. In fact, with 93 samples, the maximum observed value corresponds still to 95% of all possible outcomes, with at least 99% confidence.

The derivation of Wilks' formula is presented in Appendix A.

Graphical Representation and Interpretation

Figure 2.4 of IAEA Report No. 52 [1] provides a clear schematic of the BEPU process: starting from uncertainty distributions on input parameters, a set of best estimate code calculations are carried out, and the resulting output variables are statistically analyzed. A critical output of the process is the derivation of a value (e.g., the 95th percentile of peak cladding temperature) which is then compared to regulatory safety limits.

Benefits and Implications

The BEPU methodology supported by Monte Carlo propagation and Wilks' statistics enables:

- More realistic, less conservative estimates of plant behavior;
- Quantitative confidence in safety margins;

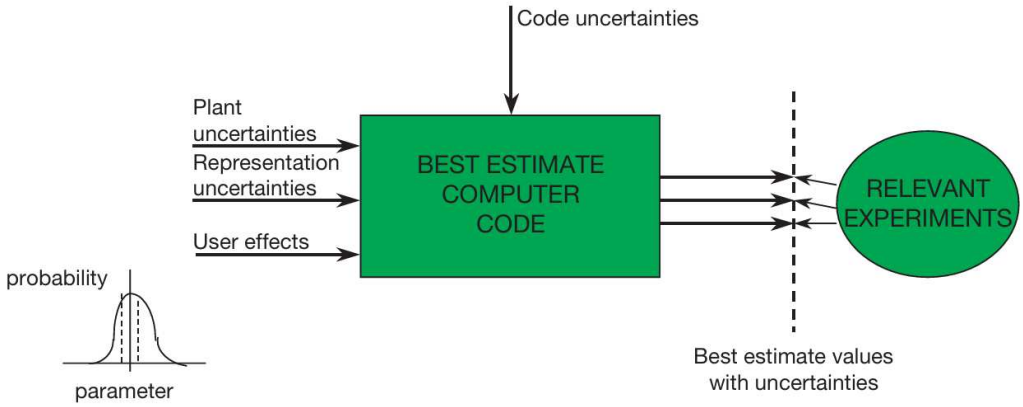

Figure 2.4: Evaluation process and main sources of uncertainties [1].

- Explicit inclusion of model and data uncertainties;
- Justification of reduced conservatism with statistical rigor.

This approach reflects a paradigm shift in nuclear safety analysis, enabling more informed regulatory decision-making and optimization of plant operations.

2.4 Uncertainty Analysis (UA): Inverse Uncertainty Quantification

Having established the critical role of input parameter uncertainty quantification in BEPU analyses, we now introduce the Inverse Uncertainty Quantification (IUQ) methodology, which allows for the calibration of uncertain model inputs based on experimental data, thereby enhancing the realism and robustness of BEPU evaluations.

Indeed, IUQ aims to estimate uncertain input parameters of a physical model by using experimental data, thereby reducing the discrepancy between model predictions and observations. Unlike forward UQ, which propagates input uncertainties to the output, IUQ addresses the inverse problem: calibrating the model's uncertain parameters so that it reproduces known physical responses with minimal error.

Techniques for Inverse Uncertainty Quantification

Several methodologies exist for IUQ, each with different assumptions, mathematical frameworks, and levels of fidelity. This subsection provides an overview of the main families of IUQ techniques applicable in nuclear system modeling [29].

1. Design of Experiments (DoEs) and Forward Uncertainty Propagation This is the most straightforward approach, often used as a preliminary step. A range of input parameters is defined using prior knowledge, and samples are generated according to a statistical design (e.g., Latin Hypercube Sampling, Sobol sequences). For each sample, the

model is run in a forward manner to produce a set of outputs, which are then compared against experimental data.

The analysis is typically visual and non-statistical, identifying parameter ranges that produce acceptable agreement with data. Although this method does not compute a posterior distribution, it helps identify regions of interest in the input space and supports sensitivity analysis.

2. Frequentist Statistical Inference The frequentist approach to IUQ seeks point estimates of uncertain parameters by minimizing a cost function, often the sum of squared residuals between model outputs and observed data. Confidence intervals can be derived through bootstrapping or asymptotic statistical theory.

This method includes optimization techniques such as Maximum Likelihood Estimation (MLE) and least-squares minimization. It is computationally less intensive than Bayesian methods, but does not provide full uncertainty distributions. Examples include the Super Moby Dick methodology and methods used in traditional code calibration frameworks.

3. Bayesian Statistical Inference The Bayesian approach uses Bayes' theorem to update the prior probability distribution of uncertain parameters in light of experimental observations. It yields a full posterior distribution that quantifies uncertainty and allows for probabilistic predictions.

Sampling methods such as Markov Chain Monte Carlo (MCMC), Hamiltonian Monte Carlo (HMC), or the No-U-Turn Sampler (NUTS) are commonly used to draw samples from the posterior. This approach is widely used in the context of BEPU methodologies for safety analysis.

4. Data Assimilation and Adjustment (DAA) This approach focuses on updating model parameters using experimental data while minimizing discrepancies between model predictions and observations. Techniques such as the Kalman Filter, Ensemble Kalman Filter, and variational data assimilation (e.g., 3DVAR, 4DVAR) are used extensively in fields such as meteorology and reactor physics.

In nuclear engineering, DAA is used for bias correction of macroscopic cross sections or tuning of system-level models using integral experiments. A key example is the adjustment of nuclear data libraries (e.g., JEFF, ENDF) via generalized least squares, where covariances and experimental uncertainties are rigorously treated.

Each IUQ approach has its strengths and limitations. While frequentist and forward methods are computationally efficient, they may not fully capture epistemic uncertainty. Bayesian and DAA methods are more robust in this regard but come at higher computational cost.

2.5 RELAP5 system code

Accurate modeling of thermal-hydraulic behavior in NPPs is essential for safety analysis, design validation, and accident management. Among the most established tools for such analysis is **RELAP5 (Reactor Excursion and Leak Analysis Program)**, a best-estimate system code originally developed by the Idaho National Engineering Laboratory (INEL) for the U.S. Nuclear Regulatory Commission. RELAP5 is designed to simulate the response of Light Water Reactor (LWR)s to a wide range of transient and accident conditions, including LOCAs, operational transients, and ATWS.

The code is based on a one-dimensional, two-phase, nonhomogeneous, and nonequilibrium flow model, and solves the associated conservation equations using a semi-implicit numerical scheme. RELAP5 allows detailed representation of reactor coolant systems through modular components and control volumes, with robust heat transfer, flow regime transition, and interphase interaction models. Its flexibility and extensibility have made it a reference tool for both experimental benchmark simulations and full-plant accident scenarios.

In recent decades, RELAP5 has been extensively validated against integral and separate effects test facilities, and it continues to be used worldwide for safety evaluations, licensing support, and the development of accident management procedures.

The contents presented in this section are mainly based on [24].

Applications of RELAP5

The robustness of RELAP5 stems from its detailed modeling of nonhomogeneous and nonequilibrium two-phase flow, its extensive library of components (e.g., pumps, valves, heat exchangers, pressurizers), and its flexibility in system nodalization. Moreover, it includes comprehensive modules for heat transfer modeling and control system simulation, which enable accurate representation of complex interactions within reactor systems.
RELAP5 has been applied in a wide range of scenarios. These include large and small break LOCAs (LBLOCA and SBLOCA), Main Steam Line Break (MSLB)s, startup and shutdown transients, and BDBAs. It is also used for single-component analyses, such as evaluating the behavior of pressurizers, steam generators, or accumulators under transient conditions.

- For instance, the ATLAS SBLOCA Test A1.1, conducted as part of the OECD/NEA international benchmark for RELAP5/MOD3.3 validation, involved simulating a 1% upper head break. RELAP5 demonstrated good predictive accuracy for key variables such as coolant inventory and clad surface temperatures [6].

- Further applications include the EU-DEMO Water-Cooled Lithium Lead (WCLL) blanket design, where RELAP5/MOD3.3 was coupled with CFD codes to analyze the thermal-hydraulic behavior of fusion reactor blankets during both operational and accidental transients [9].

- Similarly, in the MYRRHA accelerator-driven system, RELAP5-3D was used to simulate steady-state and transient conditions in the secondary water loop, with attention to the accurate modeling of low-pressure two-phase flow using optimized drift-flux correlations [21].

- In the case of the NUWARD Small Modular Reactor (SMR) concept developed by Framatome/CEA/EDF, RELAP5 simulations were performed to size components and verify the functionality of passive safety systems, such as external condensers, using a conceptual one-dimensional model [27].

As a brief overview of the employment of the RELAP5/MOD3.3 code Italian research institutions for TH safety studies and experimental facility modeling, below are representative examples that highlight the versatility and accuracy of the code in various reactor-related scenarios.

- RELAP5/MOD3.3 was applied in the simulation of the SIRIO facility at Sapienza University of Rome [8]. SIRIO is designed to investigate passive decay heat removal systems using molten salts. The study focused on both steady-state and transient behavior, modeling components such as valves, heat exchangers, and thermal storage tanks. The RELAP5 model provided accurate reproduction of the loop's behavior under varied boundary conditions, offering valuable insights for the design of passive safety systems in Gen-IV reactors.

- In another study, RELAP5/MOD3.3 was validated against data from the PERSEO Test 9, conducted by ENEA Brasimone and Politecnico di Torino [16]. This full-scale integral test explored condensation phenomena in passive heat removal systems. Observed discrepancies between the experimental results and RELAP5's predictions prompted proposed improvements to the condensation model, contributing significantly to the code's qualification for pool-type reactor safety analysis.

- The NACIE-UP loop, a lead–bismuth eutectic (LBE) experimental setup at ENEA Brasimone, was simulated using RELAP5/MOD3.3 coupled with the RAVEN framework for uncertainty quantification [18]. Both natural and forced circulation regimes were analyzed, and the study identified key uncertainty contributors in LBE thermal-hydraulic behavior. This work was part of a broader initiative to develop BEPU methodologies for advanced reactor designs.

- Lastly, a coupled analysis involving RELAP5/MOD3.3 and the PHISICS neutron kinetics module was conducted for the ALFRED reactor, a lead-cooled fast reactor demonstrator [7]. The analysis investigated transients such as Unprotected Loss of Flow (ULOF) and Unprotected Transient Over Power (UTOP). The integration of neutronics and thermal-hydraulics allowed for accurate prediction of feedback effects, supporting licensing efforts and safety demonstrations for ALFRED.

Beyond traditional transient and accident analysis, RELAP5 is also applied to uncertainty quantification, sensitivity analysis, and the investigation of real operational events. These applications support model validation and forensic reconstruction of incident sequences. The code is utilized in plant operation support, helping evaluate protection system logic, control setpoints, and dynamic behavior of interactive systems. Despite limitations in real-time performance, RELAP5 has been used in the validation of training simulators and to generate scenarios for operator instruction. In the regulatory domain, RELAP5 supports licensing audits by independently verifying vendor-supplied safety analyses and facilitating communication between plant operators and authorities. It is also

employed in PSA, where it may serve as a reference to benchmark fast-running tools. Finally, RELAP5 is a generic tool capable of modeling thermal-hydraulic transients even in non-nuclear systems, involving mixtures of steam, water, noncondensable gases, and solutes.

Although RELAP5 has established itself as a benchmark code for thermal-hydraulic transient analysis in nuclear systems, several limitations must be acknowledged regarding its modeling capabilities and numerical structure. First, RELAP5 is inherently a one-dimensional system code; although some versions (e.g., RELAP5-3D) offer limited 3D capabilities, the standard formulation cannot resolve multidimensional flow features such as lateral mixing or large-scale recirculations. The two-fluid model it employs assumes non-homogeneous but equilibrium-based interphase transport, relying heavily on empirical closure relations. This approach may yield inaccurate predictions in complex flow regimes—particularly during regime transitions or in conditions far from thermal or mechanical equilibrium.

Moreover, the code lacks precise interface tracking, making it unsuitable for problems where the interfacial topology (e.g., in stratified or slug flows) is essential. Geometrical modeling is restricted to channel-like structures, often requiring considerable simplification of real systems. RELAP5 also does not include an internal neutronic solver; coupling with external codes is required for multiphysics simulations involving feedback between reactor kinetics and thermal-hydraulics.

From a numerical standpoint, RELAP5 uses a semi-implicit finite-volume scheme with first-order spatial accuracy, which introduces significant numerical diffusion, especially in strongly advective problems. The algorithm's stability is ensured through tight coupling between pressure and velocity fields and adaptive time step control, but this can lead to high computational costs, particularly for finely resolved systems or long transients. Finally, the code's scalability is limited by its solver architecture, making large-scale parallel computation inefficient compared to modern high-performance computing standards.

Field Equations

RELAP5 is based on a non-equilibrium, non-homogeneous two-fluid model for the simulation of two-phase flow in light water reactors. The model considers separate balance equations for liquid and vapor phases, allowing the description of phase slip and thermal non-equilibrium. RELAP5 solves eight conservation equations for eight primary dependent variables at each nodal point of the hydrodynamic domain. The primary dependent variables are:

- Pressure, P;
- Phasic specific internal energies, U_f and U_g (for liquid and vapor phases, respectively);
- Vapor volume fraction (void fraction), α_g;
- Phasic velocities, v_f and v_g;
- Noncondensable gas quality, X_n;

- Boron concentration, ρ_b.

The independent variables are time, t, and spatial position along the flow path, x. Secondary dependent variables—used in the formulation of the field equations—include:

- Phasic densities, ρ_f and ρ_g;
- Phasic temperatures, T_f and T_g;
- Saturation temperature, T_{sat};
- Mass fraction of each noncondensable component X_{ni} in the gas phase.

The hydrodynamic model consists of the following eight conservation equations:

1. Mass continuity for the liquid phase;
2. Mass continuity for the vapor phase;
3. Momentum conservation for the liquid phase;
4. Momentum conservation for the vapor phase;
5. Energy conservation for the liquid phase;
6. Energy conservation for the vapor phase;
7. Boron transport equation;
8. Mass continuity for noncondensable gases.

Moreover, RELAP5 incorporates a dedicated heat conduction module to simulate solid structures in thermal contact with the fluid, referred to as *heat structures*. These may be of rectangular (e.g., slabs), cylindrical (e.g., fuel rods), or spherical (e.g., particle beds) geometry. The one-dimensional heat conduction equation is solved for each structure using temperature-dependent thermal conductivity and volumetric heat capacity. The heat structures are thermally coupled to the adjacent hydrodynamic volumes, allowing for detailed modeling of heat transfer between fluid and solid boundaries.

1. **Mass Conservation**: Mass conservation is enforced independently for both phases. Under the assumption of no external mass sources or sinks, the interfacial mass generation term in the liquid phase is the negative of that in the vapor phase. The interfacial mass transfer rate $\dot{m}_i$ is decomposed into two contributions:
   - Bulk interfacial mass transfer, $\dot{m}_{ig}$, which occurs in the fluid core;
   - Wall interfacial mass transfer, $\dot{m}_w$, which occurs in the thermal boundary layer near solid walls.
2. **Boron Transport:** The boron transport equation tracks the evolution of dissolved boron concentration, which is crucial for reactivity control in PWRs. Boron is assumed to be transported with the liquid phase and does not participate in phase change processes.

3. **Noncondensable Gases:** Noncondensable gases—such as nitrogen—may be present in the vapor phase, particularly after safety injection events involving accumulators. RELAP5 models noncondensables as moving with the vapor phase, assuming they share the same temperature and velocity. The conservation of noncondensable mass is handled through an additional transport equation.

4. **Momentum Conservation:** The momentum equations are formulated under several simplifying assumptions, justified by the secondary role of momentum in reactor safety analyses relative to mass and energy conservation:

   - Phasic pressures are assumed equal;
   - Interfacial and phasic pressure differences are neglected (except in stratified flow);
   - Viscous stresses and Reynolds stresses are neglected;
   - Covariance terms are assumed unity;
   - Interfacial momentum storage is neglected;
   - Interface forces include pressure and viscous components;
   - Normal wall forces are handled through a variable-area momentum flux model.

5. **Energy Conservation:** The energy equations for each phase are based on the following simplifications:

   - Reynolds heat flux is neglected;
   - Covariance terms are taken as unity;
   - Interfacial energy storage and intraphase heat conduction are neglected;
   - Only wall friction and pump work are included as dissipative effects.

   The dissipation effects due to interfacial mass transfer, interfacial friction, and virtual mass are neglected in the energy equations, as they are considered negligible compared to other terms.

Numerical Solution Strategy

The RELAP5 code solves the hydrodynamic field equations at each mathematical node using time and volume averaged quantities. A key approach used is the donor-cell (upwind) technique, in which transported properties are taken from upstream cells, enhancing numerical stability. For phenomena dependent on transverse gradients, such as wall friction or interfacial heat transfer, RELAP5 uses the bulk concept combined with empirical correlations or, when necessary, additional physical models.

RELAP5 provides two mathematical options for solving the system of equations:

- A semi-implicit finite-difference technique (default and recommended);
- A nearly-implicit finite-difference method, which allows violation of the Courant limit and is better suited for steady-state or quasi-steady calculations.

Only the semi-implicit method is described here, as it was employed in all simulations presented in this work.

Semi-Implicit Finite-Difference Technique

This method replaces the original partial differential equations with finite-difference approximations that are partially implicit in time. In this formulation, the equations resemble an upwind differencing scheme typically used for incompressible flow in constant-area ducts. Variables are interpreted as space-time averaged quantities, and time steps are selected such that implicit terms remain approximately linear, enabling efficient solution via finite differences. A critical feature of this technique is the use of staggered grids: scalar quantities (e.g., pressure, enthalpy, density) are stored at the centers of control volumes, while velocity components are defined at the cell faces (junctions). This layout avoids odd-even decoupling of pressure fields, a common numerical artifact in colocated grid schemes.

Due to the linear structure of the system and the fact that velocities at junctions depend only on pressures at the new time level, the volume equations can be reduced to a single equation in terms of unknown pressures and velocities. Once the pressure field is determined, all other field variables can be updated. The algorithm is state-dependent and accounts for all combinations of phase conditions between adjacent cells (e.g., two-phase to single-phase, etc.). The most general case—two-phase to two-phase—is handled by the following seven-step algorithm:

1. **Pressure Calculation:** Construct a linear system using state-variable data from the previous time step and solve for new-time pressures using a sparse matrix solver.

2. **Velocity Update:** Use pressure differences to compute the new-time liquid and vapor velocities at each junction.

3. **Intermediate Thermodynamic Quantities:** Calculate preliminary values for void fractions, internal energies, and non-condensable gas concentrations using results from the previous steps.

4. **Mass Conservation Check:** Evaluate mass balance errors. If errors exceed tolerances, reduce the time step and repeat from step 1. Otherwise, continue.

5. **Interphase Mass Transfer:** Compute phase change rates (e.g., evaporation, condensation) based on updated thermodynamic conditions.

6. **Final Update:** Use updated pressures, velocities, and interphase transfer terms to finalize void fractions, internal energies, and non-condensable gas fractions.

7. **Time Advancement:** Proceed to the next time step and repeat the cycle.

This algorithm allows RELAP5 to maintain conservation of mass, momentum, and energy while providing numerically stable solutions even for complex two-phase transients involving strong coupling, compressibility, and phase change.

Nodalization in RELAP5

The nodalization process in RELAP5 ([25],[26]) is a critical modeling step whereby the physical system is discretized into a network of interconnected control volumes and junctions. This process transforms the continuous geometry of a nuclear system into a set of

one-dimensional, spatially discrete elements suitable for numerical solution. Each control volume, also called a *hydrodynamic volume*, represents a finite region of the fluid domain, while junctions represent the flow paths between adjacent volumes.

1. **Hydrodynamic Nodalization**

   RELAP5 models fluid flow and heat transfer using a one-dimensional approximation. The entire thermal-hydraulic system (e.g., reactor core, steam generators, piping) is represented by a sequence of volumes and junctions:

   - **Control volumes** contain the fluid and store scalar quantities such as pressure, void fraction, internal energy, and noncondensable mass fraction.
   - **Junctions** connect adjacent volumes and define phasic velocities through momentum conservation equations.

   Each control volume may contain single-phase or two-phase flow and is characterized by a fixed geometry (length, cross-sectional area, hydraulic diameter). Thermodynamic and transport properties in each volume are assumed to be uniform or space-time averaged.

2. **Heat Structure Coupling**

   Heat transfer between the fluid and surrounding solid materials (e.g., fuel cladding, pipe walls) is modeled through *heat structures*, which are independently defined and thermally connected to specific control volumes. A heat structure may span several control volumes and consists of discrete axial and radial mesh points where the one-dimensional heat conduction equation is solved.

3. **Junctions and Flow Paths**

   Flow between volumes is defined at junctions. A junction connects two adjacent volumes and allows RELAP5 to solve the momentum equation based on pressure differences and interfacial forces. Junctions can represent:

   - Straight pipes or channels,
   - Sudden expansions/contractions,
   - Components with losses (e.g., valves, bends),
   - Pumps or flow restrictions.

   Special junction models account for elevation changes, area variation, or non-uniform phasic distributions.

4. **Component-Based Modeling**

   RELAP5 adopts a modular, component-based modeling strategy. Each part of the physical system (e.g., pipe, pump, heat exchanger, reactor vessel) is modeled using a specific component that defines:

   - Geometrical parameters,
   - Boundary and initial conditions,

- Interconnections with other components.

Components are assembled through a user-defined input deck that specifies the network topology and nodalization. A typical system model includes hundreds or thousands of control volumes and junctions, depending on the level of spatial resolution required.

5. **Guidelines for Nodalization**

   Accurate nodalization is essential for ensuring numerical stability and physical fidelity. Key considerations include:

   - **Resolution of key phenomena:** Areas with strong gradients (e.g., phase change, temperature spikes) require finer nodalization.
   - **Geometric fidelity:** The nodal model should preserve the geometry and flow path lengths of the physical system.
   - **Numerical stability:** Excessively fine nodalization may introduce numerical stiffness and reduce the permissible time step.
   - **Validation:** Nodalization should be supported by experimental data or sensitivity analysis to verify accuracy.

   In RELAP5, the user is responsible for choosing an appropriate nodalization strategy that balances resolution, computational cost, and physical realism. Poor nodalization may result in artificial oscillations, mass/energy imbalances, or inaccurate transient response.

Closure Laws

The mathematical formulation of two-phase flow in RELAP5 requires a set of closure laws to complete the system. These *constitutive models* describe the interactions between the liquid and vapor phases and between the fluid and the system boundaries. Without such models, the system would be underdetermined. RELAP5 includes a broad suite of physically motivated and empirically calibrated closure laws, ensuring accuracy and stability under a wide range of flow conditions [26].

Flow Regime Maps and Constitutive Model Selection

To unify and apply the closure laws consistently, RELAP5 uses *flow regime maps* to determine the flow topology and assign appropriate interfacial and wall interaction models. Three distinct flow regime maps are employed:

- Vertical flow regime map, for vertical components;
- Horizontal flow regime map, for horizontal or nearly horizontal flows;
- High mixing regime map, used primarily in pumps and high-turbulence regions.

Flow regime determination is based on key quantities such as void fraction and the phasic relative velocity. The regime map governs the calculation of interfacial area concentration and the individual wall contact area for each phase, which are then used to select suitable closure correlations.

Categories of Closure Laws

The closure relations in RELAP5 can be broadly classified into four functional categories:

1. **Interphase Heat and Mass Transfer**

   Heat and mass transfer between phases can occur both in the fluid bulk and in a thermal boundary layer near the wall. The former results from energy exchange driven by bulk phase temperature differences, while the latter involves local temperature gradients near heated surfaces. The phase-change process is modeled at a saturated interface, with the driving potential being the difference between the bulk fluid temperature and saturation temperature. RELAP5 includes multiple heat transfer mechanisms such as:

   - Free and forced convection;
   - Subcooled and saturated boiling;
   - Film boiling;
   - Wall and bulk condensation.

   A complex logical structure is used to select the applicable model based on system parameters like pressure, wall superheat, void fraction, phasic temperatures, total mass flux, and noncondensable gas content.

2. **Interphase Drag**

   Momentum exchange between the vapor and liquid phases is governed by interfacial drag. Two modeling approaches are used:

   - The **drift flux model**, applied mainly in bubbly and slug flows in vertical geometries;
   - The **drag coefficient model**, which calculates interfacial drag based on empirical drag coefficients varying with flow regime.

   These models are essential for determining the phasic slip velocities and contribute significantly to the momentum conservation equations.

3. **Wall Heat Transfer**

   The wall heat transfer model accounts for energy exchange between the solid structures (e.g., fuel rods, pipe walls) and the fluid. It includes convective and phase-change mechanisms such as nucleate boiling and condensation. The local heat transfer coefficient is selected based on the current heat transfer mode, which may include up to twelve distinct regimes ranging from single-phase convection to transition boiling and film boiling. Solid heat conduction is modeled separately via a 1D transient conduction equation with temperature-dependent thermal properties.

4. **Wall Friction and Local Losses**

   Wall friction is modeled by computing the shear stress at the wall based on flow regime and phasic velocities. The flow regime map also determines how the friction

is apportioned between the phases. Only wall shear effects are included in the wall friction term. Additional pressure losses due to geometric discontinuities (e.g., elbows, area changes, valves) are calculated using a separate *form loss* model.

Interfacial Area Transport

For improved accuracy in the modeling of interfacial mass, momentum, and energy exchanges, RELAP5 may employ an optional interfacial area transport model. This equation tracks the time evolution of interfacial area concentration by accounting for coalescence and breakup mechanisms. If this model is not activated, the interfacial area is estimated using steady-state correlations conditioned on flow regime and void fraction.

In summary, the constitutive models in RELAP5 are a cornerstone of the code's predictive capabilities. Their implementation via regime-dependent closures ensures flexibility and accuracy across a wide range of flow patterns and thermal-hydraulic conditions, especially those involving phase change, noncondensable gases, and wall heat transfer.

Chapter 3

The ATRIUM Project

3.1 Project Overview

The ATRIUM project [14] is an international benchmark organized by the OECD/NEA Working Group on Analysis and Management of Accidents (WGAMA). It is designed to advance the State of the Art in IUQ, and validation methodologies for system thermal-hydraulics codes, particularly in the context of regulatory decision-making and safety demonstration for nuclear power plants. The main objectives of ATRIUM are to:

- provide a robust framework for quantifying model and input uncertainties in thermal-hydraulic simulations,
- promote and compare different statistical methods for IUQ in a consistent experimental context,
- improve confidence in predictive safety analyses through a formal validation step,
- foster international collaboration and harmonization of best practices in IUQ and model validation for nuclear safety applications.

By combining IUQ with experimental validation, ATRIUM serves as a stepping stone toward a more systematic, transparent, and quantitative approach to uncertainty management in nuclear system analyses.

The ATRIUM benchmark comprises three progressively complex exercises designed to evaluate inverse uncertainty quantification and forward propagation methodologies.

- **Exercise 1 – Separate Effect Test (SET) based IUQ:** The first step focuses on the analysis of a well-controlled experimental database composed of SETs, which enables the isolation of specific physical phenomena and simplifies the uncertainty quantification process. The phenomenon selected is the *critical flow* at the break, which plays a key role in the initial stages of a LOCA. The reduced complexity of the scenario facilitates a more precise calibration of input parameters and model correlations involved in the choked flow regime.
- **Exercise 2 – Combined Effect Test (CET) based IUQ:** The second exercise increases the complexity by involving experiments in which multiple coupled thermal-hydraulic phenomena interact simultaneously, also referred to as CETs. In

particular, the focus is on *post-Critical Heat Flux* heat transfer, where mechanisms such as film boiling and quenching dominate the thermal response. The presence of multiple interacting effects poses a challenge for uncertainty quantification and model adequacy evaluation.

This progressive IUQ approach allows for the incremental development and application of best practices. Special attention is given to the adequacy assessment of the experimental datasets, particularly with regard to their extrapolation capability toward full-scale nuclear reactor applications under LOCA conditions.

In this context, it is essential to justify the choice of influential input parameters and physical correlations (e.g., through preliminary sensitivity analysis).

Ultimately, the input model uncertainties derived from Exercises 1 and 2 need to be propagated to the representative **Integral Effect Test (IET)**, the LSTF-ROSA IB-HL-01 experiment (i.e. Test 1: Intermediate-Break Loss of Coolant Accident (IBLOCA) in a Hot Leg), to assess and validate their applicability in complex, integrated transient scenarios. This is the core of **Exercise 3**.

Each exercise follows a structured workflow.

Exercise 1: Critical Flow

1. **Database Analysis**: Collection and review of experimental data on critical (choked) flow from dedicated separate-effect tests.

2. **Adequacy Assessment**: Verification that the selected dataset is complete, relevant, and of sufficient quality for IUQ calibration.

3. **Physical Model Selection**: Identification of appropriate choked flow correlations and two-phase flow models in the system code.

4. **Input Deck and Nodalization**: Construction of the simulation input file and spatial discretization, balancing resolution with computational cost.

5. **IUQ**: Calibration of uncertain input parameters using experimental critical flow data and a prescribed IUQ methodology.

6. **Analysis and Validation**: Comparison of IUQ prediction bands against measured critical mass flow rates to assess coverage and model fidelity.

Exercise 2: Post-CHF Heat Transfer

1. **Database Analysis**: Evaluation of test data related to film boiling and wall temperature behavior after CHF.

2. **Adequacy Assessment**: Ensuring data completeness and relevance for post-CHF modeling.

3. **Physical Model Selection**: Selection of post-CHF heat transfer and film boiling correlations (e.g., Groeneveld, Katto).

4. **Nodalization Development**: Creating a sufficiently detailed axial mesh for resolving temperature gradients in the CHF region.

5. **IUQ**: Adjustment of model parameters using observed wall temperature data to calibrate uncertainty.

6. **Analysis and Validation**: Evaluation of predicted uncertainty bands against wall temperature measurements to validate model behavior.

Exercise 3: Integral-Effect Test (IET) Propagation

1. **Experimental Analysis of the IET:** Identification of key transient phases and Quantity of Interest (QoI)s from the LSTF IB-HL-01 experiment, such as break mass flow rate and peak cladding temperature.

2. **Input Deck and Nodalization:** Development of a high-fidelity system model of the facility (or a subset of interest) using the participant's preferred thermal-hydraulic code (e.g., RELAP5 in the context of the present thesis - Section 3.4). This includes steady-state initialization and transient capabilities.

3. **Uncertainty Propagation:** Execution of a forward uncertainty quantification study, propagating uncertainties related to critical flow and post-CHF behavior through the full transient using Monte Carlo sampling or equivalent approaches.

4. **Comparison and Validation:** Assessment of the predictive capability of the model by comparing the uncertainty envelopes of the simulated QoIs against experimental data. This step contributes to evaluating the reliability and applicability of the propagated uncertainties in a realistic, scaled environment.

3.2 The INSAG Process

The **INSAG process** [15] is a systematic approach for conducting deterministic safety analyses in nuclear power plants, particularly within the framework of BEPU.

It consists of a structured sequence of steps designed to identify and quantify the relevant physical phenomena and uncertainties in a given accident scenario. Figure 3.1 provides a conceptual breakdown of the process, applied to ATRIUM project test study (e.g., Test 1) in the framework of this thesis.

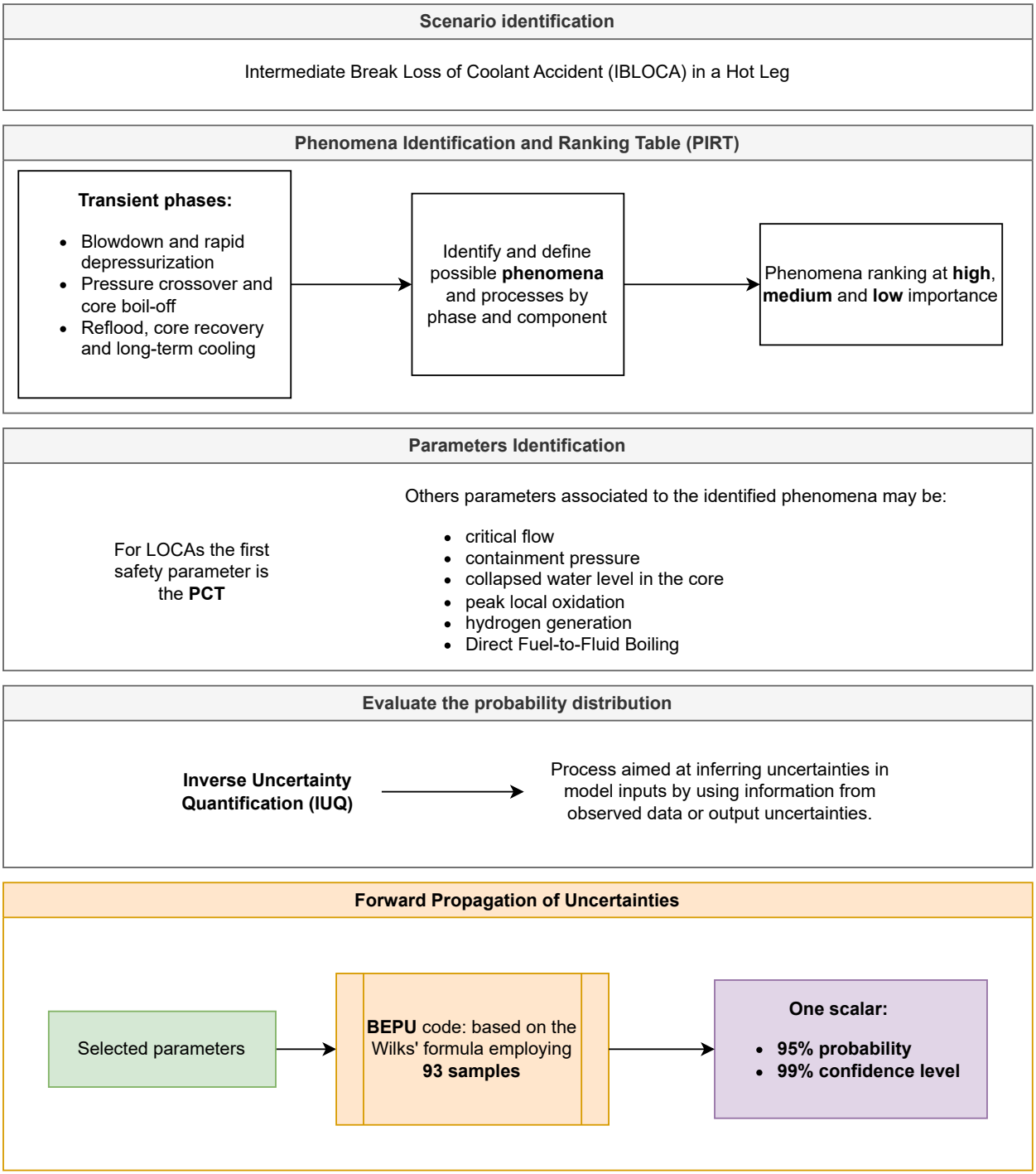

Figure 3.1: ATRIUM project process: focus on Forward Propagation of Uncertainties which represents the core objective of this thesis work. Figure generated by the author based on [15].

1. **Scenario Identification**
   Define the transient or accidental scenario to be analyzed (e.g., IBLOCA).

2. **Phenomena Identification and Ranking Table (PIRT)**
   Identify the key physical phenomena occurring during the selected scenario.
   Rank them based on their importance and the level of knowledge available.
   This step guides the modeling strategy and the treatment of uncertainties.
   Table 3.1 lists the phenomena ranked as having *high* importance, along with their classification by system, component, and associated phase.

3. **Parameter Identification**
   Determine the physical and modeling parameters influencing each phenomenon identified in the PIRT.
   This step is essential for defining the input parameters to be treated as uncertain in the UQ process.
   As will be explained in detail in Chapter 4, this thesis does not focus exclusively on the Peak Cladding Temperature (PCT)—which is traditionally the primary figure of merit in safety analyses for LOCA scenarios—but also considers other key parameters.
   Figure 3.1 illustrates a set of general parameters that may be relevant in a typical LOCA analysis. The specific parameters considered in this study will be presented in the following chapter.

4. **Inverse Uncertainty Quantification**
   Assign probability distributions to the selected uncertain parameters based on available data or output uncertainty estimates.
   For a more detailed explanation, refer to Section 2.4.

5. **Forward Uncertainty Propagation**
   Perform simulations using best-estimate thermal-hydraulic codes (e.g., RELAP5) with the previously defined uncertain input parameters.
   This step typically involves Monte Carlo sampling. In this work, the Wilks' formula is applied to reduce the number of required simulations to 93, while still ensuring a 95% probability and 99% confidence level in the statistical analysis of the results.
   For further details, refer to Section 2.3.

The final stage of the process aims to verify that key safety parameters (e.g., cladding temperature, system pressure) remain within regulatory limits with high confidence.

Table 3.1: Phenomena ranking at *high* importance. Table compiled based on Table 9 in [22]

System	**Component**	**Phenomenon**	**Phase**		
			1	**2**	**3**
RPV	Core (fuel)	Fission power (including distribution)	H	–	–
		Decay heat (including distribution)	M	H	H
		Gap conductance	M	M	H
		Rod surface heat transfer			
		- Nucleate boiling	H	H	M
		- Critical heat flux	H	L	H
		- Rewet (min. film boiling temp.)	H	–	H
		- Stable film boiling	H	–	H
		- Transition boiling	H	L	H
		- Single-phase convection to vapor	–	H	H
		Reactivity			
		- Void/moderator feedback reactivity	H	–	–
		- Scram reactivity	H	–	–
	Core (fluid)	Flashing & boiling	H	H	H
		Phase separation	–	H	H
		Vapor superheat (single-phase vapor convection)	–	H	H
		Interfacial heat transfer	M	M	H
		Interfacial drag	M	M	H
	Downcomer	Level change	–	M	H
	Upper plenum	Flashing	H	L	L
	Upper head	Flashing + level decrease (init. temp.)	H	–	–
RCS	Hot leg	Flashing	H	L	L
	Break	Critical flow	H	H	H
	RCP	Flow coastdown	H	–	–
		Pump performance	H	–	–
PZR	Vessel	Level decrease with flashing	H	–	–
SIS	SIT	Gas temp. and change (interface heat transfer)	–	–	H
		Water level and change	–	–	H
		FD resistance in high flow	–	–	H
		FD resistance in low flow	–	–	H
	SIP	SIP flow (incl. flow resistance)	–	H	H

3.3 The LSTF-ROSA IB-HL-01 experiment

The LSTF, operated by the Japan Atomic Energy Agency (JAEA), is a full-height and 1/48 volumetrically scaled integral test facility designed to simulate the thermal-hydraulic behavior of a pressurized water reactor (PWR) during transient and accident conditions, particularly LOCAs. The LSTF was originally constructed under the framework of the International Standard Problem (ISP) programs and has been extensively used in the OECD/NEA ROSA and ROSA-2 Projects to support the validation and development of best-estimate system thermal-hydraulic codes [5][4].

The facility replicates a Westinghouse-type 4-loop 3423 MW_{th} PWR with two symmetric primary loops and incorporates detailed representations of key components such as the reactor pressure vessel, hot and cold legs, pressurizer, steam generators, accumulators and safety injection systems. Despite its reduced power (10 MW_{th}) and size, the LSTF preserves the elevation, flow path layout, and pressure conditions of a reference PWR, ensuring proper simulation of important thermal-hydraulic phenomena such as natural circulation, void distribution, and critical flow.

Each loop includes a primary pump, SG U-tubes and associated piping. The secondary system consists of full-height steam generator downcomers and risers, steam lines, and feedwater systems. The facility is highly instrumented, allowing for the detailed measurement of temperatures, pressures, mass flow rates, and void fractions at multiple locations throughout the system.

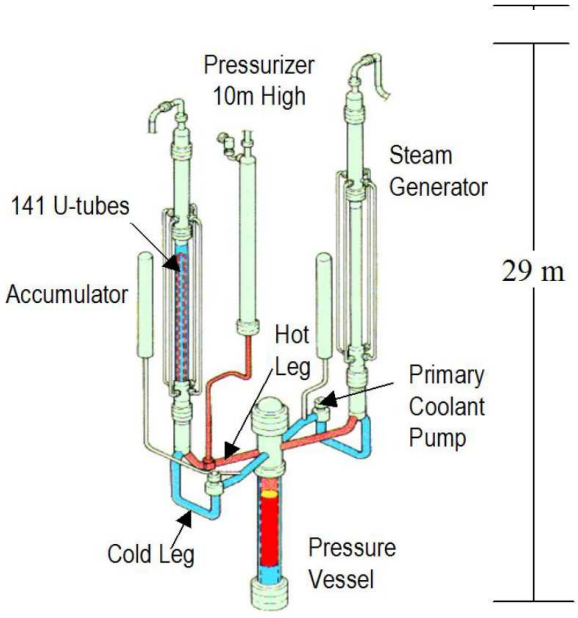

Figure 3.2: Schematic view of the LSTF.[5]

The LSTF has been extensively used to investigate small and intermediate break LOCAs, as well as other accident scenarios involving system depressurization, asymmetric loop behavior, and core cooling performance. Data from these experiments provide crucial benchmarks for code validation and uncertainty quantification in reactor safety analysis.

In the following pages, several summarizing tables are presented to provide the reader with a clearer understanding of the scaling strategy (Table 3.2), a general description of

Table 3.2: Scaling factor (PWR/LSTF): design characteristics of LSTF to a PWR [5] [23].

	Unit	LSTF	PWR	PWR/LSTF
Primary pressure	bar	160	160	1
Secondary pressure	bar	7.4	6.13	0.83
Core height	m	3.66	3.66	1
Number of fuel rods	–	1008	50952	50.55
Primary fluid volume	m^3	8.14	347	42.6
Total core power	MW	10	3423	342
Q/V	MW/m^3	1.23	8.8	8.0
Core inlet flow	$tonne/s$	0.0488	16.7	342
Pressure vessel downcomer gap	m	0.053	0.26	4.91
Number of primary loops	–	2	4	2
Hot leg inner diameter	m	0.207	0.737	3.56
Hot leg length	m	3.69	6.99	1.89
$L/\sqrt{D}$	$m^{1/2}$	8.11	8.14	1.0
Hot leg volume	m^3	0.124	2.98	24.0
Number of tubes in SG	–	141	3382	24.0
Average length of SG tubes	m	20.2	20.2	1

the test facility (Table 3.3), the timeline of the experiment (Table 3.5), and the initial steady-state conditions (Table 3.4), which also serve as inputs for the RELAP5 code simulations.

Regarding the break conditions, which define the initiating event of the transient [5]: the Double-Ended Guillotine Break (DEGB) of the PZR surge line was simulated using a nozzle installed flush with the inner surface of the hot leg, oriented in the upward direction. The configuration was selected to minimize any artificial influence of nozzle length on the mass flux. The flow area of the break corresponds to approximately 17% of the volumetrically scaled cross-sectional area of a typical PWR hot leg. The break unit is expected to be initially filled with nearly saturated coolant before the onset of the transient.

In addition, the sparger pipe at the bottom of the Storage Tank (ST) was equipped with multiple openings by removing its cover plates. Air was injected through nozzle N-5 into the sparger in order to reduce steam condensation rates and thus avoid the occurrence of water hammer phenomena in the tank.

3.4 Nodalization of the LSTF Facility Using RELAP5

This section provides a comprehensive overview of the RELAP5 input model developed for the LSTF. The RELAP5 nodalization of ROSA/LSTF is depicted in Figure 3.3.

The nodalization of the LSTF facility is divided into two main input decks: `main_MG_1_tag.i` and `BIC_test_1_tag.i`. The former includes the complete Integral Test Facility (ITF) model and the control logic required to simulate the steady-state initial-

Table 3.3: Characteristics of the LSTF IB-HL-01 integral test. Table extracted from [5].

Criteria/items	**LSTF test denoted as IB-HL-01**
Type	IET
Working fluid	Steam/water
Material properties	Electrically-heated rod cladding of Inconel 600; density, specific heat, thermal conductivity
Component and/or reactor	Overall system of PWR
Experimental conditions	• 17% hot leg intermediate-break LOCA • Total-failure of high-pressure injection system • Design flow rates of accumulator (Acc) and LPSIs to become 3:1 to cold legs in loops with and without pressurizer
Range of main parameters	• Primary pressure: max. 15.5 MPa • Core power: max. 10 MW • Cladding surface temperature: max. 607 K
Geometry	• Four primary loops of Westinghouse (WH)-type PWR are represented by two equal-volume loops to simulate two-phase flows • Full assembly has mostly the same dimensions as those of WH-type 4-loop PWR 17×17 fuel assembly to preserve heat transfer characteristics of core • Core, 3.66 m in active height, consists of 1008 electrically-heated rods in 24 rod bundles to simulate fuel rod assembly in WH-type 4-loop PWR
Scale	• Full-height model of WH-type 4-loop PWR • Volumetric scaling ratio of primary loops is 1/48 of WH-type 4-loop PWR • Time scale of simulated phenomena is one to one to those in WH-type 4-loop PWR • Flow area in horizontal leg is scaled to conserve ratio of length L to square root of pipe diameter D; $L/D^{0.5}$ of WH-type 4-loop PWR to better simulate flow regime transitions in primary loops (Froude number basis)
Covered phenomena	Critical flow; steam condensation on coolant of Acc and LPSIs; steam discharge through steam generator (SG) relief valve; coolant injection from ACC and LPSI; loop seal clearing; liquid accumulation in upper plenum due to CCFL; core two-phase mixture level; core heat transfer; core boil-off; core quench
Covered model	• Critical flow model; Ransom and Trapp model, etc. • CCFL model; Wallis-type co-relation, etc.
Validate complete system	• Experimental data are manually qualified through comparison of published ranges and uncertainty values • Bad trend data among all experimental data are excluded • Available experimental data are finally obtained
Available measurements	Pressure; differential pressure; fluid temperature; wall temperature; flow rate; liquid level; fluid density; electric power; pump rotation speed; integrated discharge flow through break
Instrumentation	Pressure transducer; differential pressure transducer; thermocouple; flow meter; gamma-ray densitometer; electric power meter; magnetic pickup; level meter

Table 3.4: Specified and measured initial conditions for LSTF IB-HL-01 test (loops with/without PZR) [4].

Item	**Specified**	**Measured**[a]
Pressure vessel		
Core power (MW)	10.0 ± 0.07	10.08
Upper plenum pressure (MPa)	15.5 ± 0.108	15.53
Downcomer-to-upper head bypass (%)	0.3	Not Measured
Primary loop		
Hot leg fluid temperature (K)	598.1 ± 2.75	598.2 / 596.9
Cold leg fluid temperature (K)	562.4 ± 2.75	563.6 / 563.4
Mass flow rate (kg/s / loop)	24.3 ± 1.25	25.13 / 24.84
Downcomer-to-hot leg bypass (kg/s)	0.049 ± 0.01	0.052 / 0.048
Pressurizer (PZR)		
Pressure (MPa)	15.5 ± 0.108	15.51
Liquid level (m)	7.2 ± 0.25	7.40
Steam generator		
Secondary-side pressure (MPa)	7.3 ± 0.054	7.33 / 7.36
Secondary-side liquid level (m)	10.3 ± 0.38	10.25 / 10.22
Steam flow rate (kg/s)	2.74 ± 0.10	2.67 / 2.62
Main feedwater flow rate (kg/s)	2.74 ± 0.05	2.75 / 2.67
Main feedwater temperature (K)	495.2 ± 2.63	497.9 / 497.1
Accumulator system		
Pressure (MPa)	4.51 ± 0.054	4.53 / 4.52
Temperature (K)	320 ± 2.3 / 2.4	320.8 / 321.6
Water level above tank bottom (m)	6.47 ± 0.12 / 7.14 ± 0.15	6.39 / 7.09
Low pressure injection system		
Temperature (K)	310 ± 2.63	311.3

[a] Averaged for 60s (-60 to 0 s)

Table 3.5: Sequence of events during the LSTF IB-HL-01 test. Table extracted from [4].

Time (s)	**Event**
−63	PZR isolation by valve closure at PZR surge line
0	Break valve open; Initiation of primary coolant pumps rotation speed increase (to 1550 rpm in 4 s)
1	Scram signal; Closure of SG main steam stop valve
4	Closure of SG MSIVs
5	Initiation of coastdown of primary coolant pumps
7	Termination of SG main feedwater
∼10	Initiation of decrease in liquid level in SG U-tube
20	Initiation of core power decay (power follows decay curve; 10 MW constant until 20 s, decay started at 19 s)
∼55	Primary pressure became lower than SG secondary-side pressure
∼155	Initiation of ACC system in both loops
∼165	Initiation of core uncover
∼180	LS clearing; Peak cladding temperature (PCT) of 607 K at Position 5 in high power bundle
∼185	Whole core quench
250	Termination of Acc system in broken loop (loop B)
252	Primary coolant pumps stop
∼290	Termination of Acc system in intact loop (loop A)
∼420	Initiation of second injection of Acc system in both loops
∼505	Initiation of LPSI in both loops
1574	Break valve closure

ization phase, typically 4900 seconds, as established in the OECD/NEA ROSA projects. The latter contains the specific boundary and initial conditions corresponding to the given experiment (e.g., Test 1). Prior to running a simulation, an external script merges the two decks to generate a final input file, `test1_tag.i`, which combines the full plant model with the experimental conditions. This workflow ensures consistency in the general nodalization across all experiments.

The LSTF model represents a detailed configuration of a pressurized water reactor, including a pseudo-3D reactor pressure vessel (RPV), two symmetric primary loops (Loop A and Loop B), steam generators (SGs), reactor coolant pumps (RCPs), a pressurizer (PZR), and ECCSs. Each primary loop comprises a hot leg, a loop seal, and a cold leg. The pressurizer is connected to the hot leg of Loop A through a surge line, while the spray line draws coolant from the cold leg of the same loop. Two accumulators are connected to each cold leg. The pump model is adapted from the RELAP5 input deck originally supplied by JAERI, with the coastdown behavior modified to match specific ROSA test conditions.

Reactor Pressure Vessel

The RPV (Figure 3.4) is modeled using a pseudo-3D approach that includes multiple parallel flow channels in both the core and downcomer regions. The core region is divided into 13 parallel channels with 19 axial levels, representing individual fuel assemblies.

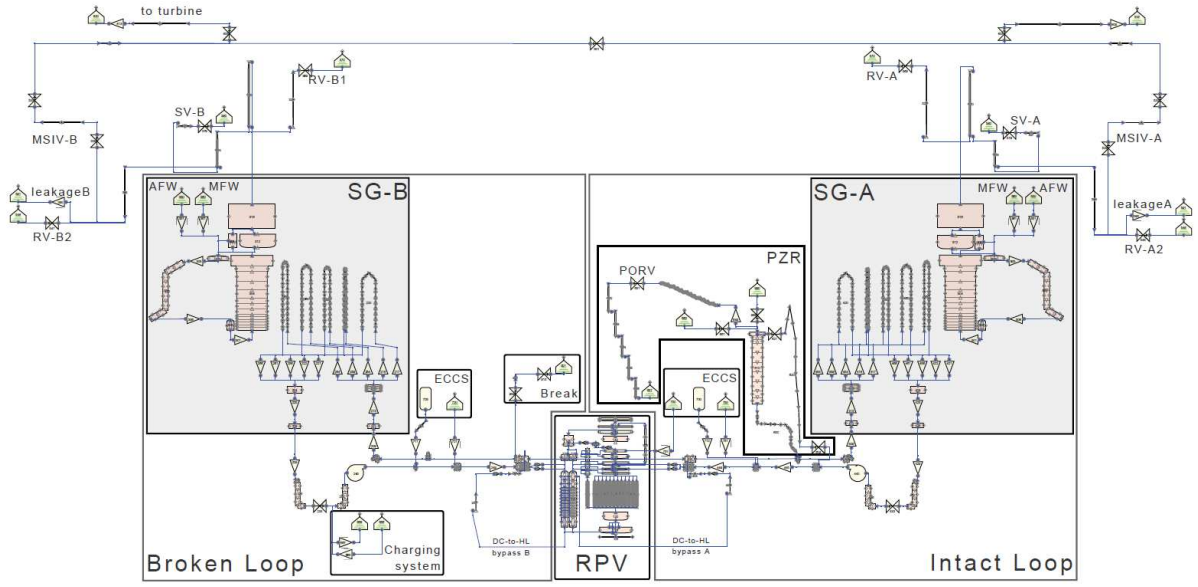

Figure 3.3: RELAP5 nodalization of ROSA/LSTF [17].

Crossflow junctions and heat structures are implemented to capture radial heat transfer and to represent instrumented elements such as thermocouples for CET measurement. The eight Core-Guide Thimbles (CRGT)s are individually modeled and connected to a common upper head volume.

The downcomer region consists of two vertically connected annular volumes. Crossflow and momentum transfer are enabled to account for possible ECCS bypass during transients. Spray and leakage bypasses between the downcomer, Upper Head (UH), and hot legs are also included, with form loss coefficients adjusted to match reported flow rates. Axially, the downcomer is discretized into 15 levels to reflect the geometric distribution of internal components and junctions.

The upper head is represented by two parallel axial flow paths to promote mixing and avoid artificial stagnation. The upper plenum is divided into five axial levels, with the lower level subdivided into 13 radial channels to better resolve the CRGT inlet flow. The lower plenum is modeled using three components aligned with the core inlet and downcomer connections.

Primary Loops

The primary loops (Figures 3.5,3.5) are symmetric in layout and modeled to preserve geometric fidelity in terms of lengths, elevation differences, and relative positions of major components (SGs, RCPs, PZR connections, ECCS injection nozzles, and break locations). The RCPs are defined using RELAP5 `PUMP` components, with all performance characteristics and coastdown profiles set through control logic. Default coastdown curves are included in the main input deck and may be overridden in the BIC files for specific tests.

ECCS subsystems—HPSI, LPSI, and accumulators—are connected at fixed positions on the cold legs, in agreement with the LSTF system design. The relative distances between ECCS nozzles, RCPs, and the RPV are preserved. The HPSI and LPSI are modeled using time-dependent junctions and volumes to define injection flow rates and

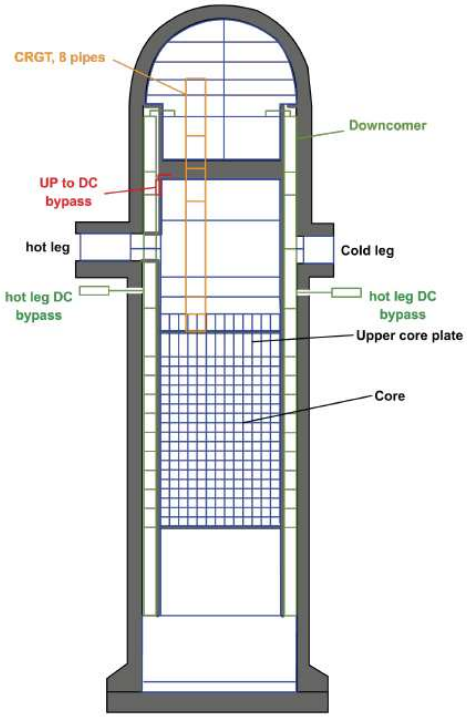

Figure 3.4: RPV nodalization [17].

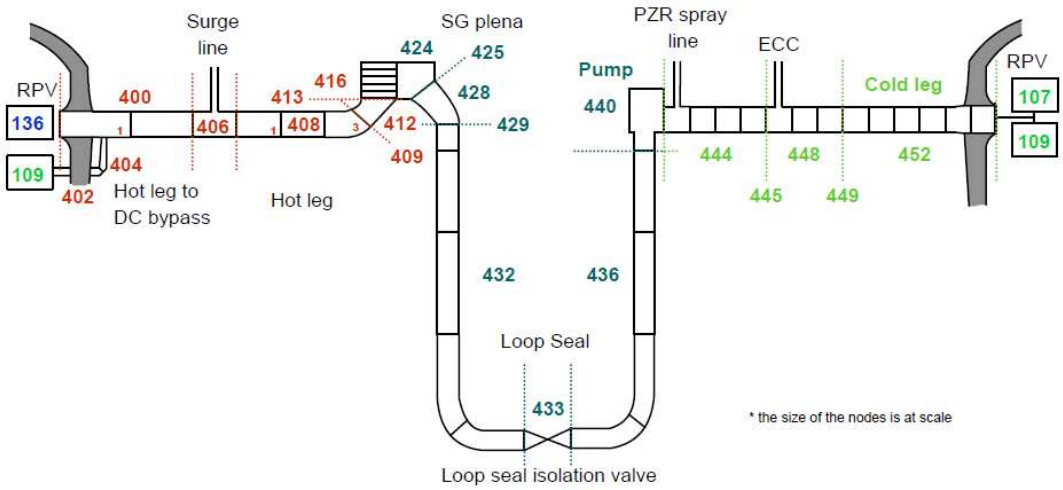

Figure 3.5: Nodalization of Loop A -intact loop, [17].

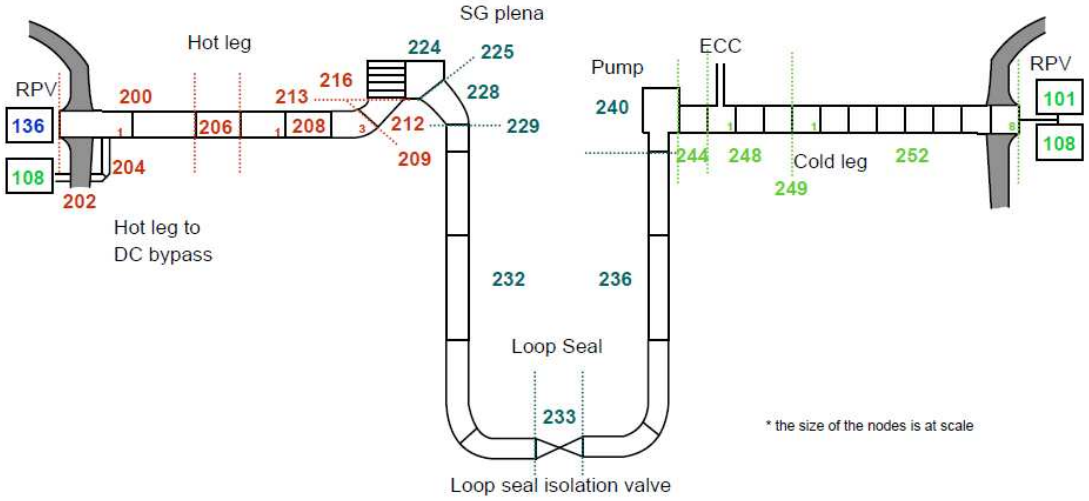

Figure 3.6: Nodalization of Loop B -broken loop, [17].

fluid conditions. The accumulator model includes gas-liquid separation, pressure loss elements, and height effects, all of which may vary slightly between experiments.

Secondary System

The secondary system includes the steam generator vessel, downcomer, riser, dome, and separator components. The model topology is inherited from a previously validated RELAP5 input deck. Both Loop A and Loop B share similar secondary side configurations. The feedwater boundary extends from the Main Feedwater (MFW) nozzle to the turbine inlet, modeled via `SNGVOL` and `TMDPVOL` components. The riser is subdivided into 16 volumes to match the thermal stratification observed in the U-tubes.

The MFW and auxiliary feedwater lines are merged and connected to a single injection point at the steam generator downcomer top. The steam lines preserve the original geometric and pressure-drop characteristics. Form losses are adjusted at riser inlets and separator outlets to match the reported recirculation ratio under steady-state conditions.

Heat Structures

Accurate simulation of heat transfer and heat losses is critical in integral test facilities. The input includes both active and passive heat structures, totaling 10,304 mesh points. Active structures simulate fuel assembly heating profiles, pressurizer heaters, and RCP motor cooling. Passive structures include all piping walls, thermal insulation layers (e.g., rockwool), and internal RPV components such as the core barrel, upper support plate, and CRGT internals.

Each heat structure is defined by its geometry, materials, axial and radial discretization, boundary conditions, and heat transfer hydraulic diameter. For non-zero values, hydraulic diameters are explicitly calculated; otherwise, the code computes them based on default formulations.

Core Power Modeling

The heater rods in the core region are modeled as cylindrical heat structures with layered materials including Al_2O_3, NiCr, MgO, and Inconel 600. Radial dimensions and discretization levels follow those defined in the original JAERI RELAP5 input model. Heating is applied to the NiCr region, and initial temperatures and diameters are set according to experimental values.

Special Models and Boundary Conditions

The Henry-Fauske model is used to represent choked flow in break components. Default discharge and non-equilibrium coefficients are set to 0.85 and 3.0, respectively, and may be refined via sensitivity analyses. Relief and safety valves in the secondary side are modeled with empirically calibrated discharge coefficients to match experimental flow data.

CCFL models are activated at key junctions, including the upper core plate, steam generator inlets, CRGTs, downcomer, U-tubes, and surge line. Wallis-type correlations are employed with site-specific coefficients, selected based on available literature and engineering judgment. Although a comprehensive sensitivity matrix has not been developed, the applied coefficients are consistent with typical values and physical expectations.

Chapter 4

Methodology

4.1 Steps of Input Uncertainty Propagation

In order to delve into the methodology adopted to obtain the results required for Exercise 3 of the ATRIUM project, a brief overview of the steps followed in this study is presented below.

Each step focuses on a different set of input parameters, with the objective of evaluating the influence of those specific uncertainties on the simulated accident transient.

- **Step 1:** This step (Section 4.4), which is still related to the previous ATRIUM exercises, involves the propagation of uncertainties associated with critical flow and post-Critical Heat Flux (post-CHF) phenomena.

- **Step 2:** In this step (Section 4.5), additional sources of uncertainty are introduced —such as geometry, material properties, and initial and boundary conditions— to supplement the model uncertainties propagated in Step 1. This extension aims to ensure adequate coverage of the experimental QoIs, which may not be fully enveloped by the first set of uncertainties alone.

- **Step 3:** This is an optional step (Section 4.6) that allows for the inclusion of further input uncertainties, enabling the definition of additional Figure of Merit (FoM)s to broaden the analysis.

4.2 Figures of Merit

As previously mentioned, the objective of this study is to estimate the 95^{th} percentile of the variables calculated using the RELAP5 code (Section 4.3), with a confidence level of 99%. Accordingly, the methodology has been specifically developed to quantify the uncertainty of scalar quantities, since the FoMs considered in this analysis are primarily scalar metrics.

Given the nature of the scenario under investigation, in which only very limited core uncovering is expected, and considering that the aim is to assess the propagation of input uncertainties, it is more representative to analyze scalar quantities that are directly related to the relevant physical phenomena, rather than restricting the analysis to PCT alone, as

was commonly done in previous exercises and is still the focus of many standard BEPU methodologies.

Table 4.1: List of FoMs, based on [23]

FoM	**Unit**	**Test1**
Related to Choked Flow		
Integrated mass through the break at 20 seconds	kg	720
Integrated mass through the break from 20 to 90 seconds	kg	1990
Integrated mass through the break from 90 to 180 seconds	kg	1420
Maximum break flow	kg/s	59.9
Fluid density downstream of the break	kg/m^3	60
Hot leg liquid level B (avg. 50–100 s)	m	0.08
Related to Core Uncover		
Maximum cladding temperature (PCT)	K	607
Time at which PCT occurs	s	182.0
Time at which cladding is exposed (CHF onset)	s	164.0
Minimum Δp in the core	Pa	1300
Time at which minimum Δp occurs	s	173.5
Minimum liquid level in core	m	0.06
Duration of core uncovering	s	15
Time at which the core is completely quenched	s	185.0
Other Relevant FOMs		
Time at which Accumulators start injecting	s	154.0
Time at which Acc-A stops injecting	s	284.5
Time at which Acc-B stops injecting	s	284.5
Time at which UP is depleted	s	170.5
Time at which UP recovers	s	187.0
Time when primary pressure falls below SG pressure	s	41.0
Time at which LPSI starts	s	504.0
Time at which LS-A clears	s	180.0
Time at which LS-B clears	s	180.0

It is now analyzed the relevance of each FoM for this case study, in order to properly understand how they influence the accidental transient.
All computations related to these scalar quantities were carried out using Python and are based on the variables extracted from the RELAP5 simulation (Section 4.3).

1. **Integrated mass through the break at different time steps** quantifies the total amount of coolant lost through the break. It is crucial for characterizing the severity of the transient and evaluating the system response, including the activation timing of safety systems and the extent of primary circuit depressurization.
   As the name suggests, it was computed by integrating the break mass flow over the selected time intervals.

2. **Maximum break flow** identifies the peak mass loss rate, which directly influences the primary pressure drop and the progression of core cooling degradation. It is a key parameter to assess the most critical phase of the transient.

3. **Fluid density downstream of the break** provides information about the phase composition (liquid/vapor) in the break region, affecting the efficiency of mass and energy discharge, and the potential for re-injection.
   This parameter was computed in the interval between 20 and 100 seconds, as it is particularly relevant during the initial stages of the transient.

4. **Hot leg liquid level B** is used to evaluate the inventory in the hot leg and the coolant availability to supply steam generators and primary pumps.
   An integral average over the interval 50–100 seconds was performed to mitigate the effect of non-uniform time steps.

5. **Peak Cladding Temperature (PCT)** is the traditional metric for assessing fuel safety. As noted in [3], compliance with the Safety Acceptance Criteria for DBA requires ensuring that cladding temperature does not exceed 1477 K, thereby preventing cladding melting and embrittlement.
   The evaluation was based on detecting the first sharp rise in cladding temperature following the initiation of the transient.

6. **Time at which PCT occurs** helps correlate the peak thermal stress on the fuel cladding with the sequence of accident events and safety system activations, providing insight into the timeliness of countermeasures.

7. **Time at which the CHF appears** marks the onset of CHF, when cladding temperature exceeds saturation temperature, initiating film boiling and heat transfer deterioration. It serves as an early indicator of possible fuel damage and defines the critical window for mitigation.
   It is important to note that CHF typically occurs immediately before the PCT.

8. **Minimum Δp in the core** indicates the point of highest flow resistance, which may be caused by boiling crisis, flow redistribution, or partial blockages. It is relevant for analyzing coolant distribution and core cooling conditions.

9. **Time of minimum Δp in the core** provides insight into the timing of flow reduction and is useful for correlating thermal-hydraulic evolution with key events such as CHF, PCT, and system actuation.

10. **Minimum core level** represents the lowest coolant level in the core during the transient. It is essential for assessing the severity and duration of core uncovery, and for correlating it with cooling failure.

11. **Duration of core uncovery** quantifies the time interval during which the core remains uncovered, which is directly associated with the risk of fuel damage. It is a critical parameter to evaluate the effectiveness of safety injection systems.
    It is defined as the time between the occurrence of CHF and the complete quenching of the core.

12. **Time at which the core is completely quenched** marks the restoration of stable cooling conditions and is a key metric for assessing the success of mitigation systems.
    This scalar was obtained by evaluating the temperature difference between the cladding and saturation temperature, starting from the end of the transient and proceeding backward in time.

13. **Accumulator injection timing** describes the time interval between the start and end of accumulator injection. Any variability or delay critically influences the system's ability to refill the core and limit uncovery duration.
    For this calculation, a minimum liquid level of 0.2 m was assumed to account for the nitrogen gas volume in the accumulator when the liquid is fully depleted.

14. **Upper plenum depletion and recovery times** mark the points at which the upper plenum inventory is exhausted and subsequently refilled. These events are indicative of core uncovery progression and rewetting dynamics, and are closely linked to pressure variations and flow redistribution within the reactor vessel.

15. **Time when primary pressure falls below SG pressure** is critical for identifying flow reversal or backflow through the steam generators and determining the triggering of pressure-based safety logics.

16. **Time at which LPSI starts** marks the activation of the low-pressure safety injection system, which is fundamental for recovery after core uncovery. Its relevance depends on the timing relative to the depressurization rate and transient evolution.

17. **Time at which LSs clearing occurs** indicates when vapor seals in the loops are cleared, which can cause sudden level changes and affect backflow to the core. This event has a strong impact on thermal-hydraulic behavior.
    To compute this scalar, a threshold pressure was used to identify the clearing phenomenon, as it was more readily extractable from the RELAP5 output.

4.3 Workflow Overview

The methodology adopted to perform the BEPU analysis and generate the results for Exercise 3 of the ATRIUM project is presented in this section. The focus is on the practical implementation of the process, including the directory structure and input generation, in order to facilitate reproducibility and understanding of the workflow by future researchers.

Since the objective of the study is the quantification and propagation of uncertainties associated with specific parameters at each step of the simulation chain, the first task consists in the generation of the RELAP5 *input tag file*. This file includes all the parameter tags associated with uncertain variables and serves as the foundation for the subsequent uncertainty analysis.

This tagged input is constructed by merging two distinct RELAP5 input files (Section 3.4):

- a **general input file**, `main_MG_1_tag.i`, common to all test cases, which defines the core geometry and system configuration of the experimental facility;
- a **test-specific input file**, `BIC_test_1_tag.i`, which contains the initial and boundary conditions relevant to Test 1, appended to the general input.

Once the *input tag file* is prepared, the actual BEPU analysis can begin. A dedicated Python script was developed to automate the following operations for generating the uncertainty analysis (UA) inputs:

- **Base case input generation**: the *tag file* is processed to replace all uncertain tags with their nominal values, resulting in the deterministic base case input.
- **Sampling of uncertain parameters**: Based on Wilks' formula[1], and using the Monte Carlo method, the script samples uncertain parameters according to the specified probability distributions (Probability Density Function (pdf)s). Differently, the uncertainties on critical flow and post-CHF are taken from the previous two exercises. The implementation supports:
  - **Normal distributions**: random values are sampled from a Gaussian distribution with a given mean and standard deviation (σ), applying a two-sided truncation at 95%, corresponding to the range $\pm 2\sigma$.
  - **Lognormal distributions**: 10,000 samples are generated using the given mean and σ, and values are truncated at the 5^{th} and 95^{th} percentiles to limit the impact of extreme tails.
  - **Uniform distributions**: samples are drawn from a flat distribution between specified lower and upper bounds; no truncation is necessary.
  - **Trapezoidal distributions**: the script uses four characteristic points to define the lower, upper, and sloped regions, and computes the probability accordingly based on linear interpolation within the sloped sides.

[1] For further details please refer to Section 2.3 and [28]

- **Generation of uncertainty cases**: 93 input files are automatically created, each corresponding to a different combination of parameter values sampled according to the defined distributions.
- **Directory organization**: a structured file system is created, as illustrated in Figure 4.1, which includes:
  - a `BASE_CASE` folder containing the nominal simulation input,
  - a `CASES` folder with all 93 uncertainty input files,
  - a `DATA` folder storing the sampled uncertainty values used in each case,
  - and an empty `STRIPS` folder, where post-processed simulation outputs will be stored.

Once all the input files are prepared, the simulations are executed. Each of the 93 uncertainty cases is run individually, and a dedicated subdirectory is created for each case within the main `CASES` directory.

To enable the post-processing phase, a predefined list of output variables is specified. These variables are selected to ensure that all the quantities required for the evaluation of the FoMs (Table 4.1) can be accurately computed from the RELAP5 outputs.

Table 4.2 presents the complete list of extracted variables, where *Alphanum* is reffered to the alphanumeric code associated to the type of variable in RELAP5.

All the data extracted from the simulations, contained in the $93 + 1$ `.dat` files, are subsequently stored in the `STRIPS` directory and are ready for post-processing.

The post-processing phase is conducted via a dedicated Python script, which executes the following operations:

- Reads both simulation and experimental datasets, interpolating all variables to a common time array. The time base adopted corresponds to that of the first `.dat` file processed.
- Constructs a matrix of results containing the upper and lower uncertainty bounds for each variable.
- For each variable, a dedicated matrix is created aggregating the results from all cases. This matrix is then sorted at each time step, and the vectors corresponding to the desired confidence bounds are extracted and stored in a new matrix, named `results`. A corresponding header array is also created, appending the suffixes `U` and `D` to indicate the *upper* and *lower* bounds respectively. These processed results are then written into a single ASCII file.
- For each simulation case, all relevant output parameters are evaluated and the scalar quantities needed for the FoMs computation (as described in Section 4.2) are calculated using an external Python function.
- Percentile curves are computed for each scalar value associated with the experimental case and the base case. A percentile plot graphically represents the value of a quantity below which a given percentage of the dataset falls, providing insight into the statistical distribution of results.

- All relevant plots are generated and stored in a dedicated output folder, including:
  1. **Percentile plots**: graphical representation of scalar distributions across all simulations.
  2. **Variable plots**: time series plots of all extracted variables, highlighting the base case in red, the experimental value in blue, and the remaining uncertainty cases in green.
  3. **Uncertainty band plots**: similar to the variable plots, but the full set of uncertainty cases is represented as a continuous shaded band between the computed upper and lower bounds.

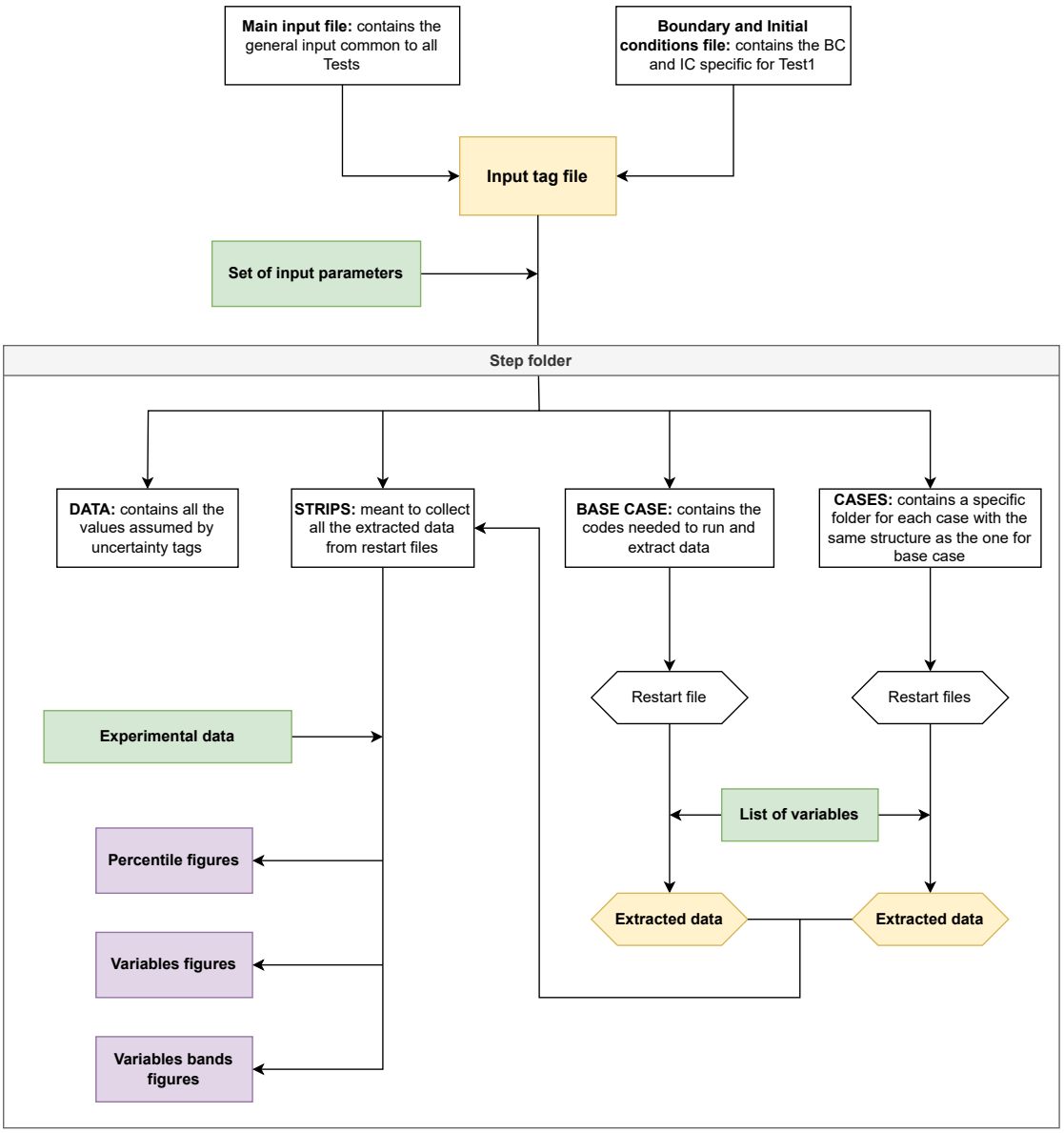

Figure 4.1: Workflow Overview, flowchart elaborated to represent the methodological process followed in each step of Exercise 3.

Table 4.2: List of output variables compiled in order to fulfill FoMs calculation requirements.

Alphanum	**Figure tag**	**Unit**
rho	Break_Density	kg/m^3
mflowj	Break_Mass_Flow	kg/s
p	Upper_Plenum_Pressure	Pa
p	SG_A_Pressure	Pa
p	SG_B_Pressure	Pa
mflowj	LPSI_A_Mass_Flow	kg/s
mflowj	LPSI_B_Mass_Flow	kg/s
cntrlvar	SG_A_Level	m
cntrlvar	SG_B_Level	m
cntrlvar	Pressurizer_Level	m
cntrlvar	Maximum_Cladding_T	K
mflowj	Accumulator_A_Mass_Flow	kg/s
mflowj	Accumulator_B_Mass_Flow	kg/s
acvliq[a]	Accumulator_Level_A	m
acvliq[a]	Accumulator_Level_B	m
tempf	HL_A_Temperature	K
tempf	HL_B_Temperature	K
mflowj	Loop_A_Mass_Flow	kg/s
mflowj	Loop_B_Mass_Flow	kg/s
cntrlvar	Core_Level	m
cntrlvar	Core_Power	W
cntrlvar	Upper_Plenum_Level	m
cntrlvar	Upper_Head_Level	m
cntrlvar	Downcomer_Level	m
cntrlvar	Cold_Leg_A_Level	m
cntrlvar	Cold_Leg_B_Level	m
cntrlvar	Hot_Leg_A_Level	m
cntrlvar	Hot_Leg_B_Level	m
cntrlvar	SGTR_Integrated_Break_Mass	kg
sattemp	Saturation_Temperature	K
cntrlvar	Dif_Pressure_Loop_Seal_A	Pa
cntrlvar	Dif_Pressure_Loop_Seal_B	Pa
cntrlvar	Dif_Pressure_Core	Pa
httemp	Peak_Cladding_T	K

[a] These variables actually represent a liquid volume, a conversion dividing by the section of the accumulators is needed.

4.4 Step 1: input parameters

In Step 1 of Exercise 3 of the ATRIUM project, uncertainty propagation is applied to two key physical models: **critical (choked) flow** and **post-CHF**, both previously calibrated via IUQ in Exercises 1 and 2.

The uncertainty in critical flow is governed by three parameters: the discharge coefficient, the non-equilibrium multiplier, and the surface roughness. Variations in these parameters affect the rate of mass discharged through the break during the initial blowdown phase of the IBLOCA. For instance, a lower discharge coefficient or higher roughness reduces the break flow rate, potentially delaying primary depressurization and prolonging high system pressure. Conversely, a higher discharge rate accelerates depressurization, which can lead to earlier core uncovering and different thermal-hydraulic conditions at the onset of heatup.

For the post-CHF regime, two uncertainty multipliers are propagated: one applied to the wall-to-fluid and wall-to-gas heat flux in heat transfer modes 3 and 8 (subcooled nucleate and superheated film boiling), and another applied to the interfacial heat transfer to gas in the annular-mist flow regime. Increasing these multipliers enhances the modeled heat transfer, resulting in lower predicted cladding temperatures and improved cooling under degraded conditions. Conversely, reducing the multipliers diminishes heat removal capabilities, leading to higher cladding temperatures and potentially more severe core heatup. The propagation of these uncertainties in RELAP5 provides a quantification of their impact on key safety parameters such as cladding temperature and system pressure evolution during the IBLOCA transient.

For illustrative purposes, the distribution of the discharge coefficient, as previously described, is presented below. The plot is intended to highlight the variability of the parameter due to the application of uncertainty.

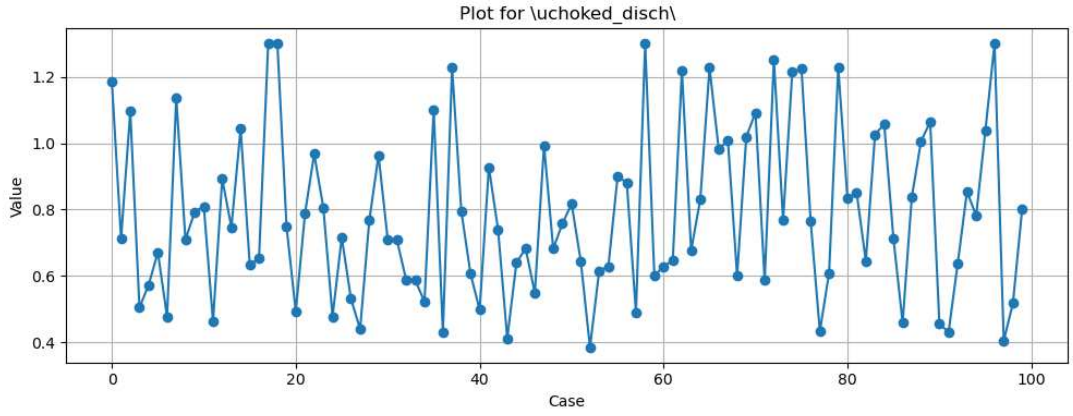

Figure 4.2: Discharge coefficient uncertainty values.

4.5 Step 2: input parameters

The new uncertain parameters included in this analysis have been grouped by physical nature into four categories: initial conditions, boundary conditions, geometrical parameters and material properties. Each category contributes differently to the TH response of the system and affects the main FoMs.
In Table 4.3 the second set of input parameters is presented with the corresponding uncertainty ranges and pdf types, where U and N refer respectively to *uniform* and *normal*. Moreover, for illustrative purposes, and in order to demonstrate the correct implementation of the uncertainty sampling function used to generate the input cases, an example distribution is provided for each category of uncertainty. Each plot shows the sampled values falling within the prescribed uncertainty range, according to the corresponding probability distribution function.

Table 4.3: Uncertainty ranges and probability density functions for the propagated parameters presented in [23] where: the geometric uncertainties associated with the break nozzle are derived from expert judgement, due to the absence of detailed design or experimental data. The remaining uncertainty ranges are taken from [12] or established based on expert evaluation.

Parameter	**Uncertainty range**	**pdf**
Initial and decay core power	±0.1 MW	N
Initial pressurizer pressure	±0.108 MPa	U
Initial pressurizer liquid level	±0.25 m	U
Initial SGs pressure	±0.054 MPa	U
Initial SGs liquid level	±0.38 m	U
Initial SGs feedwater flowrate	±0.1 kg/s	U
Initial SGs feedwater temperature	±2.6 °C	U
Accumulator pressure	±0.054 MPa	U
Accumulator temperature	±2.4 °C	U
Liquid volume in accumulators	±10%	U
LPSI pressure	±0.054 MPa	U
LPSI temperature	±2.6 °C	U
Break throat diameter	±2%	U
Break nozzle localized pressure loss (K-factor)	[0.5, 2.0]	U
U-tubes heat transfer area	±15%	N
Fuel thermal conductivity	±10%	N
Fuel heat capacity	±2%	N

Initial Conditions

- **Initial and decay core power** defines the reactor's thermal power at transient onset and the residual decay heat. It directly affects the energy to be removed from the core, impacting fuel temperature rise and coolant vaporization rate.

- **Initial pressurizer pressure** determines the primary system initial pressure, af-

fecting saturation onset, void generation, and the triggering of safety injection systems.

- **Initial pressurizer liquid level** influences the pressure control margin and the time to saturation in the pressurizer, modifying the timing and dynamics of system depressurization.

- **Initial SGs pressure** affects secondary side saturation conditions and the temperature gradient across the steam generator tubes, altering the efficiency of heat removal from the primary system.

- **Initial SGs liquid level** defines the available secondary-side inventory, influencing steam generator dryout timing and overall core cooling performance.

- **Initial SGs feedwater flowrate** controls the long-term capacity of heat removal. Reduced flow may lead to earlier dryout and increased core temperatures.

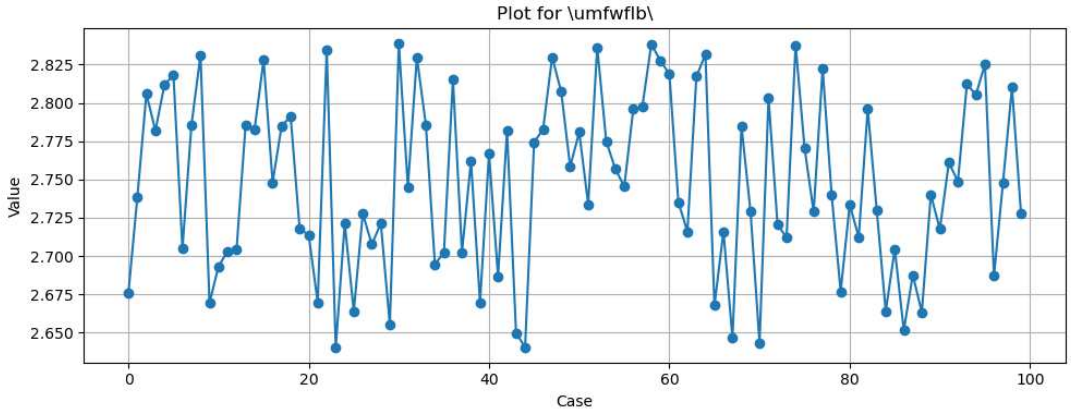

Figure 4.3: Initial SG B flowrate uncertainty values.

- **Initial SGs feedwater temperature** impacts the heat transfer rate in the steam generators. Higher feedwater temperatures reduce the temperature differential, degrading heat extraction.

Boundary Conditions

- **Accumulator pressure** sets the driving force for passive coolant injection. Higher values promote earlier and stronger injection, aiding in core cooling during depressurization.

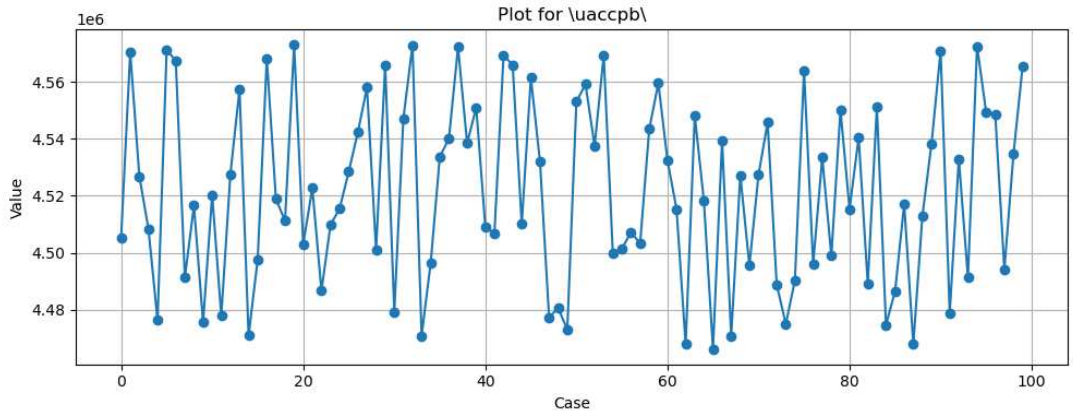

Figure 4.4: Accumulator B pressure uncertainty values.

- **Accumulator temperature** alters the density and pressure relationship in the accumulator fluid, slightly influencing injection dynamics.

- **Liquid volume in accumulators** determines the total injected volume. Smaller volumes may be insufficient for complete core reflood, affecting PCT.

- **LPSI pressure** sets the operating condition of the Low Pressure Safety Injection system. Low pressure may reduce or delay coolant delivery to the reactor core.

- **LPSI temperature** influences the thermodynamic properties of the injected coolant, potentially affecting its effectiveness in heat removal and density-driven mixing.

Geometrical Parameters

- **Break throat diameter** directly impacts the coolant discharge rate. Larger diameters cause faster inventory loss and stronger depressurization, which can accelerate core heat-up.

- **Break nozzle localized pressure loss (K-factor)** represents hydraulic resistance at the break. Higher K-values reduce discharge flow, mitigating pressure drop and coolant loss.

- **U-tubes heat transfer area** defines the efficiency of heat transfer across the steam generators. A smaller area leads to degraded heat removal from the primary side, increasing core temperatures.

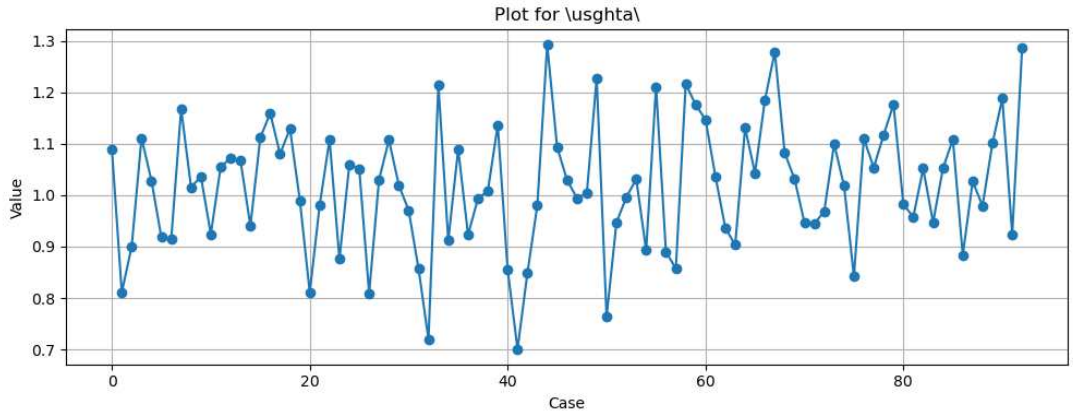

Figure 4.5: U-tubes heat transfer area uncertainty values.

Material Properties

- **Fuel thermal conductivity** affects the radial heat transfer within fuel pellets. Lower conductivity leads to higher centerline temperatures and a larger temperature drop across the fuel.

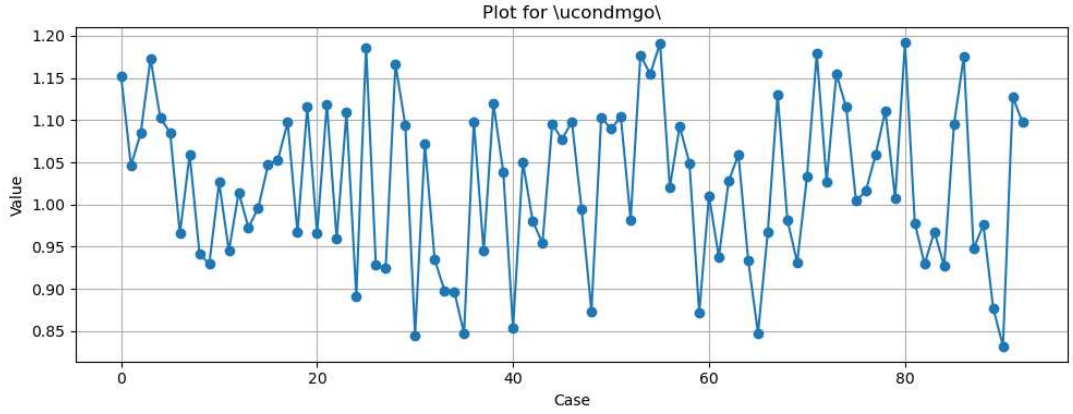

Figure 4.6: Thermal conductivity of MgO uncertainty values.

- **Fuel heat capacity** governs the amount of energy that can be stored in the fuel. A lower heat capacity results in faster temperature excursions for a given power level.

4.6 Step 3: input parameters

In order to enhance the outcomes obtained in Step 1 and Step 2, an additional set of uncertainties is now introduced into the analysis. The primary objective is to better capture the CCFL phenomena by propagating uncertainties in various locations of the plant[2], but other relevant quantities are considered as well.

As previously mentioned, this step is optional and aims to provide an overall improvement of the participants' results, thereby supporting a more robust validation of the applied BEPU methodology. The complete list of additional input uncertainties considered is provided in Table 4.4 and justified in the following lines.

- **Pressurizer surge line Kloss** affects the ability to relieve or accept coolant from the pressurizer. A higher loss may delay pressure equalization, impacting pressure control and potentially worsening transient responses.

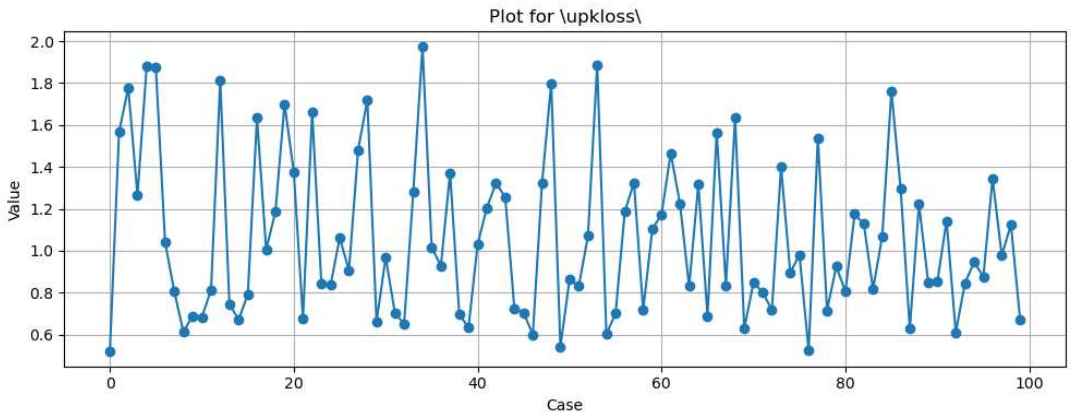

Figure 4.7: Pressurizer surge line Kloss uncertainty values.

- **Kloss DC-UH**, (uncertainties in the loss coefficient between Downcomer and Upper Head) influence flow distribution in the vessel upper plenum, affecting cooling and vapor transport during transients.

- **Kloss DC-UP** affects the flow resistance between the downcomer and upper plenum. Variations can influence core outlet flow rates, impacting temperature distribution and steam separation.

- **Kloss core grids**represents friction losses through core spacer grids. Variability impacts the core pressure drop and can modify the coolant mass flow rate through the fuel assemblies, thus affecting heat removal efficiency.

[2]Please refer to Section 5.1 for further details.

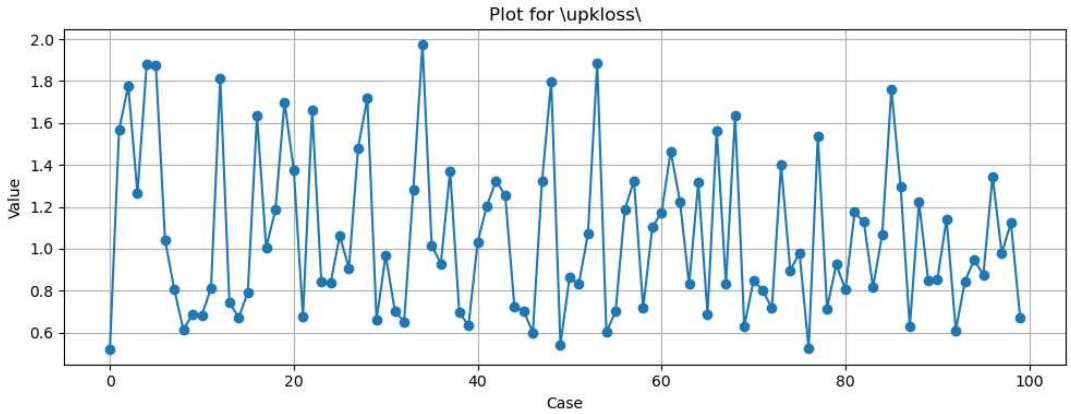

Figure 4.8: Kloss of core grids uncertainty values.

- **Primary loop mass flow** directly affects the heat transport capability of the primary system. Deviations from nominal flow can significantly alter core outlet temperatures and system pressure response during accidents.

- **Heat losses to environment** accounts for the uncertainty in the thermal losses from the system to the surroundings. Variations can affect the global energy balance, potentially leading to under- or overestimation of core cooling efficiency and secondary side heat transfer during transients.

- **CCFL UP c** (critical CCFL condition in the Upper Plenum) influences the maximum achievable liquid penetration during counter-current flow; affects reflooding and cooling efficiency during two-phase conditions.

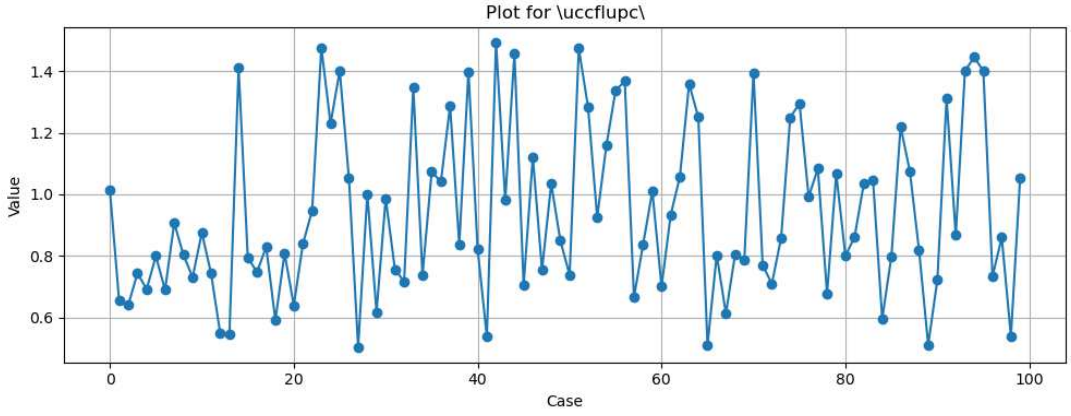

Figure 4.9: Critical CCFL condition in Upper Plenum uncertainty values.

- **CCFL UP m** (mass flow rate at which CCFL occurs) variations may shift the onset of flow limitation, impacting the coolant delivery to the core.

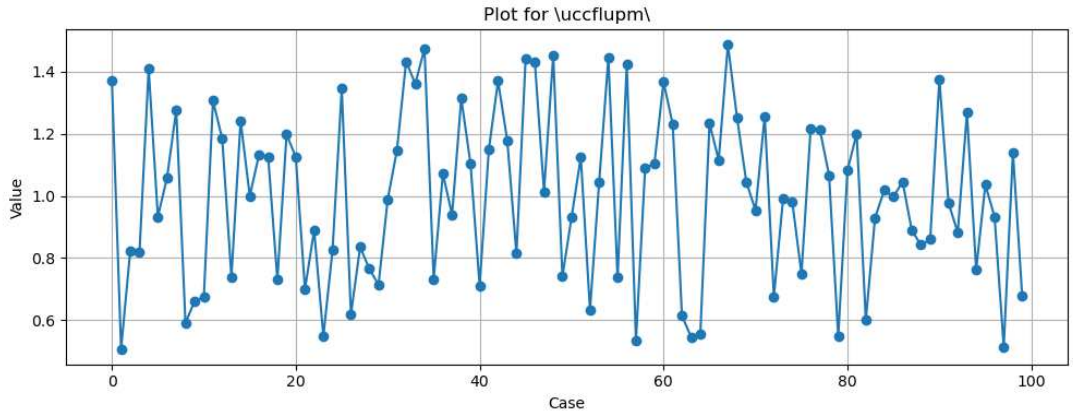

Figure 4.10: Mass flow at which CCFL occurs in Upper Plenum uncertainty values.

- **CCFL SG-inlet c** (critical CCFL condition at the steam generator inlet) influences the capacity of liquid to enter the SG during reflood or blowdown phases, impacting secondary-side heat transfer.

- **CCFL SG-inlet m** (uncertainty in the limiting flow rate) affects when and how much coolant can flow into the SG inlet under counter-current conditions, modifying system pressure response.

- **CCFL Surge line c** affects flow reversal behavior in the surge line during transients. Critical condition uncertainty could impact pressurizer level and pressure stability.

- **CCFL Surge line m** determines the flow rate limit due to CCFL in the surge line. Influences the dynamics of coolant exchange with the pressurizer.

- **CCFL U-tubes c** impacts the ability of liquid to flow into or out of the U-tubes during two-phase flow conditions. Relevant during blowdown and reflooding phases.

- **CCFL U-tubes m** affects heat removal efficiency through the steam generator under two-phase counter-current conditions.

- **Kloss loop seal** affects coolant circulation and phase separation. High losses may hinder natural circulation, particularly in low-pressure transients.

- **Kloss SG-inlet leg** determines pressure losses entering the SG. Influences flow stability and coolant inventory in the steam generator, especially under two-phase flow or depressurization.

Table 4.4: Uncertainty ranges and probability density functions for the propagated parameters chosen for Step 3.

Parameter	Uncertainty range	pdf
Pressurizer		
Pressurizer surge line Kloss	[0.00; 0.42]	LN
Flow repartition		
Kloss DC-UH	[0.00; 0.42]	LN
Kloss DC-UP	[0.00; 0.42]	LN
Kloss core grids	[0.9; 1.1]	U
Initial conditions		
Primary loop mass flow	±1.25 kg/s	N
Heat losses		
Heat losses to environment	[0.9; 1.1]	U
CCFL		
CCFL UP c[b]	[0.5; 1.5]	U
CCFL UP m[c]	[0.5; 1.5]	U
CCFL SG-inlet c	[0.52; 0.95]	U
CCFL SG-inlet m	[0.397; 1.0]	U
CCFL Surge line c	[0.5; 1.5]	U
CCFL Surge line m	[0.5; 1.5]	U
CCFL U-tubes c	[0.5; 1.5]	U
CCFL U-tubes m	[0.5; 1.5]	U
Kloss loop seal	[0.00; 0.42]	LN
Kloss SG-inlet leg	[0.00; 0.42]	LN

[b] *Critical/choking condition* — refers to the point at which the flow is critically limited, for example when the maximum capacity of the counter-current two-phase flow is reached.

[c] *Mass flow rate* — indicates the value of the mass flow rate corresponding to the counter-current flow limitation.

Chapter 5

Results

5.1 TH Phenomenology

Core cooling represents a cornerstone of nuclear safety analysis, as the removal of the heat generated by fission is essential to prevent cladding failure and subsequent fuel degradation. In accident scenarios such as the IBLOCA investigated in Exercise 3 of the ATRIUM project, the reduction in coolant inventory significantly compromises the system's ability to remove heat.

The analyzed transient involves a break in the hot leg, which progressively depletes the primary circuit and drives the core through a wide range of thermal-hydraulic regimes. These regimes are characterized by distinct heat transfer mechanisms and complex flow behavior in the reactor channels.

As illustrated in Figure 5.1, heat removal is initially governed by forced convection of subcooled liquid, resulting in high heat transfer coefficients and stable cladding temperatures. As the coolant and fuel temperatures rise and system pressure decreases, subcooled nucleate boiling develops at the cladding surface. This regime enhances heat removal through latent heat of vaporization and remains favorable for core cooling. Its accurate modeling is crucial and was the focus of the first ATRIUM exercise.

However, as flow continues to decline, vapor generation eventually surpasses the liquid's capacity to re-wet the cladding surface, leading to the onset of critical heat flux (CHF). CHF marks the boundary between efficient nucleate boiling and the transition to deteriorated heat transfer conditions.

Beyond CHF, the system enters the post-CHF regime, where intermittent dryout zones develop and the cladding surface becomes increasingly enveloped by a vapor film. In this regime—targeted in the second ATRIUM exercise—the heat transfer coefficient drops significantly, as heat is transferred primarily through conduction and radiation across the vapor layer, both far less effective than nucleate boiling. The transition to film boiling introduces additional phenomena, including the formation of an insulating vapor blanket (Leidenfrost effect), droplet entrainment in the vapor core, surface rewetting attempts, and interfacial instabilities. These effects contribute to large spatial and temporal variations in wall temperature, posing significant challenges for both measurement and predictive simulation.

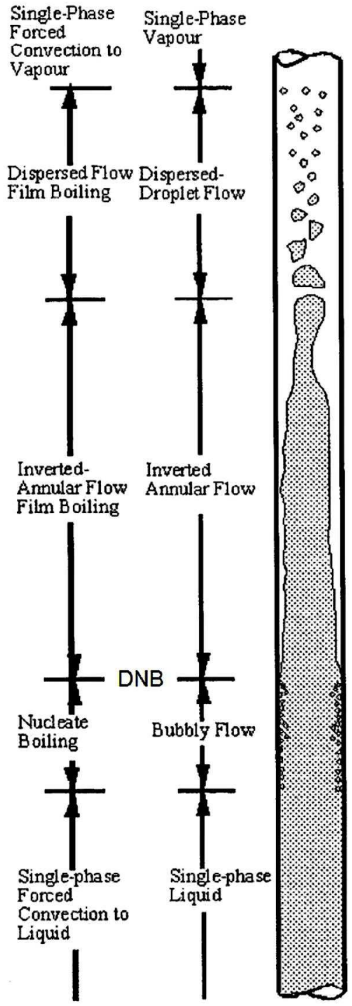

Figure 5.1: Heat transfer and flow regimes for low quality flow. Wall and fluid temperature variations are also shown. Figure adopted from [19].

Among the phenomena that characterize the post-CHF regime, Counter-Current Flow Limitation (CCFL) plays a critical role in determining the core cooling efficiency, especially in hot leg break scenarios. When the break occurs in the hot leg, the path from the core to the break is relatively short and unobstructed, favoring the early onset of CCFL as soon as core uncover begins. In such cases, flow reversal and vapor escape toward the break hinder the downward penetration of liquid from the upper plenum into the core, particularly near the upper core plate and the hot leg connection.

This mechanism becomes especially relevant in the time window between the initiation of core boiling and the actuation of the accumulators. As observed in Test 1 of the ATRIUM benchmark [13], CCFL phenomena develop briefly when the primary pressure drops below the secondary side pressure and the break transitions to single-phase vapor flow. At this stage, the core begins to boil off, but the system rapidly reaches the accumulator setpoint, leading to injection and loop seal clearance. Although this sequence limits the duration of core uncovery, the temporary inhibition of liquid fallback due to CCFL significantly contributes to the localized peak cladding temperature. Even within this narrow timeframe, the presence of CCFL at the top of the core proves to be a dominant

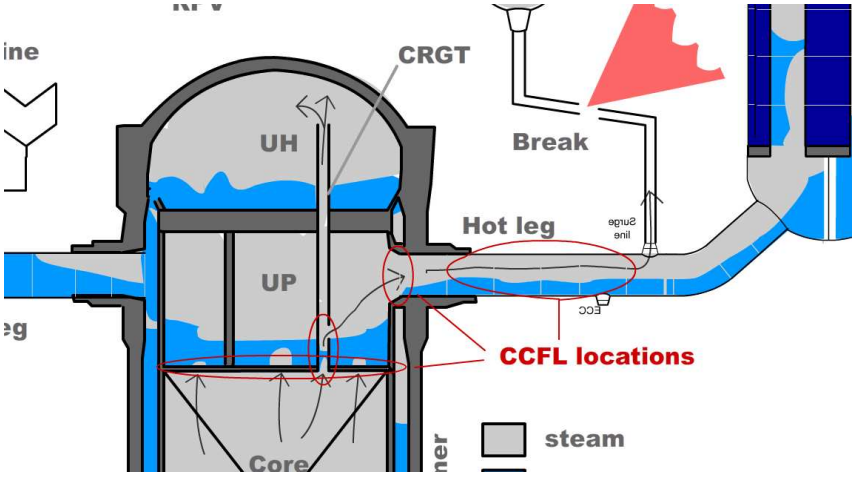

Figure 5.2: Schematic Description of the Possible CCFL Locations during an IBLOCA at the Hot Leg. Figure taken from [13].

factor in the thermal response. Figure 5.2 shows the schematic description of the possible CCFL phenomenon locations during a Hot Leg Break.

A practical quantitative view of these thermal-hydraulic phenomena is now presented through time-dependent plots concerning both the nominal simulated scenario and experimental data, capturing the evolution of the IBLOCA scenario through distinct flow regimes. The onset of core boiling, the transition through CHF, and the development of post-CHF conditions, including film boiling and CCFL, can all be inferred from specific system responses.
It is worth emphasizing that the nominal simulation corresponds to a **best-estimate** representation of the underlying physical phenomena.

Core uncovering and reflooding dynamics are primarily represented in Figure 5.3 by **core level**, **downcomer level**, **liquid level in cold legs**, and **upper plenum level**, which indicate the availability of coolant in the lower plenum, core region, and cold legs. The depletion of these levels marks the onset of dryout and the conditions favoring CHF. Simultaneously, **PCT** (Figure 5.5) captures the thermal response of the fuel cladding. A rapid rise in cladding temperature beyond the saturation temperature is indicative of the transition to film boiling, where heat transfer is significantly degraded due to vapor film formation.

The progression of core boiling also affects the **upper plenum pressure** (Figure 5.13), as vapor generated in the core accumulates above the fuel. An increase in this pressure serves as an indicator of flow reversal and CCFL, where upward vapor flow limits or prevents the downward motion of liquid from the upper plenum. **Mass flow in LSs** (Figure 5.4b) provides further evidence of flow disturbances associated with loop seal dynamics, such as loop seal clearing, which occurs when vapor displaces liquid trapped in the U-shaped region of the cold leg.

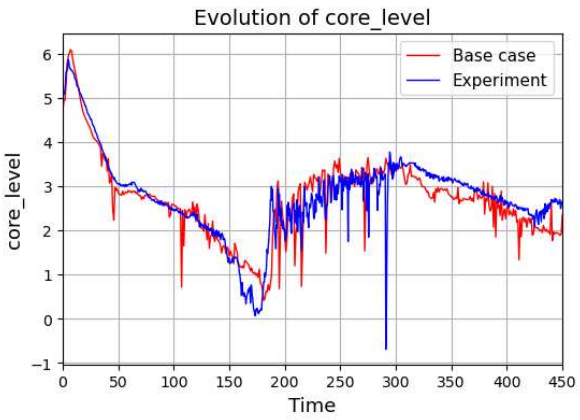

(a) Core level

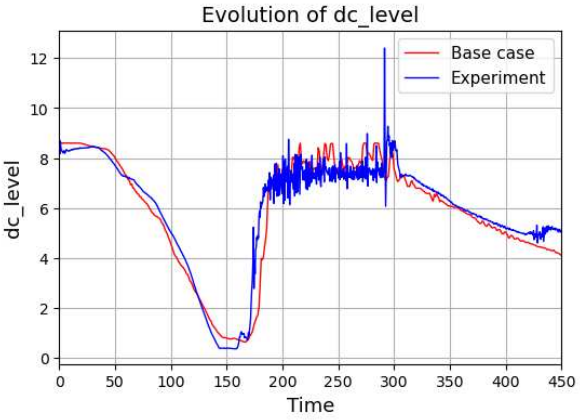

(b) Downcomer level

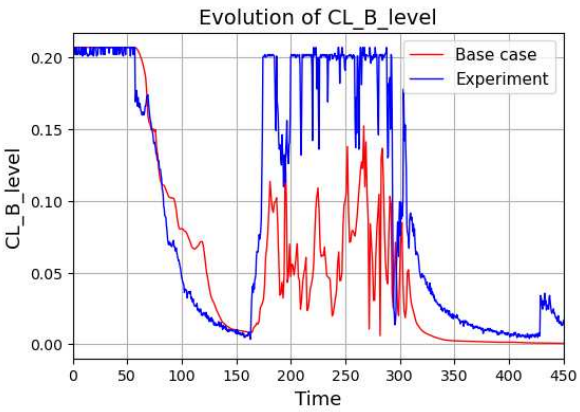

(c) Liquid level in Cold Leg

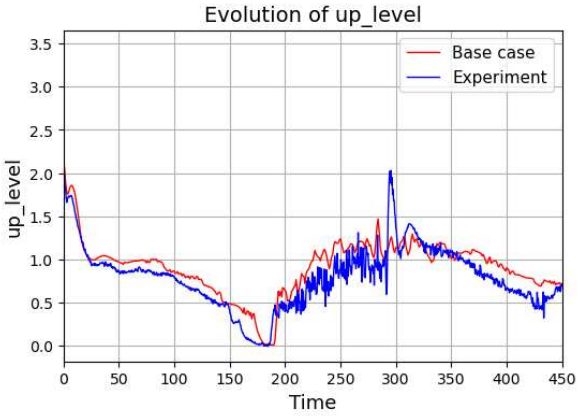

(d) Liquid level in Upper Plenum

Figure 5.3: Test 1 TH phenomenology.

The injection of emergency coolant is traced through **accumulators mass flow** (Figure 5.4d) and **accumulators level** (Figure 5.4c). These plots reveal the timing, magnitude, and duration of coolant recovery mechanisms. The effectiveness of these systems is directly linked to the observed mitigation of cladding temperatures and recovery of coolant levels. Additional insights into system depressurization and break behavior are obtained from **mass flow at the break** (Figure 5.4e), **density at the break**, and **integrated mass flow at the break** (Figure 5.4f), which characterize the discharge conditions and flow regime at the break location.

The behavior of the secondary side is captured by **SGs level** (Figure 5.4g) and **SGs pressure** (Figure 5.4h), reflecting steam generator inventory and pressure stability throughout the transient. Finally, the evolution of **PZR level** (Figure 5.4i) reflects global mass balance and system pressurization trends, while **hot legs level** (Figure 5.4j) offer additional information on primary loop circulation and stratification.

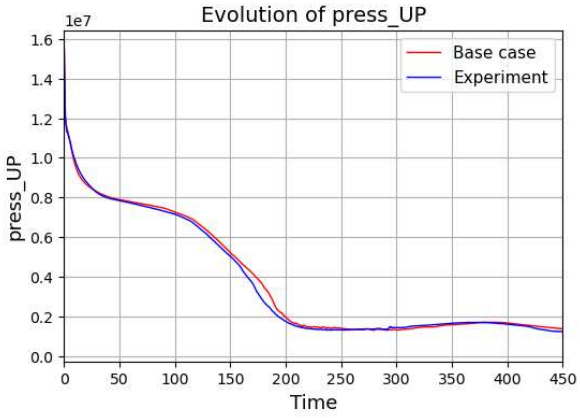

(a) Upper Plenum pressure

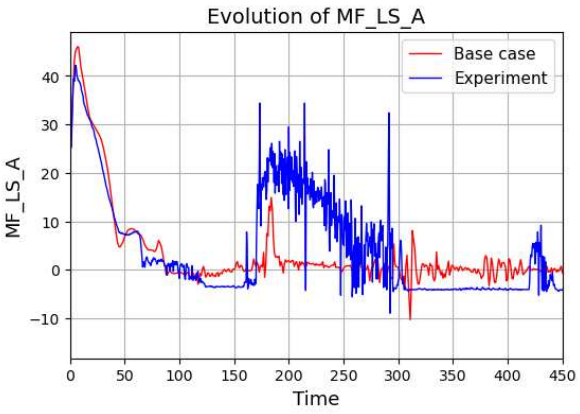

(b) Mass flow in Loop Seals

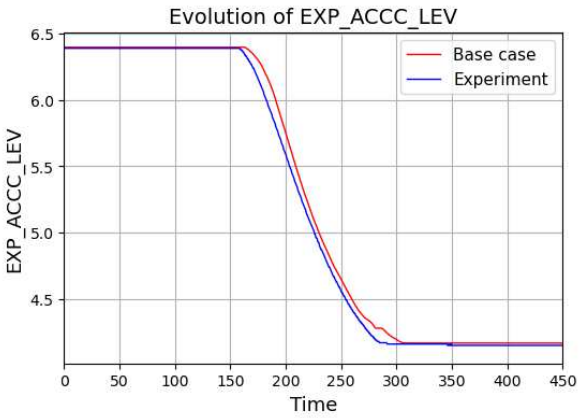

(c) Accumulator level

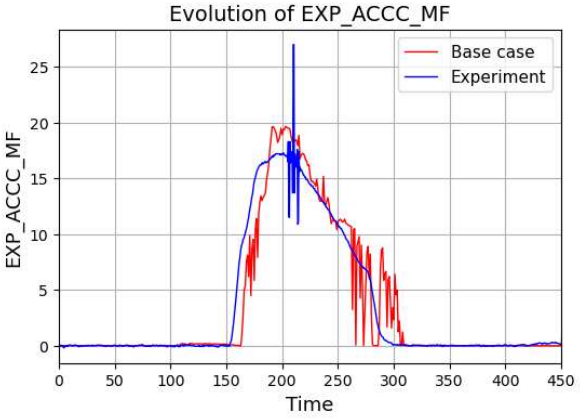

(d) Accumulator Mass Flow

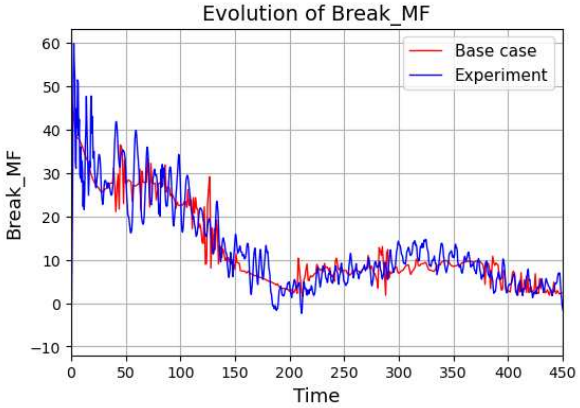

(e) Break Mass Flow

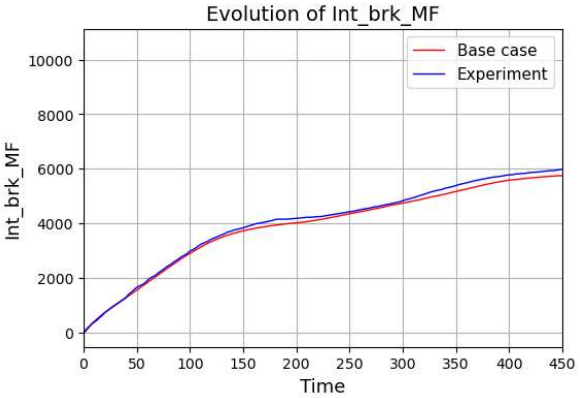

(f) Integrated Mass Flow

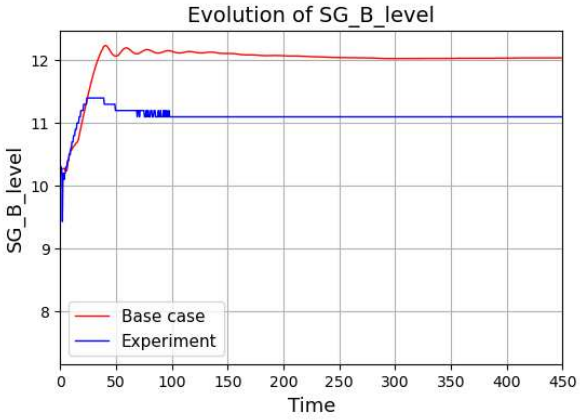

(g) Liquid level in SG

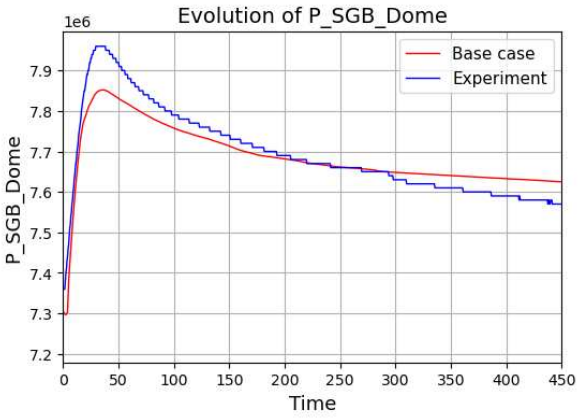

(h) SG Pressure

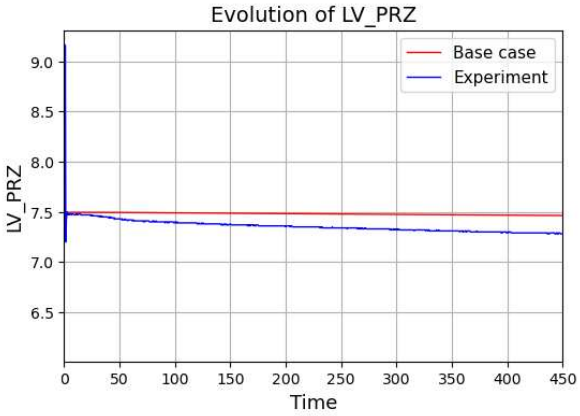

(i) PZR Level

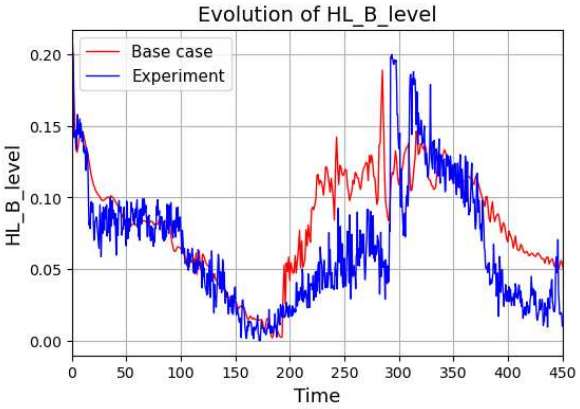

(j) Liquid Level in Hot Leg B

Figure 5.4: Test 1 TH phenomenology.

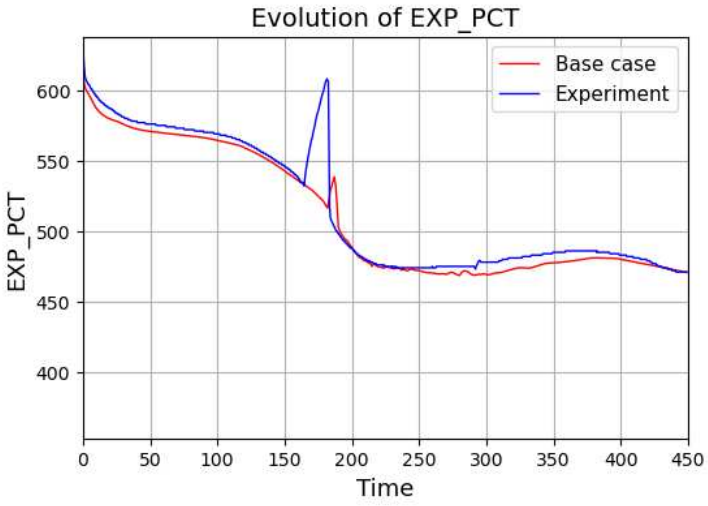

Figure 5.5: Peak Cladding Temperature

Taken together, this comprehensive set of parameters provides a coherent picture of the transient progression, and allows for the identification of critical safety-relevant events.

As clearly shown by the presented plots, the simulation successfully reproduces the key features of the experimental scenario, except for some variables that exhibit slight deviations. Unfortunately, the parameter that deviates the most from the experiment is the PCT, a key parameter in the context of nuclear safety analysis, which will be discussed in more detail in the following sections.

5.2 Step 1 - BEPU Analysis Results

This section presents the results of the BEPU analysis conducted in the context of Step 1, during which only the uncertainties associated with critical (choked) flow and post-CHF heat transfer were considered. The structure of the results includes an initial part where the time evolution of the key parameters listed in Table 4.2 is shown, followed by a discussion of the percentile plots related to the scalar quantities required by Exercise 3 of the ATRIUM project.

In practice, the large uncertainties introduced by the choked flow model—originating from Exercise 2—strongly dominate the overall variability, resulting in Step 1 and Step 2 outcomes being largely similar, with only a few exceptions.

The primary objective of this section is therefore to highlight the differences between Step 1 and Step 2, while a more detailed interpretation of time trends and percentile plots will be provided in the next section. This choice is motivated by the fact that the main focus and contributions of the present thesis are centered on the analysis performed in Step 2.

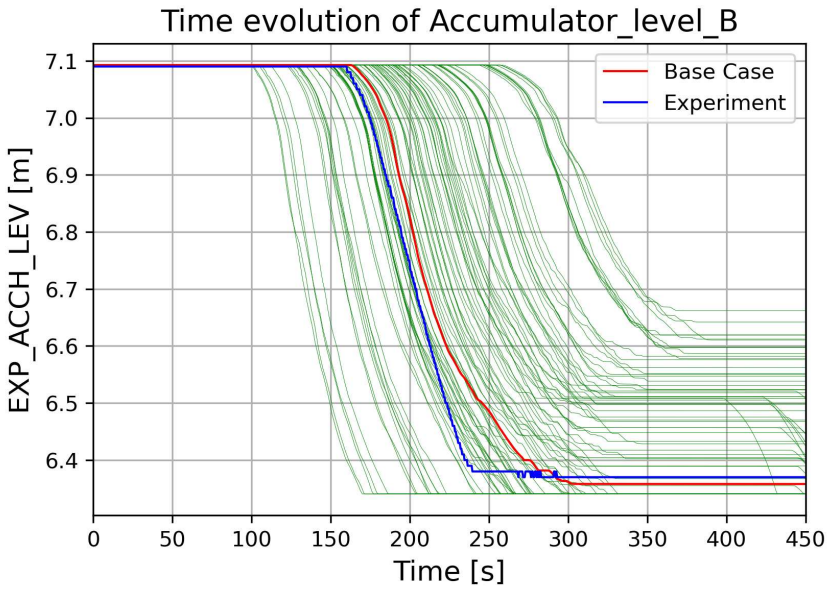

Figure 5.6: Liquid level in Accumulator B Step 1: comparison between the steps.

5.2.1 Transient Analysis Results

The main differences between Step 1 and Step 2 are highlighted in the following Figures.

Regarding the liquid level in the accumulators (Figures 5.6, 5.7), Step 2 exhibits a wider dispersion of results compared to Step 1, including cases that deviate significantly from the base case trend. Some simulations do not reach complete tank depletion, while others show irregular emptying behavior. This is primarily due to the introduction of uncertainties on the initial conditions of the accumulators in Step 2, which were not considered in Step 1.

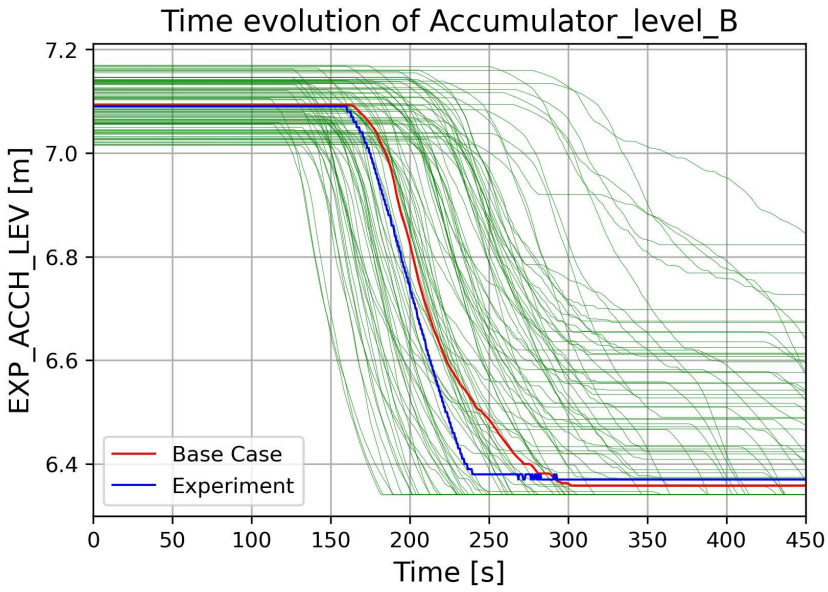

Figure 5.7: Liquid level in Accumulator B Step 2: comparison between the Steps.

A particularly noteworthy observation concerns the Peak Cladding Temperature (PCT) in Figure 5.8. In Step 1, the PCT remains consistently below the experimental threshold across all simulations. In contrast, Step 2 includes a case that not only reaches but slightly exceeds the experimental PCT value—although with a delay of nearly 200 seconds. This difference stems from the fact that, in Step 2, uncertainties in initial and boundary conditions were introduced, which were absent in Step 1.

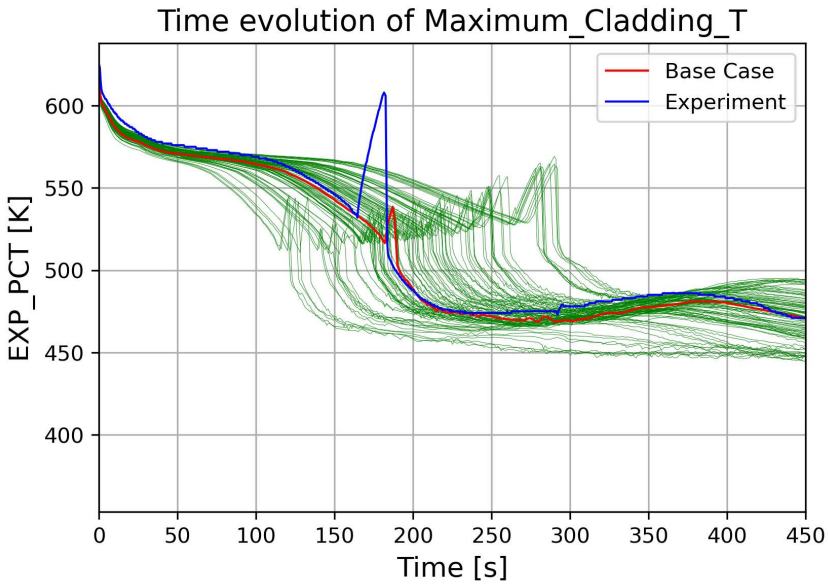

(a) Step 1

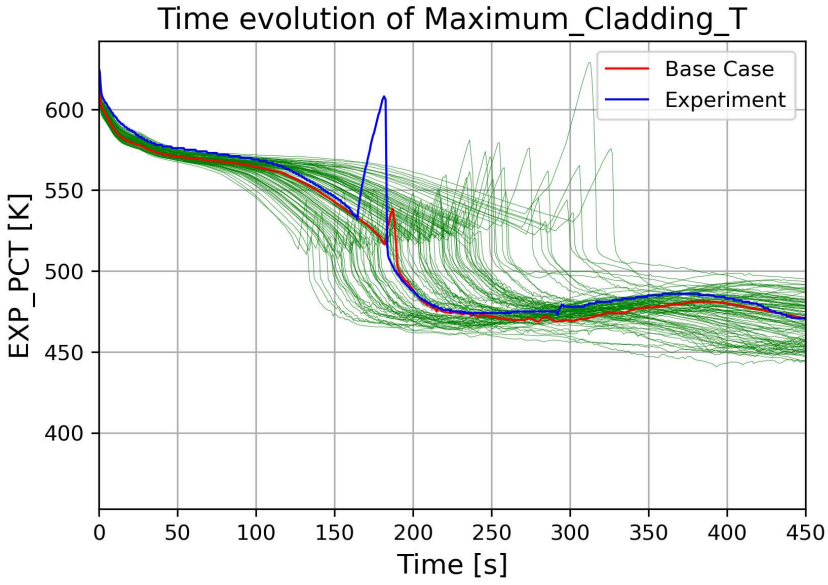

(b) Step 2

Figure 5.8: PCT: comparison between Step 1 and Step 2.

As for the liquid level in the SG in Figure 5.9, Step 1 results are tightly clustered, with minimal variation across the sampled cases, and they closely follow the base case behavior. In Step 2, however, the increased input variability leads to a broader range of responses, reflecting a greater sensitivity of this parameter to initial and boundary condition uncertainties.

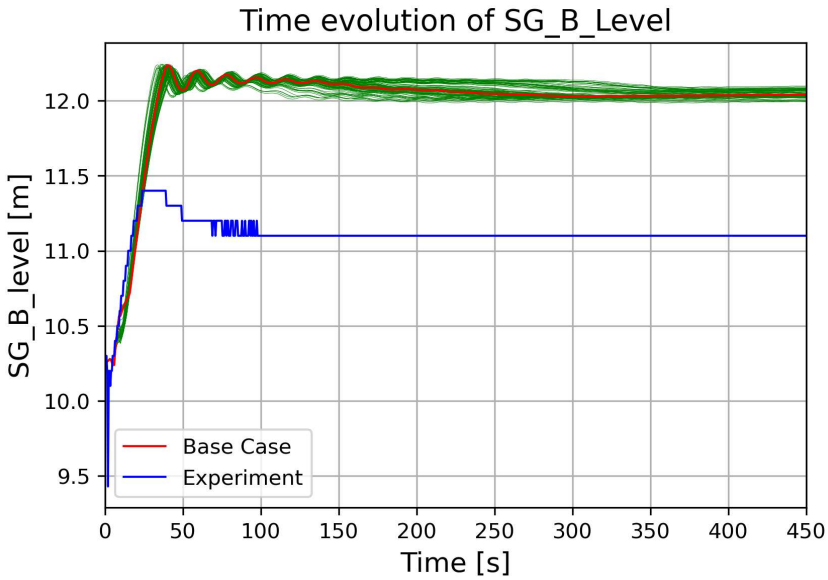

(a) Step 1

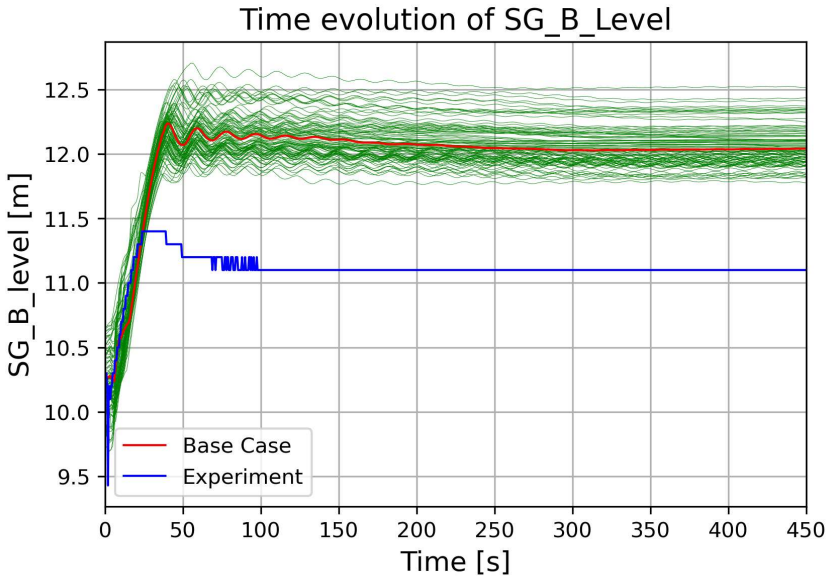

(b) Step 2

Figure 5.9: Liquid level in SG B: comparison between Step 1 and Step 2.

5.2.2 Percentile Plots Analysis

The percentile plots are now addressed to complete the analysis.

Once the ensemble of results is obtained, the output values of interest are sorted at each time step across all simulations. From this sorted data, and after including the base case and the experimental data, statistical percentiles (e.g., 95th) are computed, and percentile curves are constructed as a function of time. These curves represent the statistical bounds of the system's response: for instance, the 95th percentile curve indicates that 95% of the simulations lie below that value at each time step, providing a conservative envelope of the predicted behavior.

The interpretation of these plots is essential in BEPU frameworks, where safety margins must be assessed under uncertainty. The median (50th percentile) curve typically reflects the best-estimate behavior, while the higher percentiles are used to evaluate the likelihood of exceeding safety limits. If all relevant safety thresholds remain unviolated across the high percentile bands (e.g., 95th), one can demonstrate compliance with regulatory criteria in a statistically meaningful way. Thus, percentile plots serve both as a diagnostic and decision-support tool in uncertainty-informed safety analysis.

As in the previous section, only the main differences with respect to Step 2 are addressed here. In fact, the only significant discrepancy lies in the timing of the onset of the CHF condition, as it can be stated from Figure 5.10.

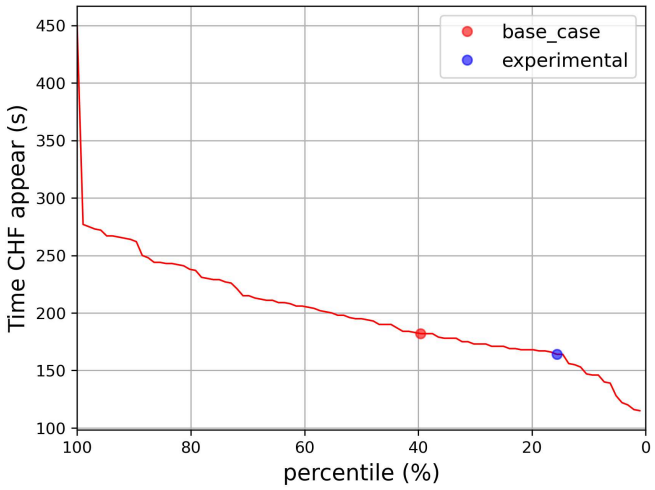

(a) Step 1

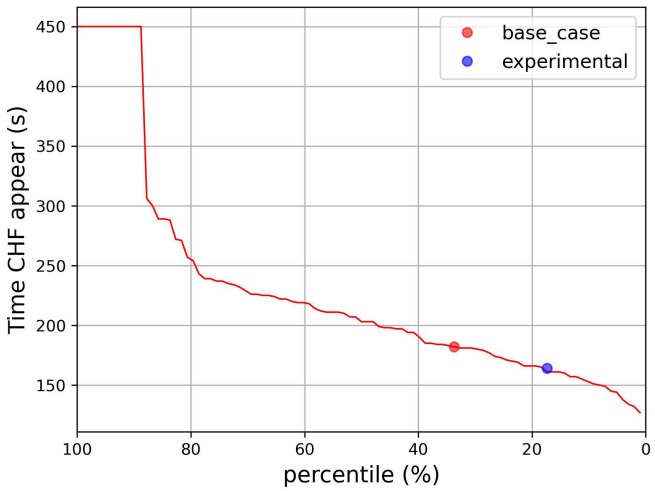

(b) Step 2

Figure 5.10: Time at which CHF appears: comparison between Step 1 and Step 2.

As shown in Figure 5.10, Step 1 includes only one case in which CHF is not reached. This behavior can be attributed to the absence of uncertainties on initial and boundary conditions in Step 1, which leads to a more constrained system response. In contrast, Step 2 introduces broader variability in these conditions, potentially altering the timing

and occurrence of the critical heat flux event.

In summary, the results of Step 1 are overall consistent with the experiment. They are also of comparable quality to those obtained in Step 2, which will be presented in more detail in the following section. The two sets of results exhibit strong similarities, especially in the general trends and the majority of key output variables. The main differences arise in a limited number of cases and parameters—particularly those sensitive to the timing of critical phenomena such as CHF onset or accumulator depletion. The similarities are primarily driven by the dominant impact of the uncertainties associated with choked flow, which were already present in Step 1 and largely govern the system response, even in the absence of additional variability from initial and boundary conditions.

5.3 Step 2 – BEPU Analysis Results

This section presents the results of the BEPU analysis carried out in the context of Step 2, during which additional sources of uncertainty were propagated beyond those previously considered—namely, critical flow and post-CHF heat transfer.

5.3.1 Transient Analysis Results

The correspondence between simulation results and experimental data is illustrated in the time-history plots of the key parameters listed in Table 4.2.

Overall, the simulations successfully capture the temporal evolution of the main system variables, as also confirmed by the percentile plots that will be presented. The propagated uncertainties related to initial and boundary conditions generally result in narrow uncertainty bands, with only a few cases falling outside of these bounds as clear outliers.

The quality of the simulations varies across parameters, as evident in the plots presented in this section. Quantities such as the break mass flow rate (Figure 5.11), total discharged mass, upper plenum pressure and level, loop B mass flow, hot leg temperatures (especially in loop B, where the break occurs), downcomer level, core power, core liquid level (except for rare negative oscillations), and core differential pressure are well captured, with minimal presence of outliers. The agreement with experimental trends is strong and further supported by the corresponding percentile analysis.

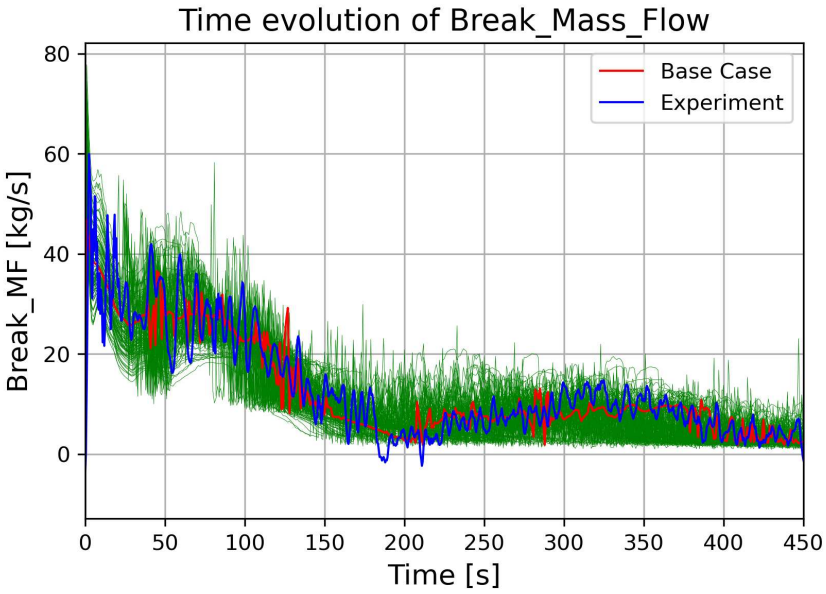

Figure 5.11: Time evolution of Break Mass Flow.

In contrast, parameters related to the accumulator systems (Figure 5.12) show greater variability. While the base case aligns closely with experimental data, several cases deviate both in magnitude and in curve shape. For instance, in some scenarios, the accumulators do not fully discharge, contrary to experimental observations.

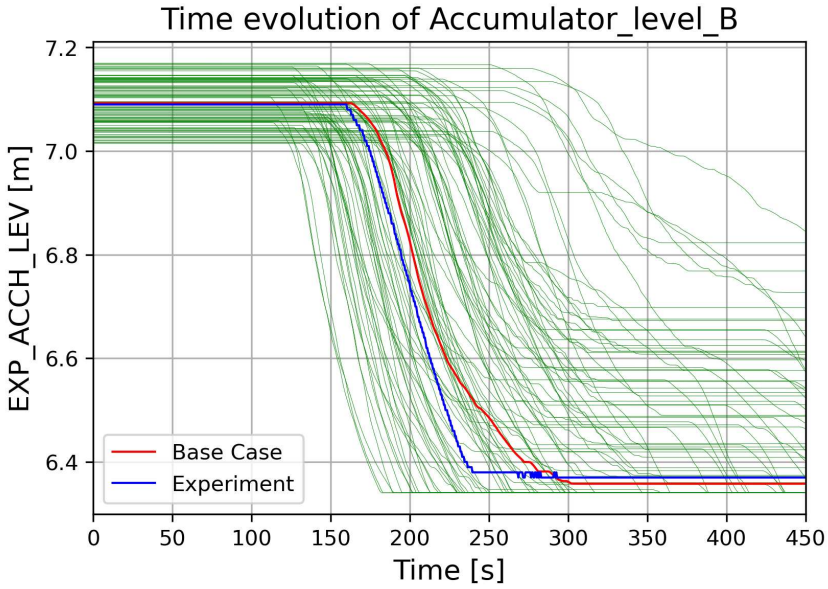

Figure 5.12: Time evolution of liquid level in accumulator B.

This behavior is consistent with trends in upper plenum pressure (Figure 5.13), which acts as a proxy for the primary system pressure: in cases where pressure variations are smoother or less pronounced, the pressure drop is insufficient to trigger the opening of the accumulator check valves. As a result, part of the nitrogen gas volume remains trapped, and the fluid is not injected.

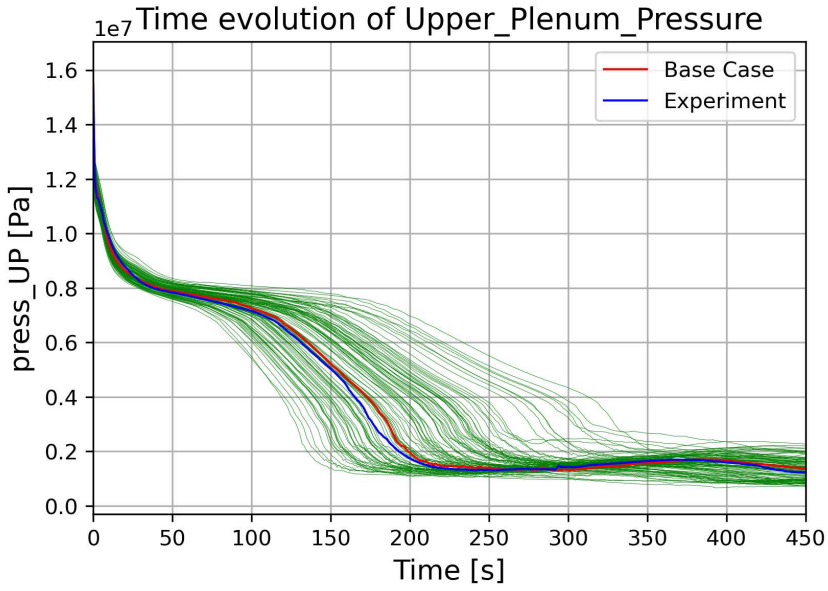

Figure 5.13: Time evolution of the Upper Plenum Pressure.

This dynamic contributes to the wider spread observed in the cold leg levels (Figure 5.14), where the accumulators discharge. The hot leg levels (Figure 5.15), on the other hand, show better agreement with both the base case and the experimental data, with fewer outliers.

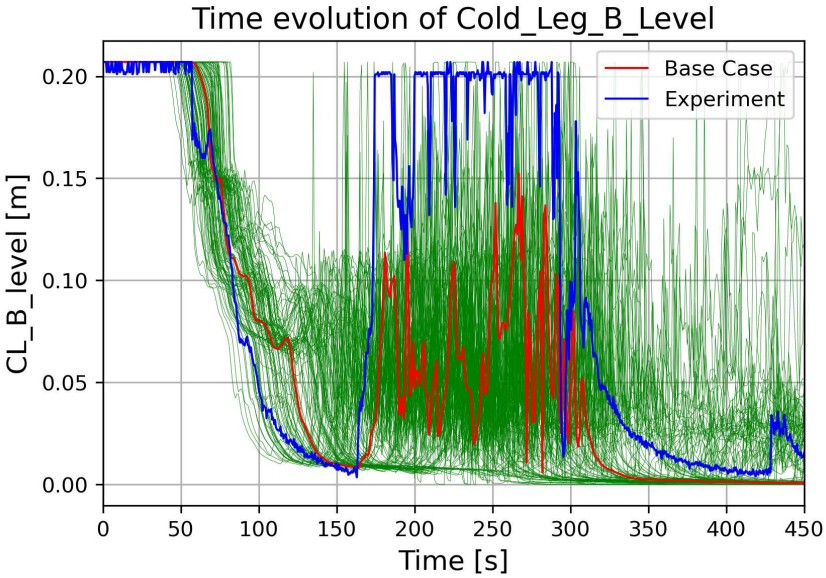

Figure 5.14: Time evolution of Cold Leg B.

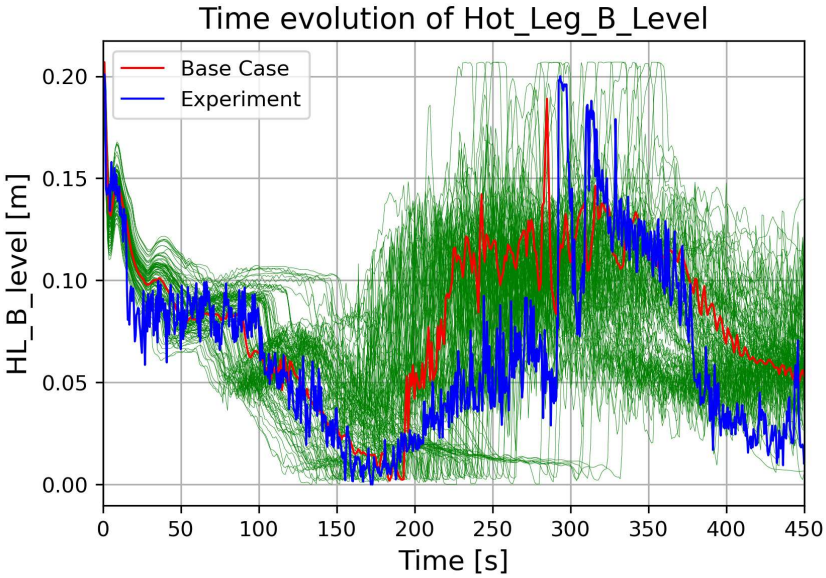

Figure 5.15: Time evolution of Hot Leg B.

The behavior of the steam generator parameters is slightly different (Figures 5.16 and 5.17). Here, all simulation cases follow the same trend as the base case, with differences limited to amplitude variations due to input uncertainties. However, this common trend diverges somewhat from the experimental curves — particularly for pressure and level — suggesting a systematic modeling discrepancy.

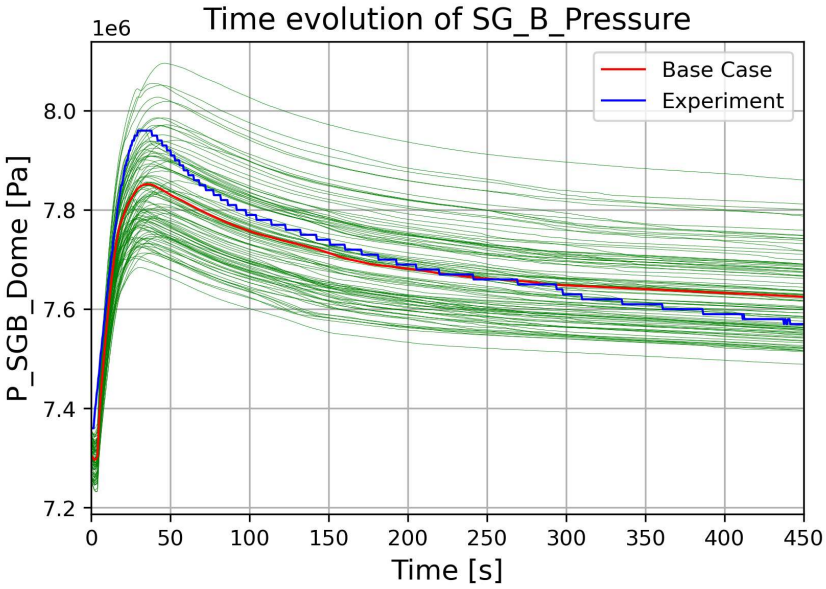

Figure 5.16: Time evolution of SG B Pressure.

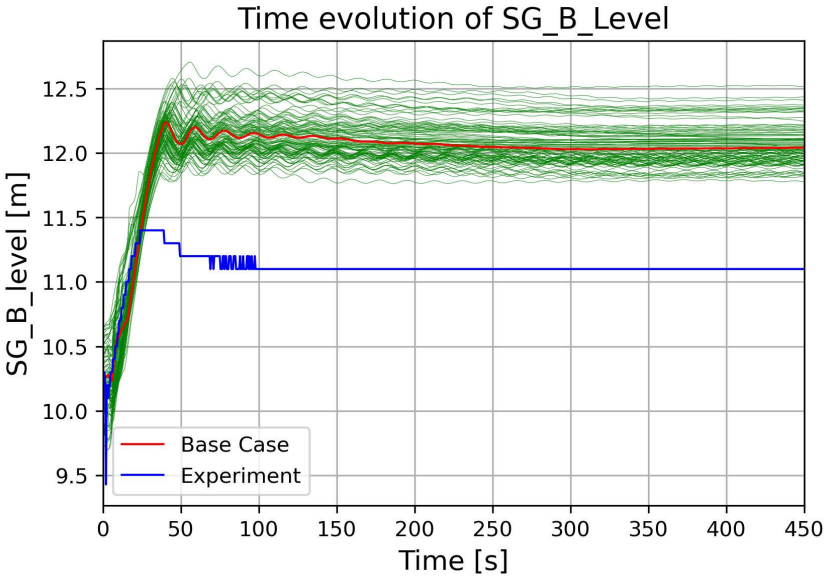

Figure 5.17: Time evolution of SG B Level.

A similar deviation is observed in the fluid density near the break (Figure 5.18). However, this may be due to differences between the measurement location in the experimental facility and the nodalization point used in RELAP5 for density calculation.

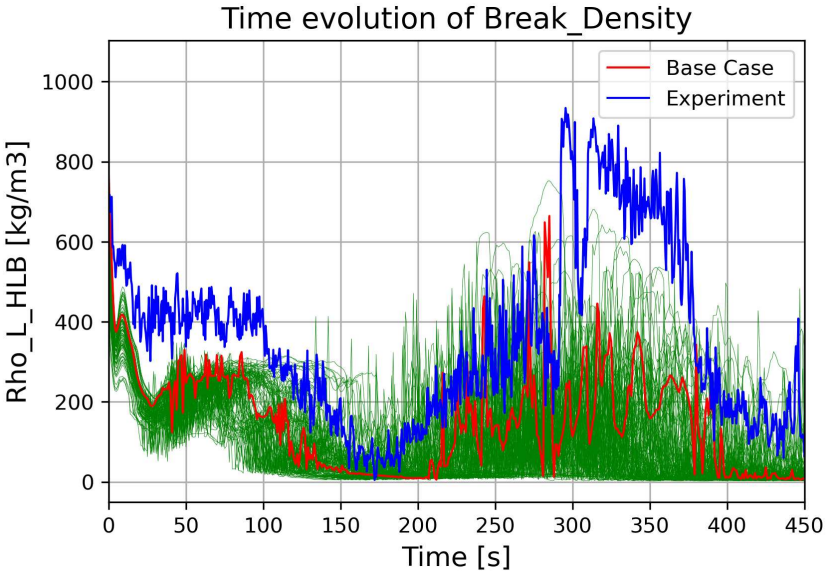

Figure 5.18: Time evolution of Density at the Break.

The upper head level (Figure 5.19) shows consistent discrepancies between simulations and experiment, the cause of which should be further investigated. Similarly, the downcomer level (Figure 5.20) exhibits a delayed rise in some cases, potentially due to delayed mass redistribution or flow path blockage — further analysis is warranted.

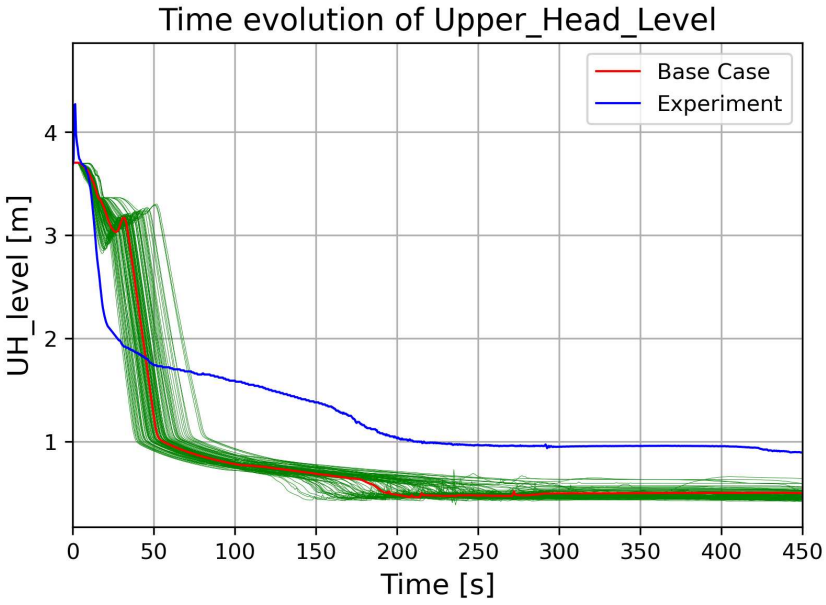

Figure 5.19: Time evolution of Upper Head Level.

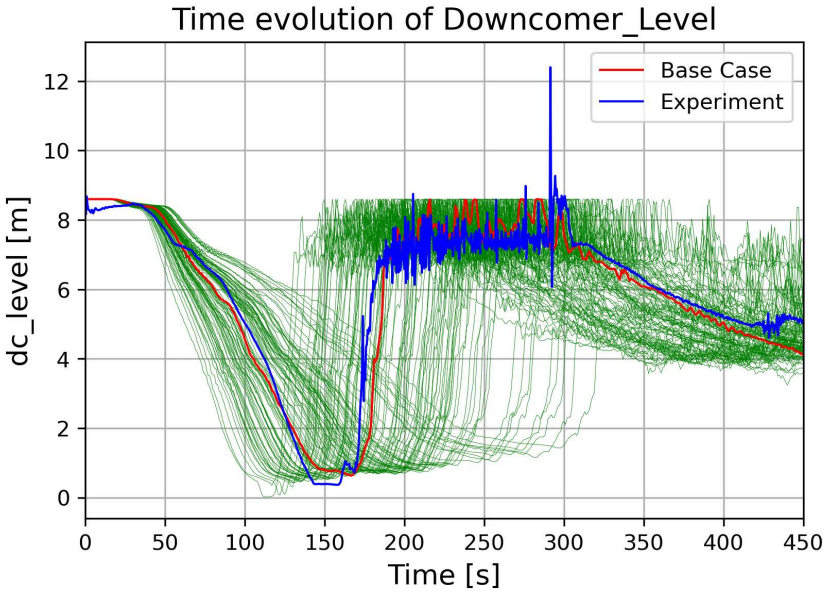

Figure 5.20: Time evolution of Downcomer Level.

As for the LPSI systems, the one in loop A appears more effective in the BEPU simulations, likely because it is farther from the break and subject to more favorable pressure conditions. The LPSI in loop B (Figure 5.21), being located near the break, appears to be affected by backpressure or direct mass loss, which reduces injection efficiency. Comparison with experimental data suggests that in both loops, the pressure threshold required for injection may not have been reached. The inconsistency with experimental trends indicates that the backpressure effects or the pump activation logic may not be adequately captured in the model.

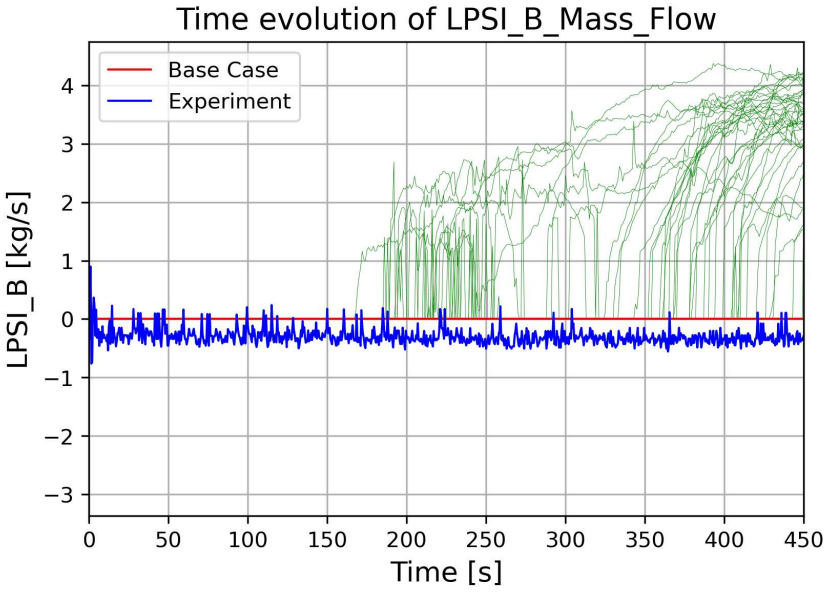

Figure 5.21: Time evolution of Low Pressure Injection System.

A critical issue in the current BEPU analysis is the underestimation of the experi-

mental PCT (Figure 5.22), which reaches approximately 610 K. The base case fails to reproduce this peak, and only a small number of BEPU trajectories capture it — often with a significant delay and followed by strong oscillations. These fluctuations may reflect instabilities or uncertainties in modeling key thermal-hydraulic phenomena such as rewetting or boil-off. This discrepancy is especially concerning given the importance of PCT in licensing applications, where it serves as a benchmark for evaluating cladding integrity (e.g., burst, oxidation).

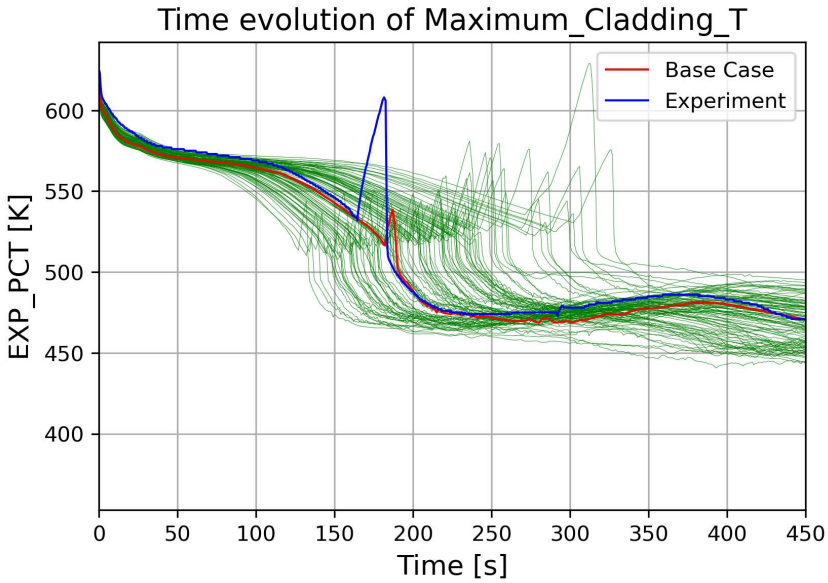

Figure 5.22: Time evolution of the PCT.

One possible explanation for this mismatch may lie in the modeling of CCFL, inaccuracies in local core pressure prediction, or an incomplete representation of LPSI system performance.

The failure to capture the experimental PCT peak could lead to a false sense of safety, particularly since the base case shows a smooth and uninterrupted cooldown, with no apparent criticality. Consequently, the simulation lacks credibility in reproducing realistic worst-case scenarios, compromising the conservative character of the analysis. It is still important to remember that the primary goal of the present work is to envelope the experimental data related to the scalar quantities required by the ATRIUM exercise, not to reproduce the full time evolution, which would require millions of simulations — meaning that these results are, in fact, quite reasonable.

In conclusion, while the simulation set generally reproduces the experimental trends with satisfactory accuracy, the presence of significant outliers — and, more critically, the systematic underestimation of the PCT — raises concerns. A discrepancy of this magnitude in a safety-critical parameter undermines the model's ability to support conservative and reliable safety evaluations.

5.3.2 Percentile Plots Analysis

As in Step 1, the quality of the percentile plots is evaluated to assess the simulations' predictive capability against experimental data.

In general, the uncertainty propagation adopted in this step does yet ensure a quite satisfactory representation of the experimental behavior. Only in a few cases, the deviation is not marginal, but rather indicative of a systematic under- or overestimation of the physical phenomena involved.

Some of the most representative scalars are shown below along with their description. The complete set of percentile plots is presented in Appendix B.1.2.

Break Parameters

Focusing on the break-related quantities in Figure 5.23, the quality of the simulation is variable.

The **break fluid density** is systematically overpredicted in all simulations. Both the base case and the experimental value lie at opposite extremes of the output distribution, highlighting a marked inconsistency likely attributable to modifications in boundary conditions introduced in the input model.

For the **maximum break flow rate**, the agreement improves: the experimental and base case values fall within the 95% bounds, although they occupy different locations within the distribution, indicating some level of uncertainty but a qualitatively acceptable match.

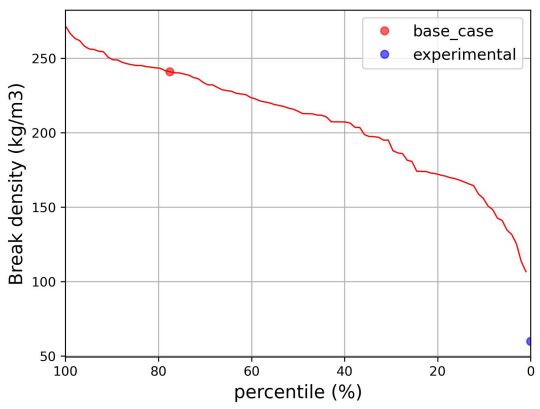

(a) Density of the fluid at the break: percentile plot.

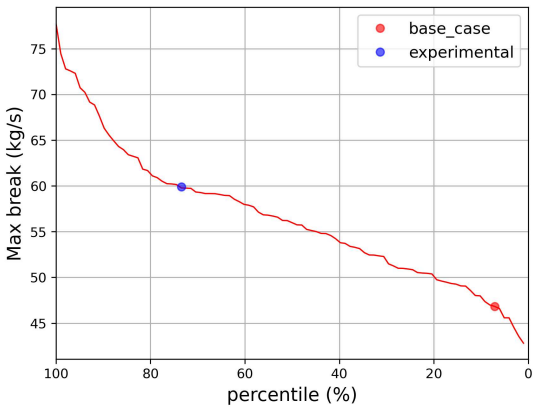

(b) Maximum break flow rate: percentile plot.

Figure 5.23: Break Parameters.

Core Behavior

The **core uncovery duration** (Figure 5.24) is reproduced with moderate accuracy: while the experimental value lies near the upper bound, approximately 15% of simulations incorrectly predict a negative uncovery time, i.e., no uncovery. This suggests potential modeling issues or overly optimistic assumptions in certain uncertainty realizations.

The **minimum collapsed water level in the core** is significantly underpredicted. Both the base case and the experimental value coincide, but lie above the 100th percentile of the simulation results. This likely reflects a physical floor at 0 meters, unaccounted for in many simulations, and is consistent with the pressure drop trends discussed below.

The **minimum core pressure drop** is reasonably well captured: the experimental value lies within the Wilks' bounds and above approximately 80% of the simulations. However, the base case slightly overpredicts the expected pressure behavior.

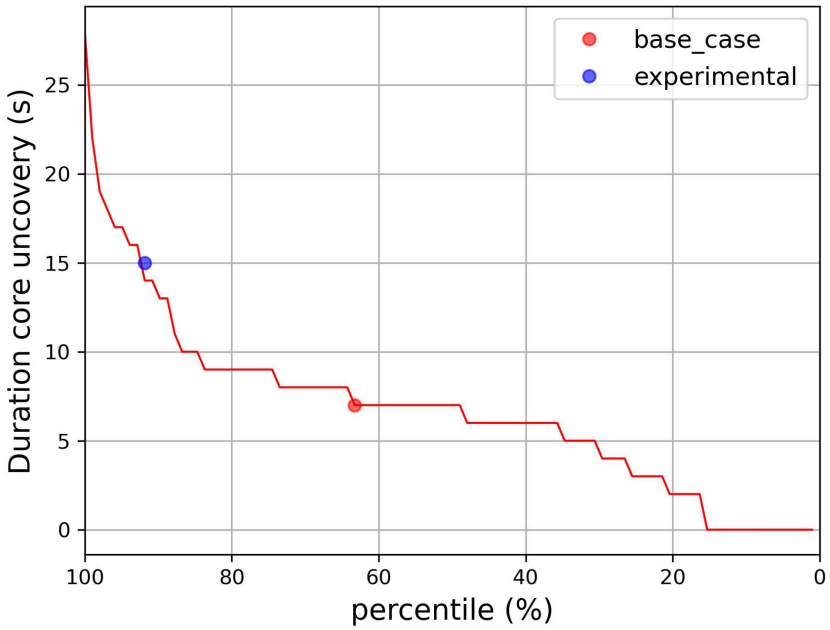

Figure 5.24: Duration of core uncovery: percentile plot.

Heat Transfer and Safety Parameters

The **Peak Cladding Temperature (PCT)** (Figure 5.25a), a critical safety parameter, is notably underestimated. The experimental value lies well above the 95th percentile of the simulated distribution, with only ∼15% of simulations exceeding the base case. This mismatch may be attributed to incomplete modeling of phenomena such as **Counter-Current Flow Limitation (CCFL)** and/or inadequacies in the **post-CHF heat transfer treatment**, as largely stated above.

In contrast, the **time to reach the PCT** (Figure 5.26b) is well predicted. Both the base case and the experimental value lie within the uncertainty bounds and are closely aligned, indicating accurate temporal modeling of the thermal excursion. It is crucial to notice that all the negatives values depicted in Figure 5.25 are related to a percentage of cases (round 15%) in which PCT is never reached, as it can also assessed looking at the correlate plot in Figure 5.25a. In the latter, the temperature in those cases is set equal to the saturation one.

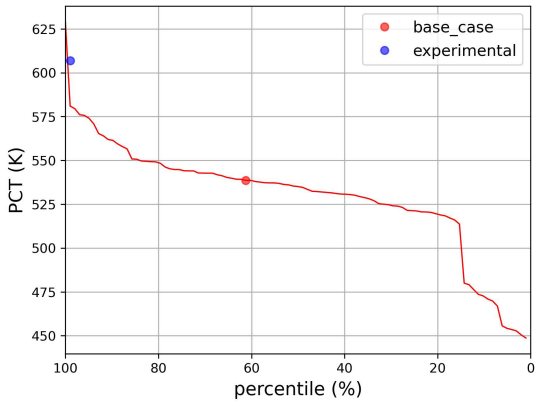

(a) PCT: percentile plot.

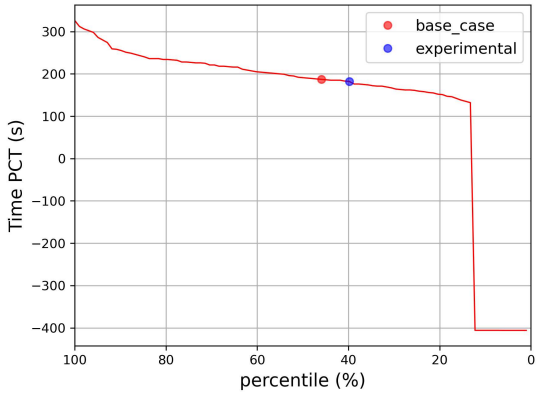

(b) Time to reach PCT: percentile plot.

Figure 5.25: Heat Transfer and Safety Parameters.

Integral and System-Level Parameters

The **integral break mass flow** shows a consistent and physically realistic decreasing trend across all simulations. The base case and experimental values lie within the uncertainty bounds and are in good agreement across all three evaluations.

For the **hot leg liquid level** (connected to the break), both the base case and the experimental value fall within the Wilks' bounds, close to the 40th percentile and in close proximity to each other, suggesting reliable reproduction of the experimental trend.

A number of scalar quantities show consistent and satisfactory agreement between simulations and experiment (Figure 5.26). These include:

- **Accumulator injection start and end times**,
- **Upper plenum depletion and refill times**,
- **CHF onset and complete quench times**,
- **LPSI (Low Pressure Safety Injection) initiation time**,
- **Minimum core temperature time**,
- **Liquid Seal (LS) clearing times (first and second occurrences)**.

These quantities generally exhibit percentile distributions with smooth, monotonically decreasing trends. Experimental and base case values lie within the Wilks' bounds, often near the center of the distributions, indicating strong consistency and robust modeling for these events. It is relevant to notice that in Figure 5.26 the plot shows a flat zone at $450s$, this behavior can be explained by assessing that in around 15% of cases CHF is never reached.

A discrepancy is observed for the **time at which the primary system pressure drops below that of the steam generator**. This quantity is overestimated across all simulations, with the experimental value falling below the simulated range. This may point to deficiencies in the system pressure balance modeling or an overly conservative treatment of break and system depressurization dynamics.

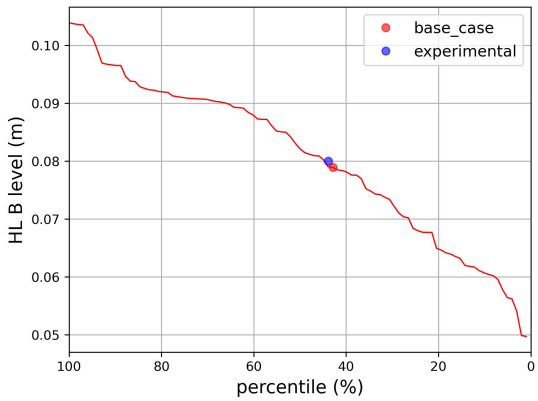

(a) Hot Leg B liquid level: percentile plot.

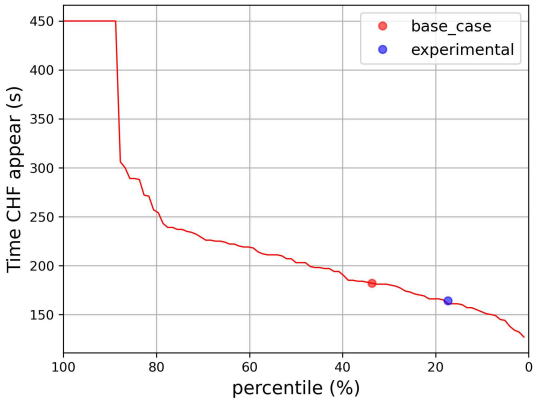

(b) CHF onset time: percentile plot.

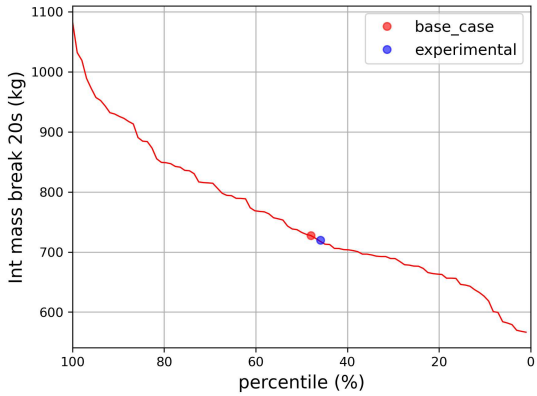

(c) Integral mass flow at the break at 20s: percentile plot.

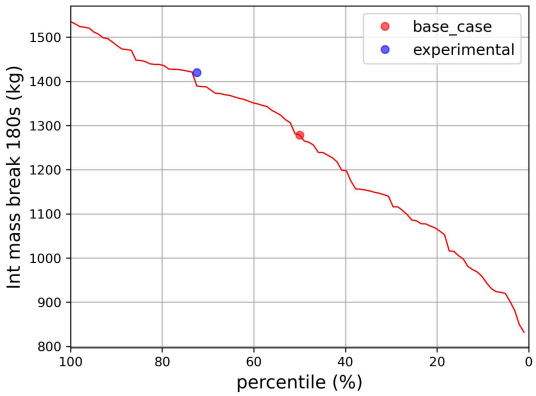

(d) Integral mass flow at the break at 180s: percentile plot.

Figure 5.26: Integral and System-Level Parameters.

In summary, the Step 2 BEPU analysis demonstrates generally good simulation accuracy, especially for integral and timing-related parameters such as accumulator and system injection events. However, notable discrepancies persist for critical safety-related variables like PCT and core liquid inventory, which are consistently under- or overestimated. Excluding these specific outliers—already discussed in detail above—the overall agreement between simulations and experiment is acceptable, with approximately 85–90% of the results exhibiting physically meaningful and smoothly distributed trends within the Wilks' bounds.

For completeness, plots including uncertainty bands are provided in Appendix B.1.3, offering a clear visual representation of the predictive performance of the simulation set.

5.4 Step 3 – BEPU Analysis Results

This final step is intended to synthesize and optimize the results obtained in the previous phases. As mentioned earlier, the uncertainty space has been expanded in this step — for instance, by including the CCFL phenomenon among the uncertain parameters.

However, it is not possible to conclude that a significant improvement has been achieved. Once again, the uncertainties related to the choked flow remain dominant, effectively "choking" or masking the influence of the additional uncertainties introduced in this step. This dominance limits the ability to observe any meaningful change in the overall response of the system.

The transient plots generated in this step are nearly identical to those from Step 2, suggesting little to no variation in system behavior over time. That said, a few minor considerations can be made based on the percentile plots, which, although still very similar to those of the previous step, offer some noteworthy differences. For instance, in Step 3, there is a single case where core uncovery extends up to 200 seconds (Figure 5.27) — a significantly delayed recovery compared to the rest of the ensemble, which aligns closely with prior results.

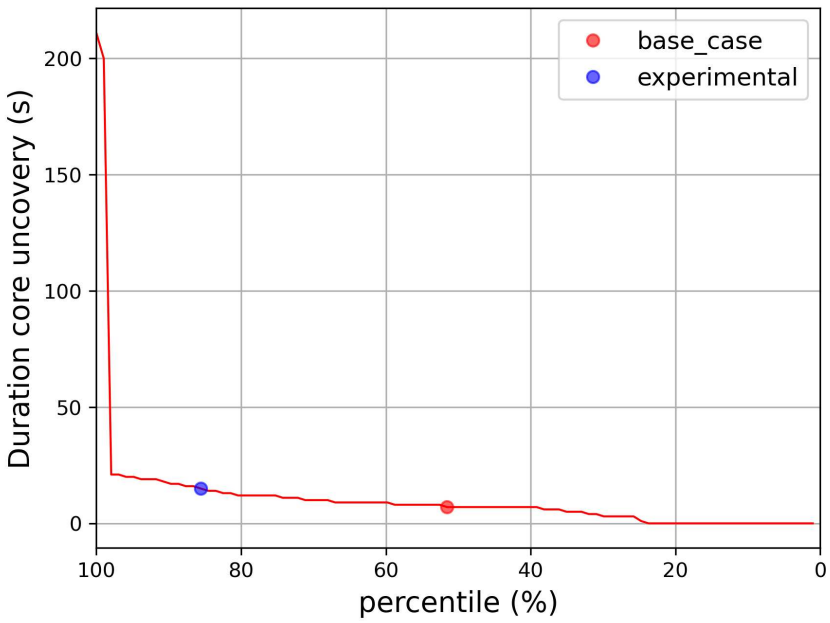

Figure 5.27: Duration of core uncovery: percentile plot.

Focusing on variables related to core uncovery, we can observe a modest increase in the number of cases where Critical Heat Flux is not reached (Figure 5.28). This results in a broader percentage of scenarios where the Peak Cladding Temperature remains lower (Figure 5.29). Moreover, the experimental peak value of PCT is not reached in any of the simulations this time, as is can be assessed from Figure 5.30 — not even with a time delay, as observed in earlier steps.

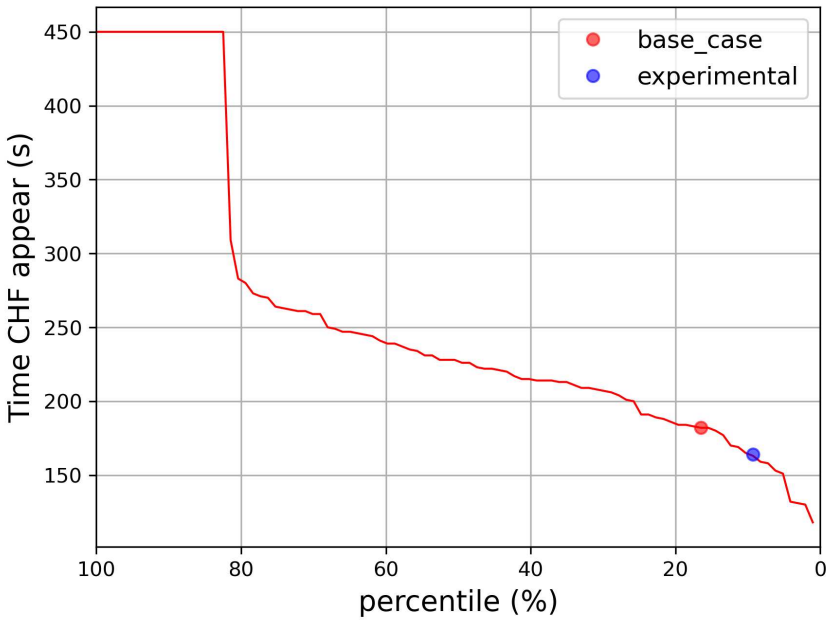

Figure 5.28: Time at which CHF appears.

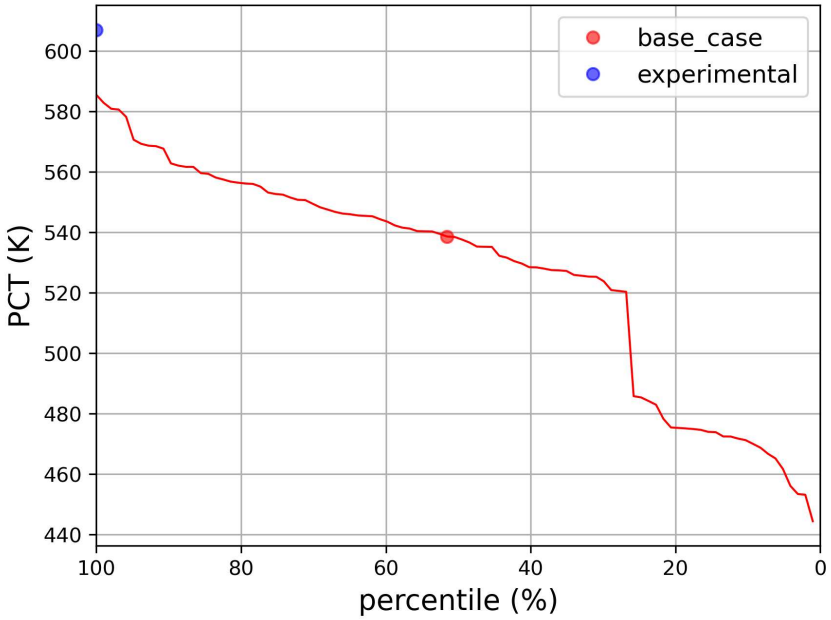

Figure 5.29: PCT: percentile plot.

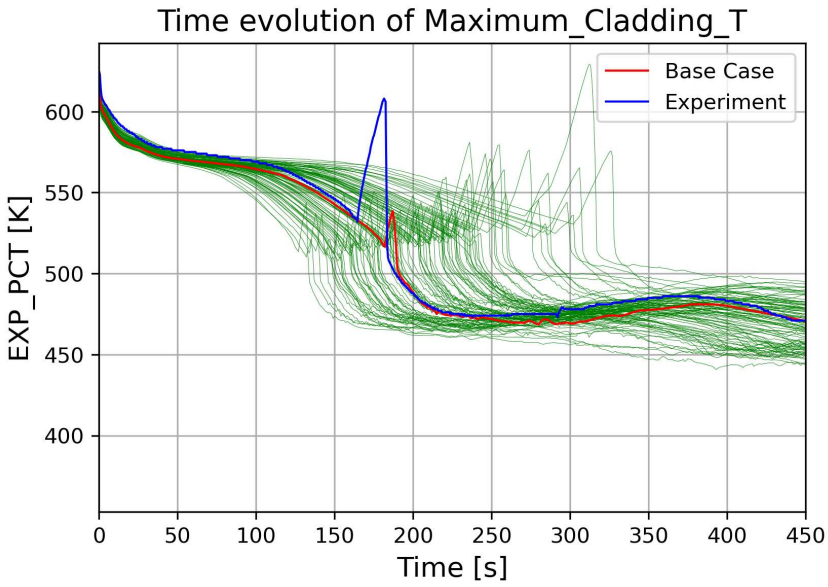

(a) Step 2

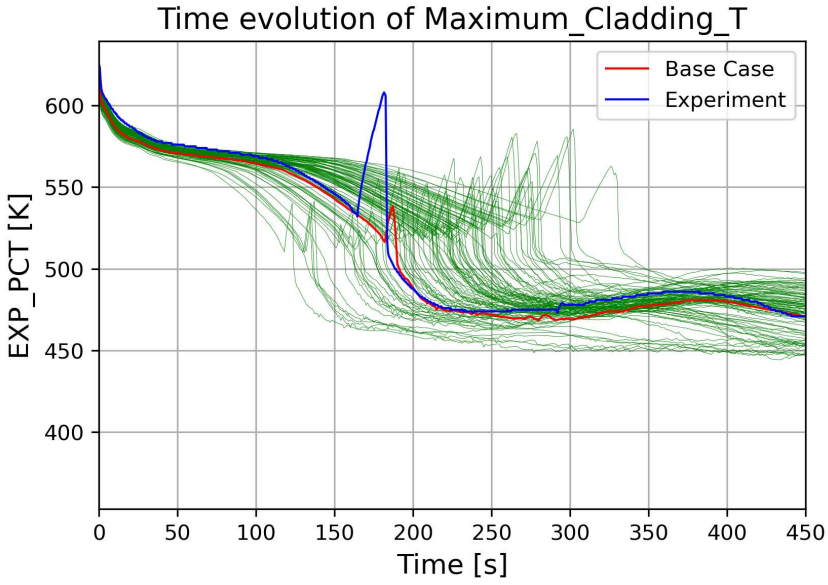

(b) Step 3

Figure 5.30: PCT: comparison between Step 2 and Step 3.

Overall, the trends observed in Step 2 are generally reproduced here. In some cases, there is a higher fraction of simulations falling into the outlier range for key scalar quantities, such as the time at which accumulator injection ends (Figure 5.31), the occurrence of CHF, and the PCT value.

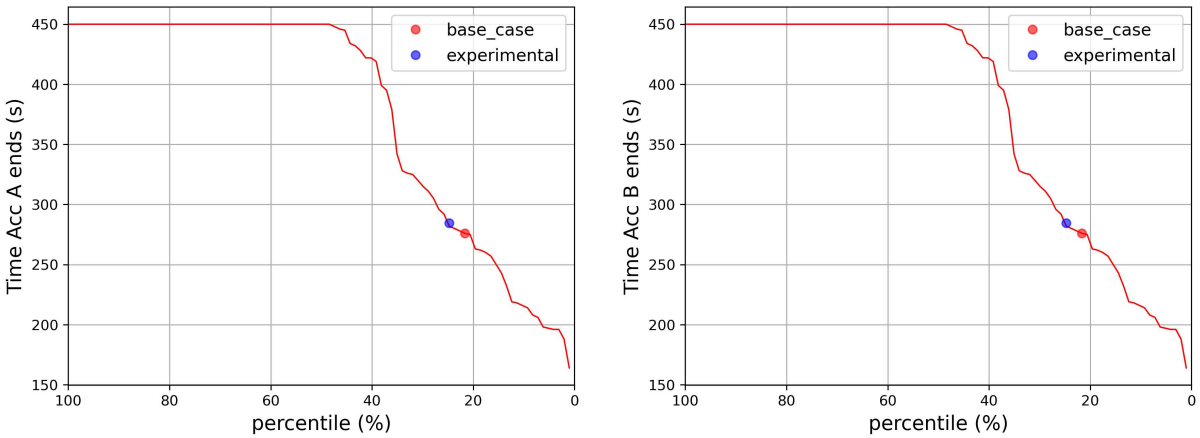

(a) Step 2 (b) Step 3

Figure 5.31: Time at which accumulators injection ends: comparison between Step 2 and Step 3.

In conclusion, although the range of scalar responses appears to be reasonably covered, no new uncertainty has had a sufficiently strong impact to meaningfully alter the core uncovery duration — which is the primary driver of the PCT peak. As a result, the fundamental limitations observed in earlier steps persist in this final assessment.

5.5 Additional considerations

It is important to highlight that all transients are capped at an upper time limit of 450 seconds. This constraint arises from significant numerical instabilities that caused many simulation cases to fail around this point in the transient. Given that this time truncation represents a substantial limitation to the analysis, it is strongly recommended to assess and improve the numerical robustness of the RELAP5 code in future work.

Actually, the only scalar affected by this cap is the time at which LPSI starts, in all the steps.

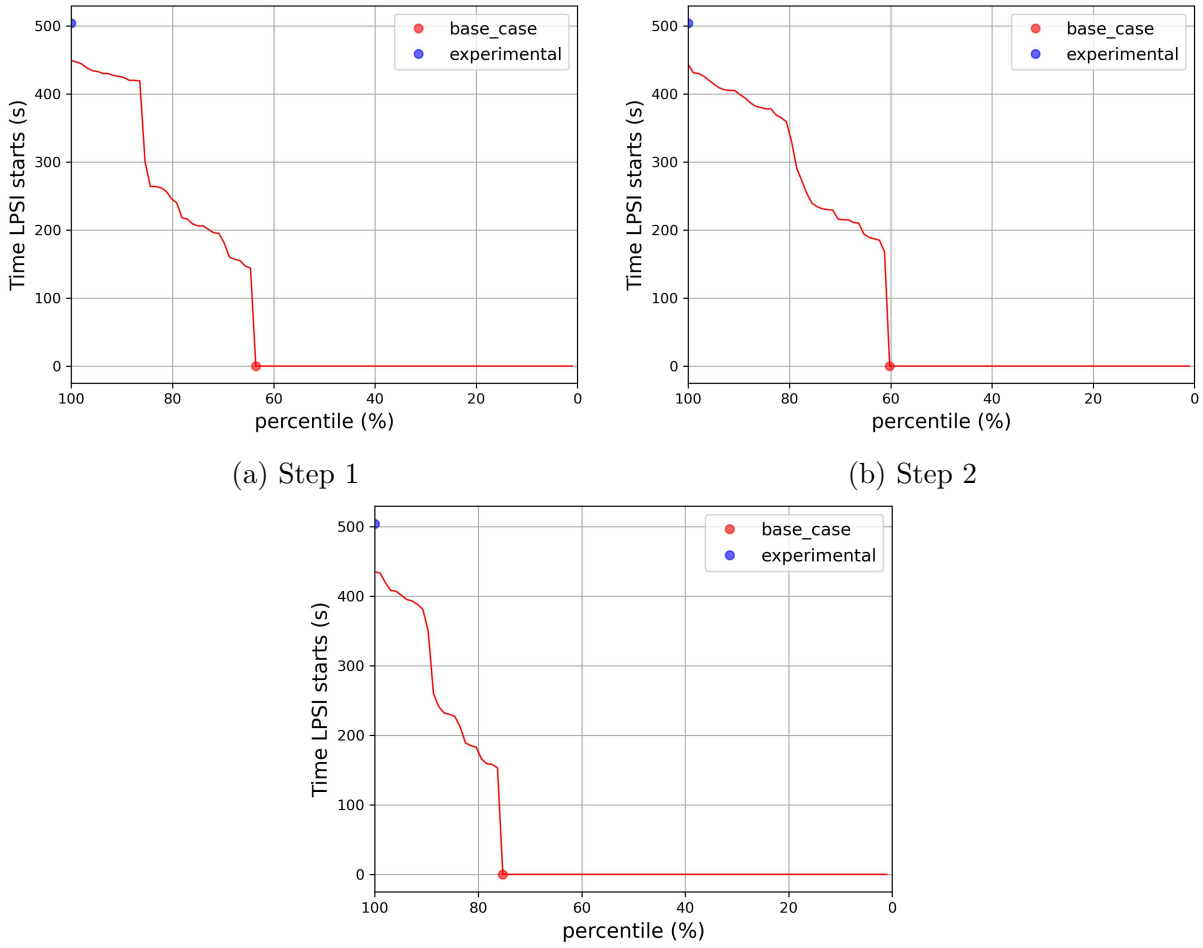

(a) Step 1

(b) Step 2

(c) Step 3

Figure 5.32: Time at which LPSI starts: percentile plot.

As illustrated in Figure 5.32, the majority of cases do not reach the point at which the LPSI system begins injecting coolant into the primary loop. This behavior is attributed to the fact that, for many simulations, the boundary conditions required to trigger LPSI activation are not met within the allowed transient time. For the remaining cases, the scalar value representing LPSI start time is simply set equal to the maximum simulation duration, i.e., 450 seconds, indicating that the injection did not occur before the simulation was terminated.

Another important aspect to consider is the Core Power (Figure 5.33). The uncertainty applied in this case appears excessively large: the power ranges from 8 MW to 12 MW, whereas the expected physical range should be much narrower, approximately from 9.8 MW to 10.2 MW. This discrepancy suggests that the uncertainty bounds do not accurately reflect the actual variability of the parameter. As a result, it becomes challenging to quantify the true impact of this overestimated uncertainty on the simulation outcomes, since it may artificially inflate the perceived sensitivity of the system to variations in core power.

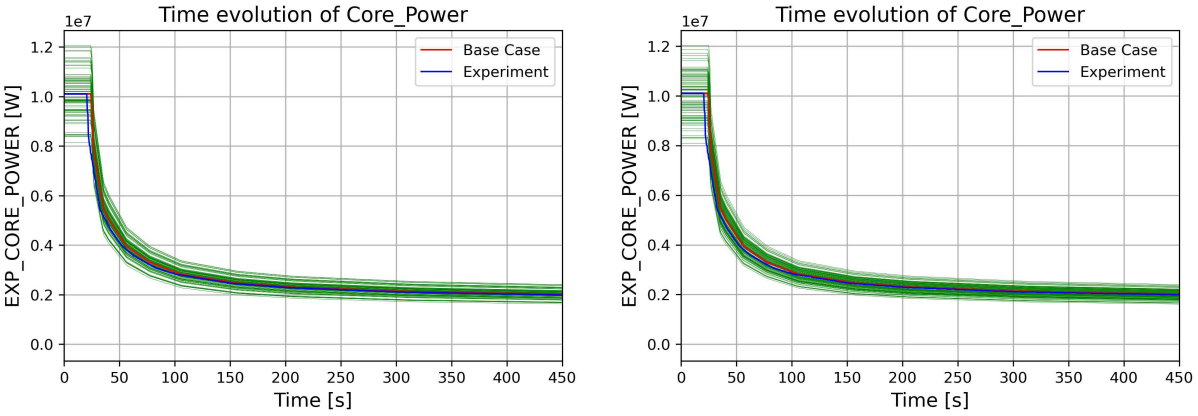

(a) Step 2

(b) Step 3

Figure 5.33: Core power: impact of the uncertainties applied on initial condition.

Chapter 6

Conclusions

The ultimate goal of this thesis was the validation of a RELAP5 model capable of accurately representing the thermal-hydraulic phenomena occurring during an Intermediate Break Loss of Coolant Accident (IBLOCA) localized in the hot leg of a pressurized water reactor (PWR). This objective is framed within the broader context of Deterministic Safety Analysis (DSA), which constitutes one of the pillars of nuclear safety assessment, alongside Probabilistic Safety Analysis (PSA). In particular, the DSA approach aims to demonstrate the compliance of a nuclear system with established safety criteria under postulated accident scenarios, using conservative or best-estimate methodologies.

The work was carried out within the scope of the ATRIUM project, focusing specifically on Exercise 3. The analysis involved comparison with experimental data from Test 1, performed at the ROSA/LSTF integral test facility in Japan.

The validation process was conducted through a forward uncertainty propagation analysis based on the Best Estimate Plus Uncertainty (BEPU) methodology, which is a widely recognized and regulatory-accepted approach for safety analysis. The uncertainty quantification required for the BEPU analysis was carried out via Inverse Uncertainty Quantification (IUQ), leveraging information from Exercises 1 and 2 of the ATRIUM project.

The analysis was structured in three successive steps. The first propagation included uncertainties solely on critical flow and post-dryout heat transfer, as characterized in the initial ATRIUM exercises. The second step extended the uncertainty domain by incorporating uncertainties on initial and boundary conditions as well. The final step was intended to incorporate additional uncertainties related to further physical phenomena — such as CCFL and heat transfer to the environment — with the aim of enhancing the overall robustness and representativeness of the simulation output. The results from all steps exhibit strong similarities, with nearly identical time trends and only marginal improvements in the percentile plots of Step 2 and 3 compared to Step 1. This limited improvement is primarily attributed to the dominant influence of the choked flow uncertainties, which heavily affect the simulation outcomes and tend to mask the impact of uncertainties associated with other parameters.

Overall, the simulation process can be considered successful, with the majority of key output variables — including the base case — closely matching the experimental trends. However, approximately 15%-20% of the cases showed significant deviations from experimental behavior.

Despite these generally positive outcomes, a major concern remains regarding the ac-

curate prediction of the Peak Cladding Temperature (PCT). Among all propagated cases across the three steps, only a single simulation in Step 2 reaches a temperature close to the experimental peak — and even then, with a substantial time delay. This discrepancy is particularly critical, as the PCT is the primary safety criterion adopted to assess compliance with IAEA regulatory limits. The inability of the current model to reproduce this metric with sufficient accuracy implies that the system cannot yet be considered fully validated for safety-related applications. This deficiency is most likely linked to the limitations of the CCFL model currently implemented in RELAP5, which may not fully account for the complex physical mechanisms governing flow reversal and flooding dynamics under transient conditions. The final step of the analysis aimed precisely at addressing this limitation by extending the uncertainty space to include additional phenomena and the expectation was that such an extension would lead to a better representation of the physical behavior, particularly during the core reflooding phase.
Unfortunately, this enhancement did not result in a significant improvement of the results. One of the persistent shortcomings is the failure to accurately reproduce the core uncovery duration, which is a key driver of the cladding temperature escalation. As a consequence, even though the simulated outputs do envelope most of the scalar metrics required by the ATRIUM project the most safety-relevant quantity, the PCT, remains inadequately captured.
Given the pivotal role of PCT in nuclear safety assessments, further refinement of the CCFL modeling approach is strongly recommended, with particular attention to its coupling with heat transfer mechanisms and reflood behavior.

Looking ahead, future work should prioritize a more detailed phenomenological analysis aimed at improving the prediction of core uncovery dynamics and their impact on PCT. Additionally, the relative dominance of choked flow uncertainties should be critically reassessed, to allow the influence of less dominant — but still relevant — phenomena to emerge more clearly within the uncertainty propagation process.

This work reaffirms the fundamental role of safety analysis as a cornerstone of nuclear engineering, not only as a regulatory requirement but as a scientific tool to deepen our understanding of complex accident scenarios and to ensure the highest levels of protection for both the public and the environment.

Bibliography

[1] Best estimate safety analysis for nuclear power plants: Uncertainty evaluation. Technical report, International Atomic Energy Agency, 2008.

[2] *Deterministic Safety Analysis for Nuclear Power Plants*. Number SSG-2 (Rev.1) in Specific Safety Guide. INTERNATIONAL ATOMIC ENERGY AGENCY, Vienna, 2019.

[3] International Atomic Energy Agency. Accident analysis for nuclear power plants with pressurized water reactors. *Safety Report Series*, 30, 2003.

[4] OECD Nuclear Energy Agency. Final integration report of the rig-of-safety assessment (rosa-2) project (2009–2012). Nea/csni/r(2016)10, OECD Nuclear Energy Agency, Committee on the Safety of Nuclear Installations (CSNI), Paris, France, 2016. Final integration report, OECD Publishing.

[5] OECD Nuclear Energy Agency and Japan Atomic Energy Agency. Final data report of rosa-2/lstf test 1: Hot leg intermediate break loca (ib/hl/01). Jaea report / oecd nea rosa-2, OECD Nuclear Energy Agency & Japan Atomic Energy Agency, 2011. Large Scale Test Facility IB-HL-01 data report.

[6] Abdulrahman S. Al-Awad. Thermal–hydraulic phenomenology analysis and relap5/mod3.3 code assessment for atlas 1% upper head sbloca test. Master's thesis, UPC – Escola Tècnica Superior d'Enginyeria Industrial de Barcelona, July 2020. Master's thesis.

[7] A. Bortot et al. Neutron kinetic–thermal hydraulic coupled analysis of alfred reactor using phisics/relap5 3d. In *UIT Conference on Heat Transfer*, 2020.

[8] E. Cirillo et al. Transient analysis of sirio using relap5/mod3.3 system code. In *EPJ Web of Conferences*, 2023.

[9] Cristiano Ciurluini, Lorenzo Melchiorri, Vincenzo Narcisi, Gianfranco Caruso, Alessandro Tassone, and Fabio Giannetti. Transient analysis and thermal-hydraulic assessment of the primary cooling circuit of the eu-demo wcll breeding blanket. Master's thesis, Sapienza Università di Roma, 2022. Master's thesis.

[10] Francesco D'Auria. *Thermal-Hydraulics of Water Cooled Nuclear Reactors*. Woodhead Publishing Series in Energy. Woodhead Publishing, 2017.

[11] Francesco D'Auria, Carlos Camargo, and Oscar Mazzantini. The best estimate plus uncertainty (bepu) approach in licensing of current nuclear reactors. *Nuclear Engineering and Design*, 248:317–328, 2012.

[12] J. Freixa, T.-W. Kim, and A. Manera. Post-test thermal-hydraulic analysis of two intermediate loca tests at the rosa facility including uncertainty evaluation. *Nuclear Engineering and Design*, 264, 2013. SI:NURETH-14.

[13] J. Freixa, V. Martínez-Quiroga, K. Martin-Gil, and F. Reventós. Modelling Guidelines for CCFL Representation During IBLOCA Scenarios of PWR Reactors. NUREG/IA-0550 IA-0550, U.S. Nuclear Regulatory Commission, Washington, DC, October 2024. Prepared under the Thermal–Hydraulic Code Applications and Maintenance Program (CAMP). Manuscript completed February 2024.

[14] IAEA. Atrium benchmark – application tests for inverse uncertainty quantification in thermal-hydraulics. `https://www.oecd-nea.org/jcms/pl_71614/atrium-project`, 2023. Accessed: 2025-06-25.

[15] International Atomic Energy Agency. Best estimate safety analysis for nuclear power plants: Uncertainty evaluation. Technical Report SSG-23, IAEA, 2008. Safety Standards Series No. SSG-23.

[16] P. Mancusi et al. Qualification of relap5-3d code condensation model against full-scale perseo test 9. *Progress in Nuclear Energy*, 2021.

[17] Víctor Martínez-Quiroga, Kevin Martin, Max Casamor, Marina Pérez-Ferragut, Carme Pretel, and Jordi Freixa. *LOCUST LSTF Input Model*. UPC ANT, July 2020. Engineering Handbook of the UPC, Confidential.

[18] A. Del Nevo et al. Uncertainty quantification method for relap5 3d© using raven and application on nacie experiments. *Annals of Nuclear Energy*, 2019.

[19] Nuclear Power Knowledge Base. Flow patterns – two-phase flow. `https://www.nuclear-power.com/nuclear-engineering/fluid-dynamics/two-phase-fluid-flow/flow-patterns-two-phase-flow/`, 2023. Accessed: 2025-07-15.

[20] Nuclear-Power.com. Defence-in-depth principle – nuclear safety. `https://www.nuclear-power.com/nuclear-power/reactor-physics/nuclearsafety/defence-in-depth-principle/`, 2015. Accessed: 2025-06-11.

[21] Krzysztof Otlik and Tewfik Hamidouche. Assessment of relap5-3d two phase flow models for myrrha secondary cooling system conditions. Master's thesis, ENSTA ParisTech – École Nationale Supérieure de Techniques Avancées Paris, September 2021. Master's thesis.

[22] Hae Min Park, Jong Hyuk Lee, Chiwoong Choi, Kwi-Seok Ha, Byung Hyun You, Jaeseok Heo, Kyung Doo Kim, Sung Won Bae, Seung Wook Lee, Dong Hyuk Lee, Sang Ik Lee, Chan Eok Park, Bub Dong Chung, and Kwang Won Seul. Development of a phenomena identification and ranking table (pirt) for intermediate break loss-of-coolant accident in pwrs. *Nuclear Engineering and Technology*, 57(1):103141, 2025.

[23] Lucia Sargentini, Alberto Ghione, Jordi Freixa, Ziyu Xie, and Xu Wu. Specifications for the atrium project – 3rd exercise. Internal project document, CEA-Saclay, UPC, NCSU, 2025. Unpublished report.

[24] Jordi Freixa Terradas. *SBLOCA Transients with Boron Dilution in Pressurized Water Reactors*. PhD thesis, Universitat Politècnica de Catalunya, 2007. Ph.D. thesis.

[25] U.S. Nuclear Regulatory Commission. Relap5/mod3.3 code manual, volume ii: User's guide. Technical Report NUREG/CR-5535, INEEL-95/0174, Idaho National Engineering and Environmental Laboratory (INEEL), Idaho Falls, Idaho, USA, 2001. Prepared by the Idaho National Laboratory for the U.S. NRC.

[26] U.S. Nuclear Regulatory Commission. Relap5/mod3.3 code manual, volume iv: Models and correlations. Technical Report NUREG/CR-5535, INEEL-95/0174, Idaho National Engineering and Environmental Laboratory (INEEL), Idaho Falls, Idaho, USA, 2001. Prepared by the Idaho National Laboratory for the U.S. NRC.

[27] Ashwin Bala Vidya. The design and thermal-hydraulic simulation of a nuward-like smr using relap5. Master's thesis, Politecnico di Milano, 2022. Master's thesis.

[28] Samuel S. Wilks. Determination of sample sizes for setting tolerance limits. *The Annals of Mathematical Statistics*, 12(1):91–96, 1941.

[29] Xu Wu, Ziyu Xie, Farah Alsafadi, and Tomasz Kozlowski. A comprehensive survey of inverse uncertainty quantification of physical model parameters in nuclear system thermal-hydraulics codes. *arXiv preprint arXiv:2104.12919*, 2021. Review paper categorizing IUQ into Design-of-Experiments, Frequentist, Bayesian, empirical and more, with comparative metrics.

Appendix A

Wilks' Formula derivation

The following derivation follows the formulation in [28].

Let's begin by recalling the *Beta distribution*, defined on $[0, 1]$ with shape parameters $a > 0$, $b > 0$. Its probability density function (pdf) is:

$$f(u; a, b) = \frac{1}{B(a, b)} u^{a-1}(1-u)^{b-1}, \quad u \in [0, 1] \tag{A.1}$$

where $B(a, b)$ is the Beta function:

$$B(a, b) = \frac{\Gamma(a)\Gamma(b)}{\Gamma(a+b)} \tag{A.2}$$

The cumulative distribution function (CDF) is:

$$F(u; a, b) = \int_0^u f(t; a, b)\, dt = I_u(a, b) \tag{A.3}$$

where $I_u(a, b)$ is the *regularized incomplete Beta function.*

Wilks' method assumes a population described by a smooth CDF $G(y)$ and PDF $g(y)$. Given N i.i.d. samples $\{X_1, ..., X_N\}$, their sorted values (order statistics) are:

$$X_{(1)} \leq X_{(2)} \leq \cdots \leq X_{(N)}$$

These can be used to define coverage probabilities:

$$P_U = 1 - G(X_{(t)}), \qquad P_L = G(X_{(s)}), \qquad P_C = G(X_{(t)}) - G(X_{(s)}) \tag{A.4}$$

To study the distribution of order statistics, consider the k-th order statistic $U_{(k)}$. Its CDF is:

$$P(U_{(k)} \leq u) = \sum_{j=k}^{N} \binom{N}{j} u^j (1-u)^{N-j} \tag{A.5}$$

Differentiating gives the PDF:

$$f_{U_{(k)}}(u) = \frac{N!}{(k-1)!(N-k)!} u^{k-1}(1-u)^{N-k} \tag{A.6}$$

which matches the Beta PDF with parameters $a = k$, $b = N - k + 1$. Thus:

$$U_{(k)} \sim \text{Beta}(k, N - k + 1)$$

This allows expressing the coverage probabilities as Beta-distributed variables:

$$P_U \sim \text{Beta}(N - t + 1, t) \tag{A.7}$$
$$P_L \sim \text{Beta}(s, N - s + 1) \tag{A.8}$$
$$P_C \sim \text{Beta}(t - s, N - t + s + 1) \tag{A.9}$$

Using the regularized Beta function $I_x(a, b)$, the confidence level $1 - \alpha$ leads to:

$$I_{1-P}(N - t + 1, t) \geq 1 - \alpha \qquad \text{(upper bound)} \tag{A.10}$$
$$I_{1-P}(s, N - s + 1) \geq 1 - \alpha \qquad \text{(lower bound)} \tag{A.11}$$
$$I_P(t - s, N - t + s + 1) \leq \alpha \qquad \text{(two-sided bound)} \tag{A.12}$$

Assuming symmetry ($s = r$, $t = N - r + 1$), Wilks' bounds become:

$$I_{1-P}(r, N - r + 1) \geq 1 - \alpha \qquad \text{(one-sided)} \tag{A.13}$$
$$I_P(N - 2r + 1, 2r) \leq \alpha \qquad \text{(two-sided)} \tag{A.14}$$

These expressions allow computing the minimum sample size N for a given rank r, tolerance level P, and confidence level $1 - \alpha$. For example, for a 95%/95% one-sided bound with $r = 1$:

$$I_{0.05}(1, N) \geq 0.95 \quad \Rightarrow \quad N \geq 58.4 \quad \Rightarrow \quad \lceil N \rceil = 59$$

This value is commonly used in BEPU applications.

In the present study, **93 cases** were used. This sample size exceeds the minimum required for a one-sided 95%/95% tolerance limit with $r = 1$, and allows for increased flexibility in applying Wilks' formula. Specifically, the use of a larger sample size enables the selection of higher-order ranks $r > 1$, which can improve the statistical robustness of the results and potentially reduce the width of the resulting tolerance bounds. Furthermore, it facilitates the use of two-sided (central) intervals with the same level of confidence, which are generally more informative in uncertainty quantification applications.

Appendix B

Additional plots

B.1 Step 2

B.1.1 Time evolution plots

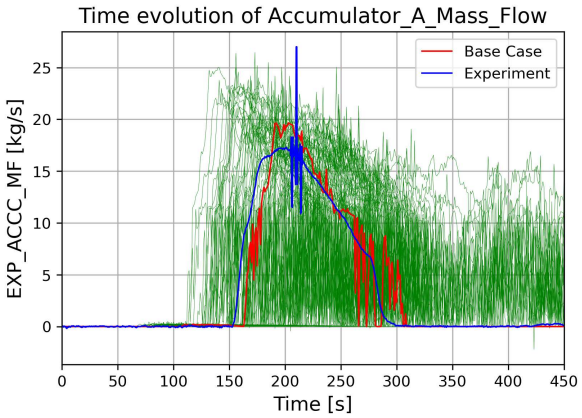

(a) Accumulator A Mass Flow

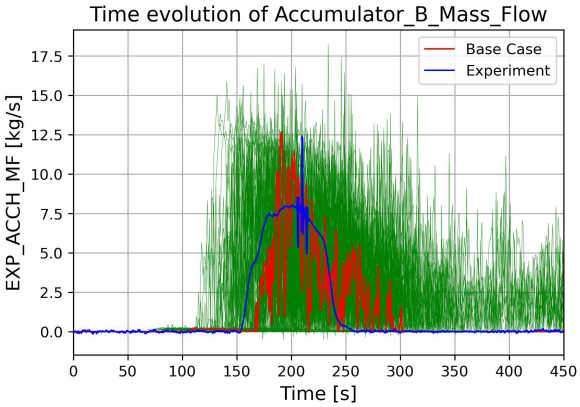

(b) Accumulator B Mass Flow

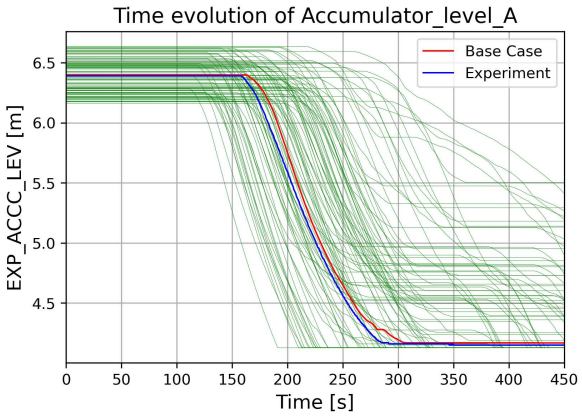

(c) Accumulator level

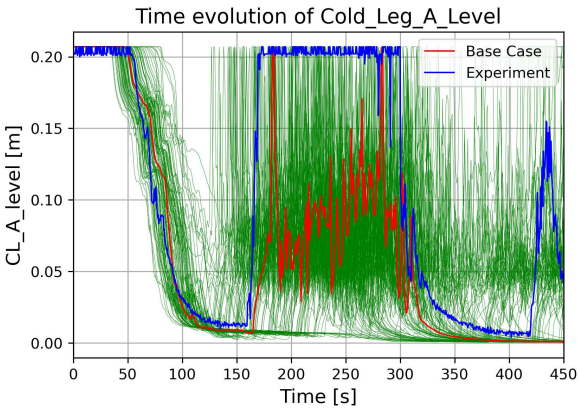

(d) Cold Leg A Level

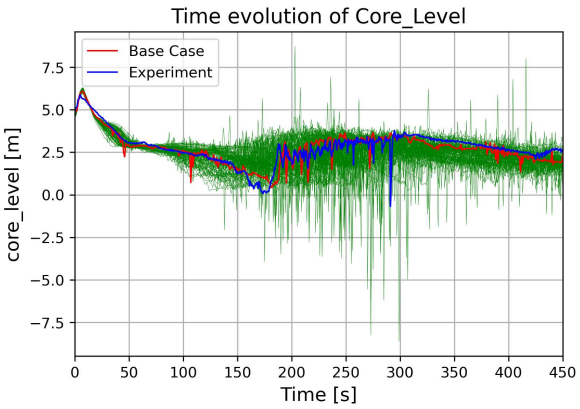

(e) Core Level

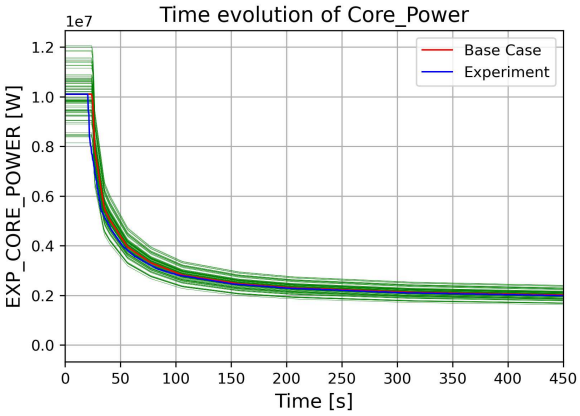

(f) Core Power

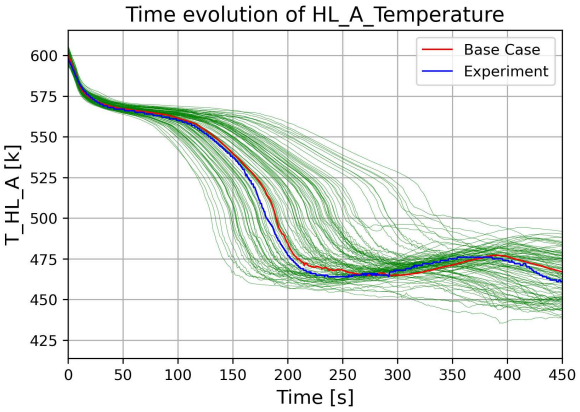

(g) Hot Leg A Temperature

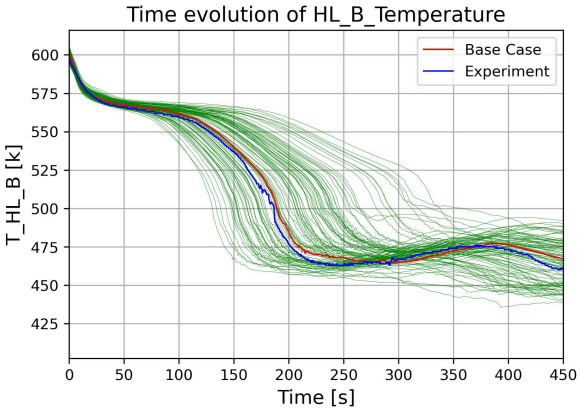

(h) Hot Leg B Temperature

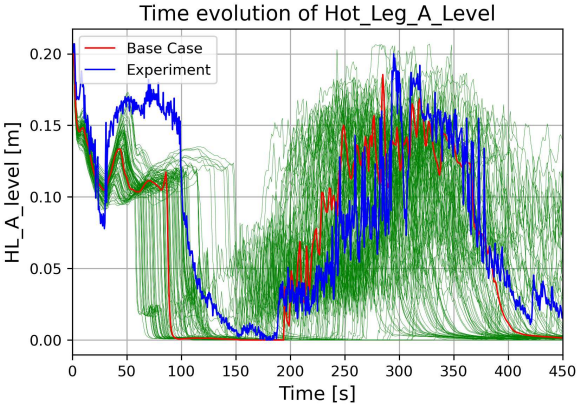

(i) Hot Leg A Level

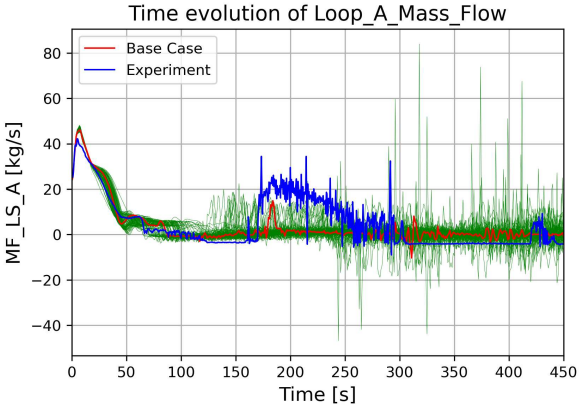

(j) Loop A Mass Flow

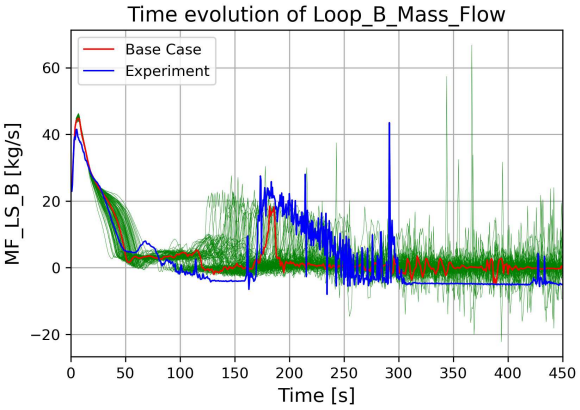

(k) Loop B Mass Flow

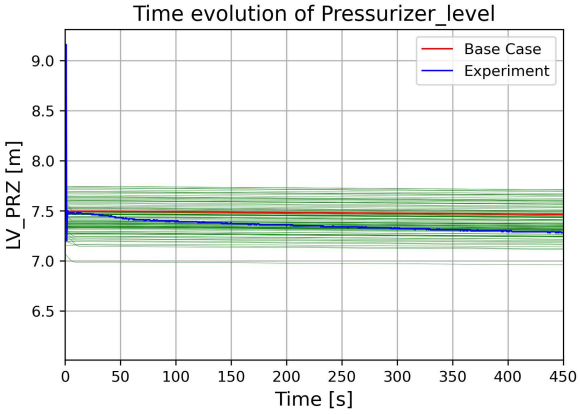

(l) Pressurizer Level

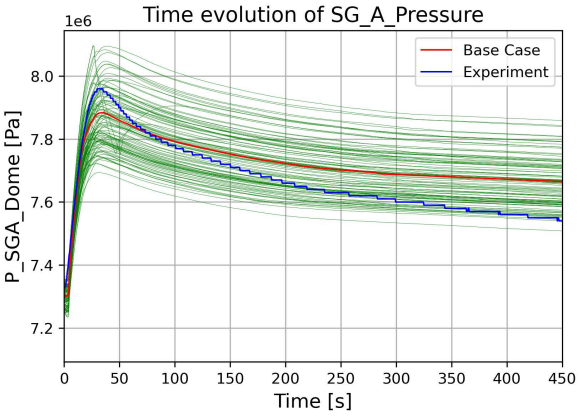

(m) SG A Pressure

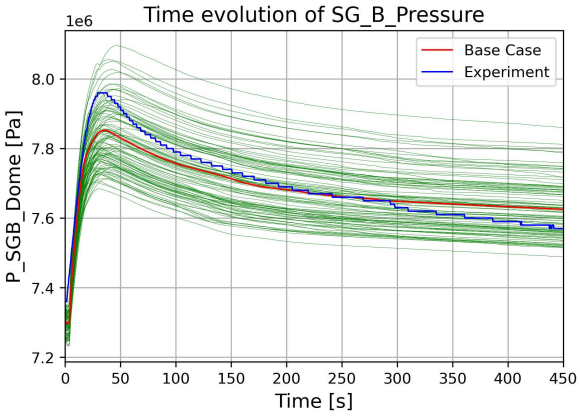

(n) SG B Pressure

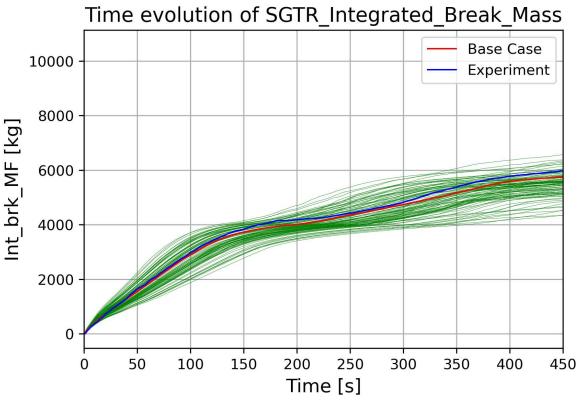

(o) Integrated Break Mass

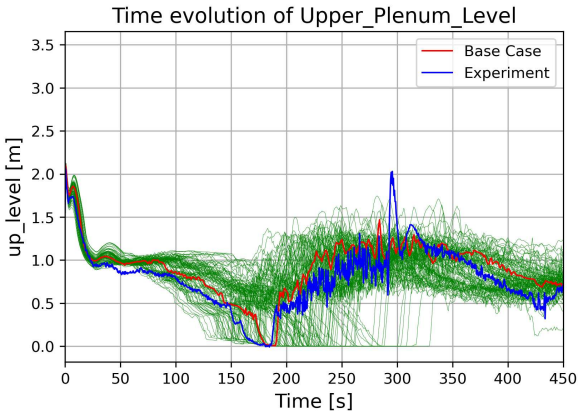

(p) Upper plenum level

Figure B.1: Time evolution plots

B.1.2 Percentile plots

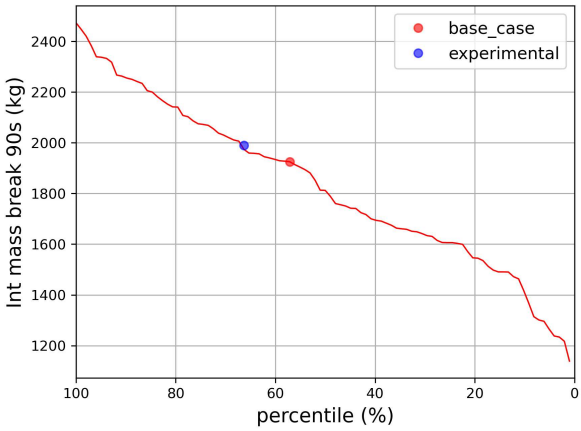

(a) Integrated Mass Flow at break at 90s

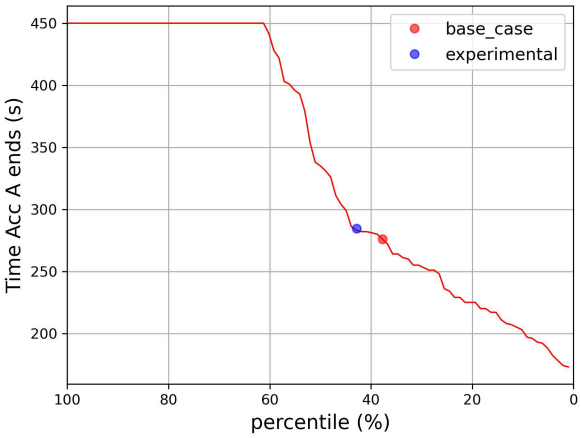

(b) Time at which Accumulator A ends

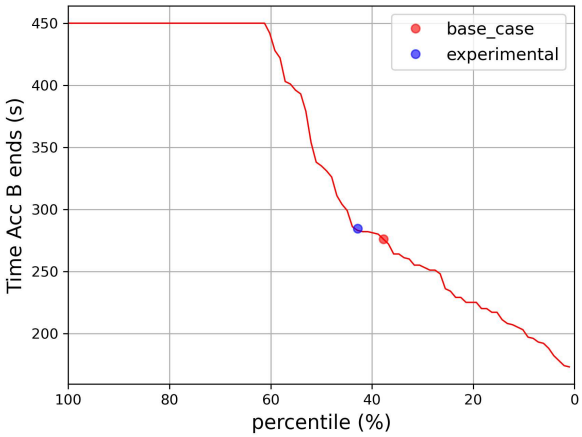

(c) Time at which Accumulator A ends

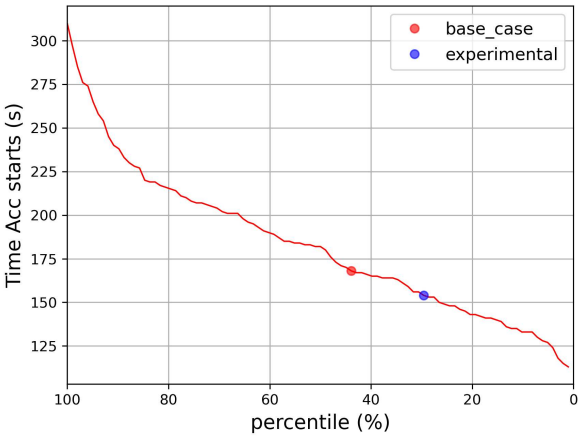

(d) Time at which Accumulators start

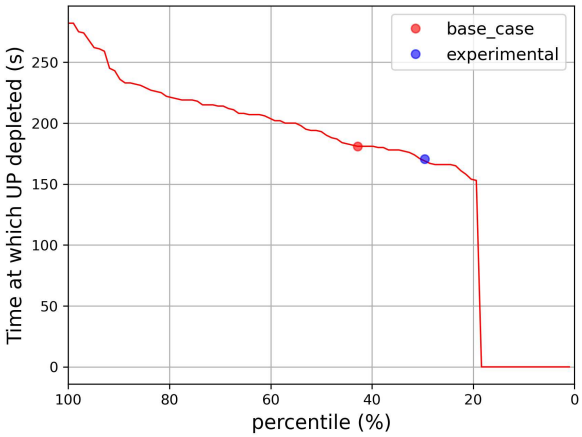

(e) Time at which UP is depleted

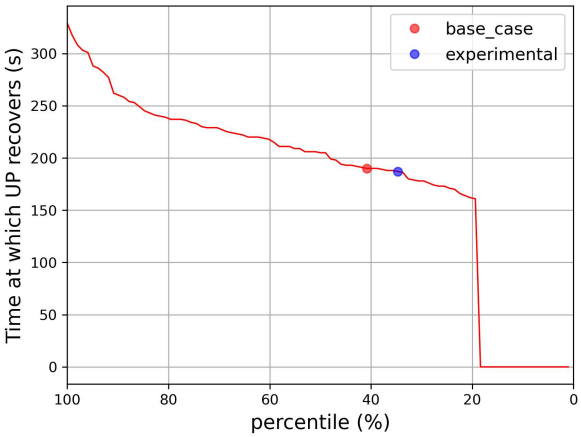

(f) Time at which UP recovers

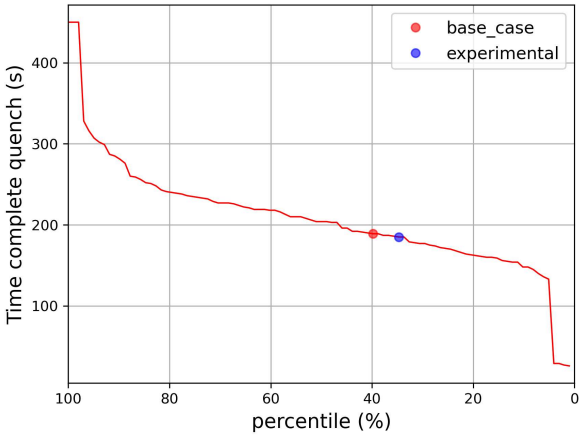

(a) Time to complete the quenching process

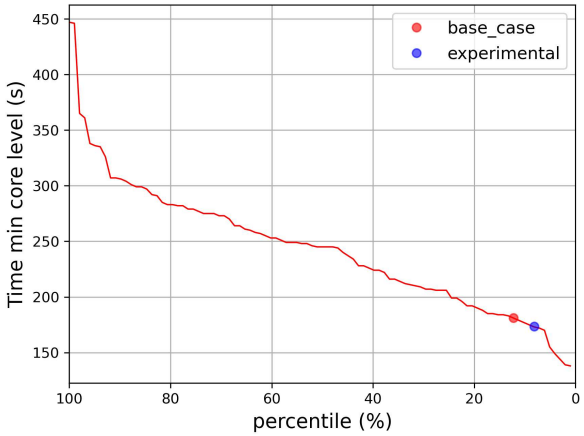

(b) Time to reach minimum core level

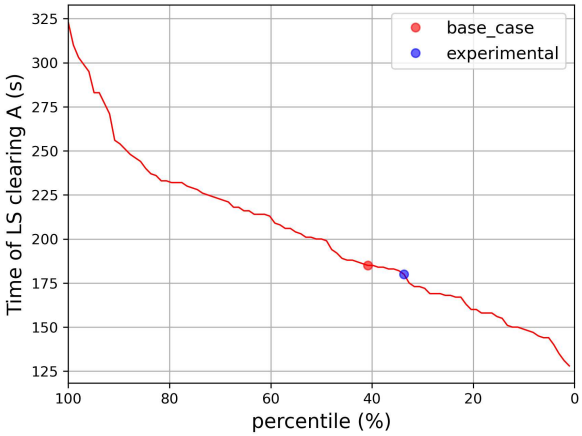

(c) Time at which LS A clears

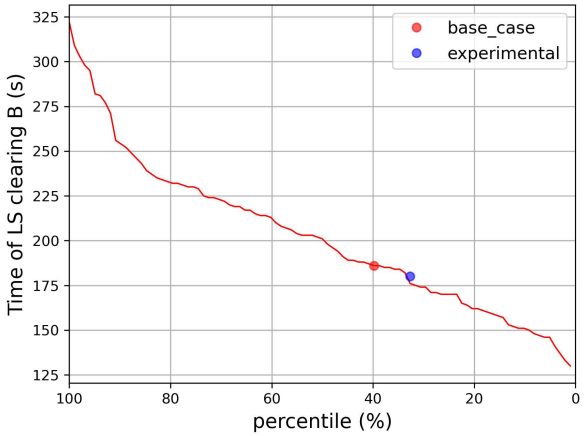

(d) Time at which LS B clears

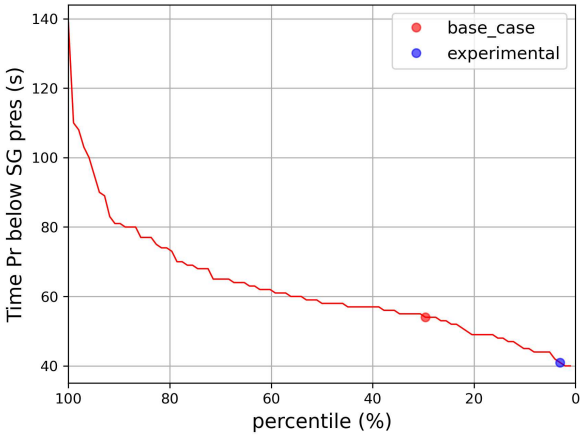

(e) Time at which PZR pressure falls below SG pressure

Figure B.3: Percentile plots

B.1.3 Time evolution plots with bands

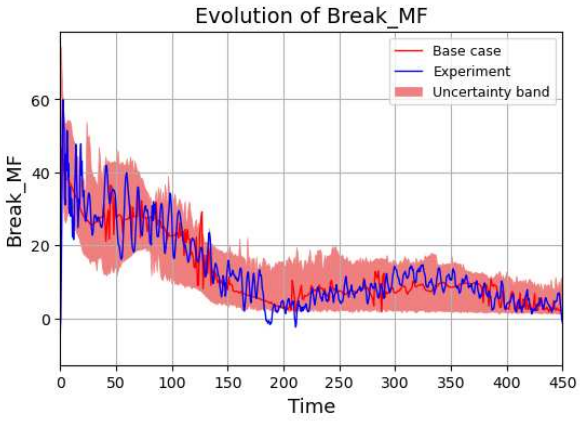

(a) Break Mass Flow

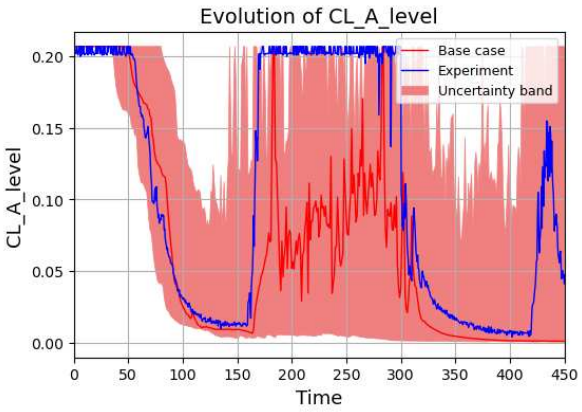

(b) Cold Leg A Level

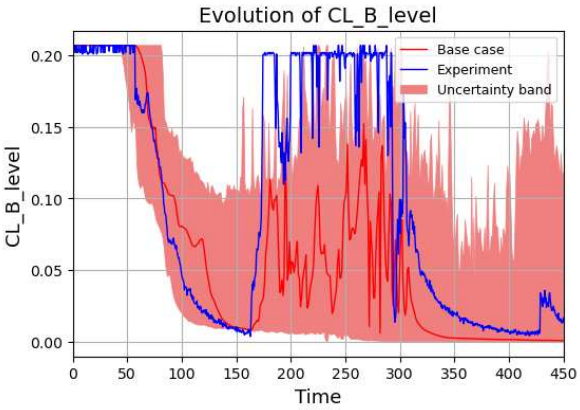

(c) Cold Leg A Level

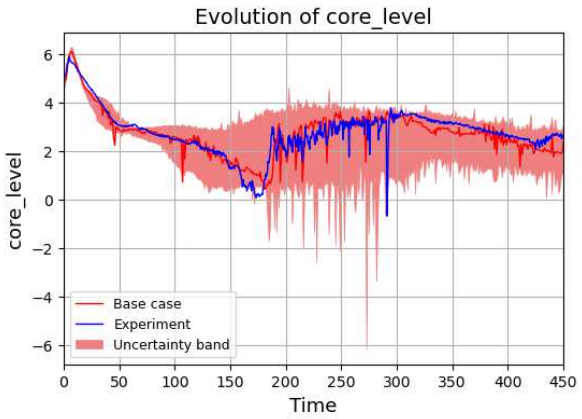

(d) Core Level

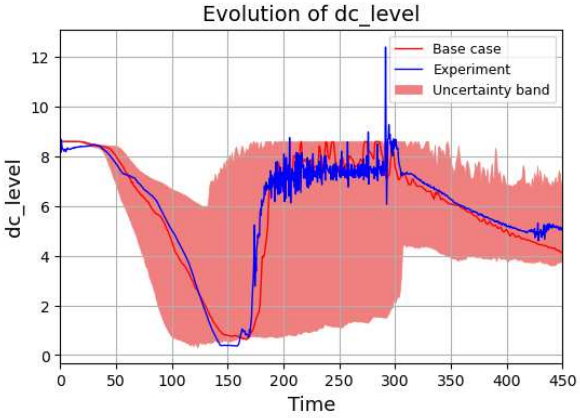

(e) Downcomer Level

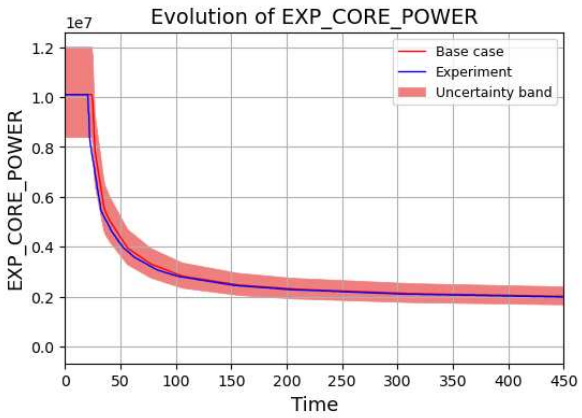

(f) Core Power

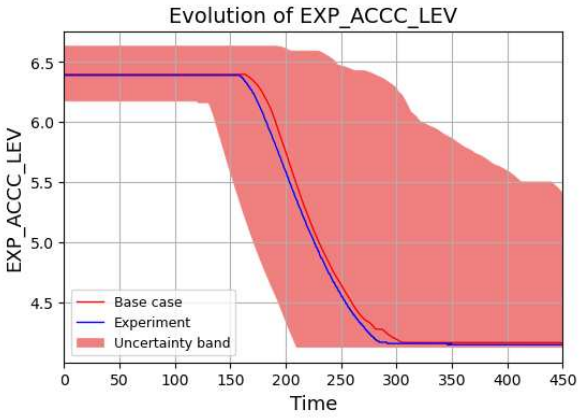

(g) Accumulator B Level

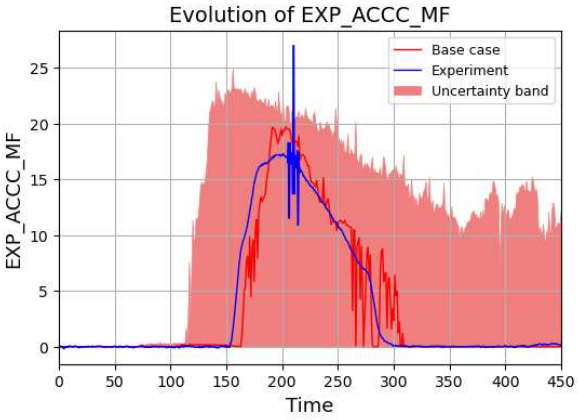

(h) Accumulator B Mass Flow

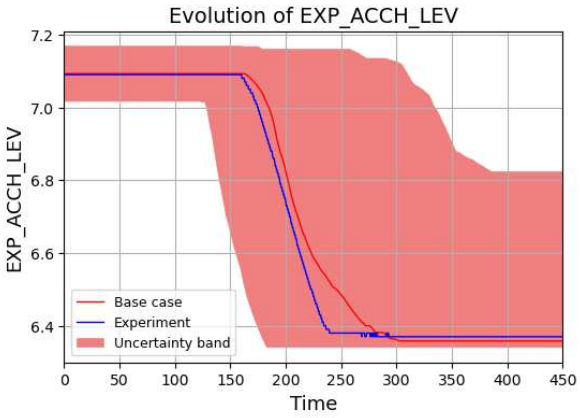

(i) Accumulator A Level

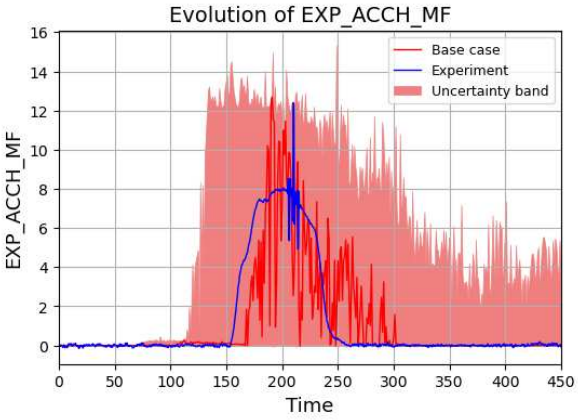

(j) Accumulator A Mass Flow

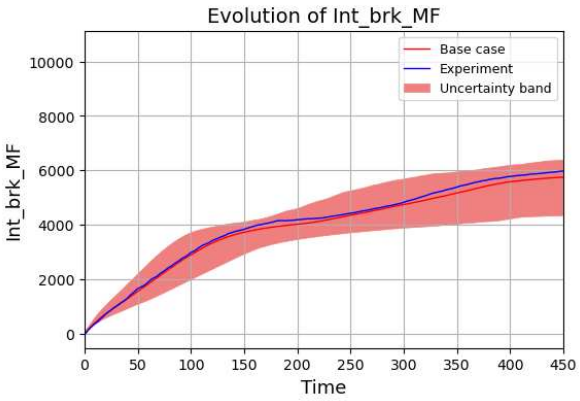

(k) Integrated Break Mass Flow

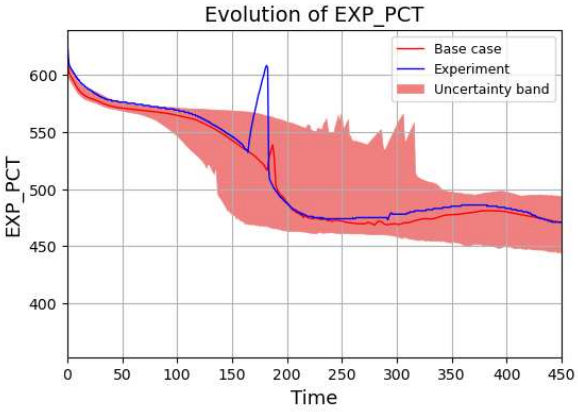

(l) Core Power

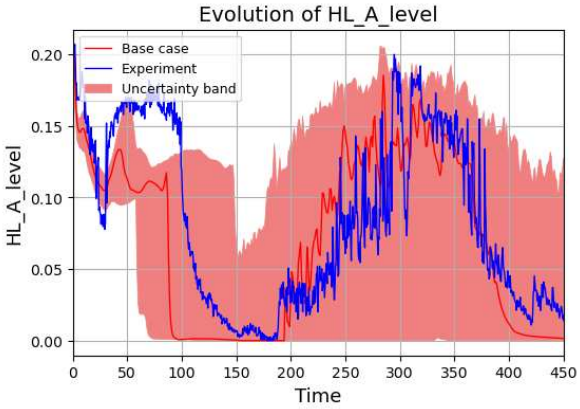

(m) Hot Leg A Level

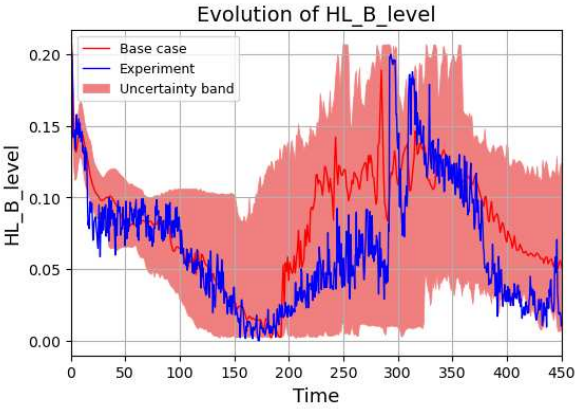

(n) Hot Leg B Level

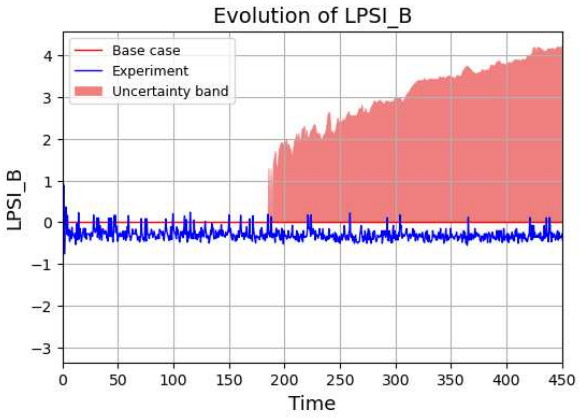

(o) LPSI B

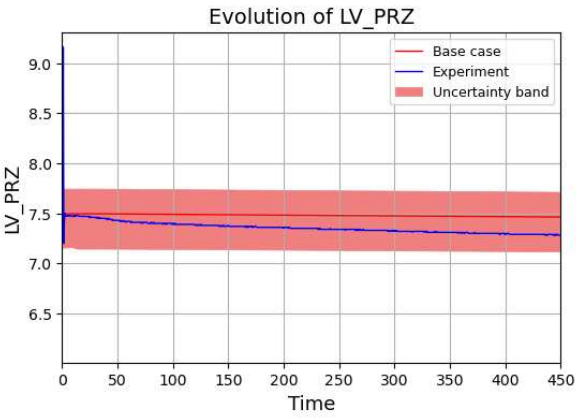

(p) Pressurizer Level

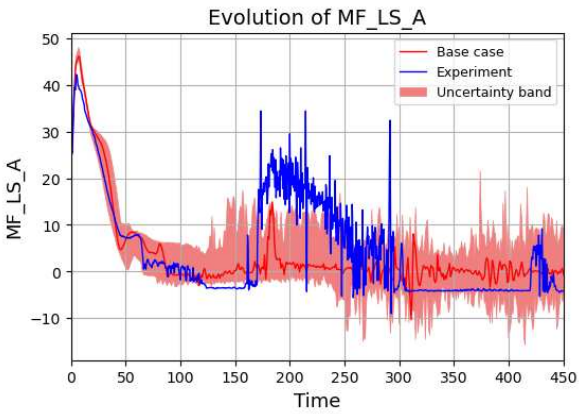

(q) Mass Flow in Loop Seal A

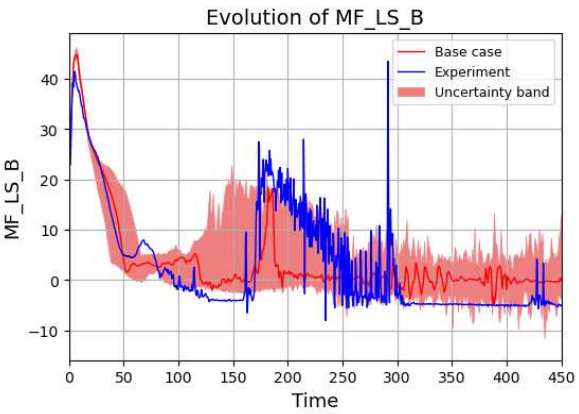

(r) Mass Flow in Loop Seal B

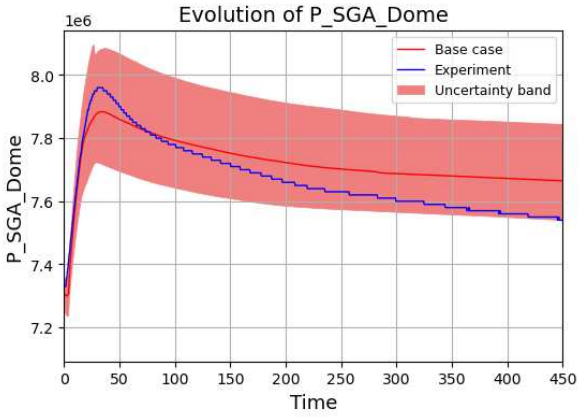

(s) SG A Pressure

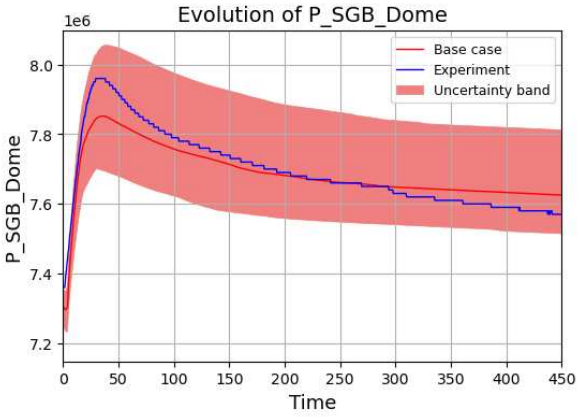

(t) SG A Pressure

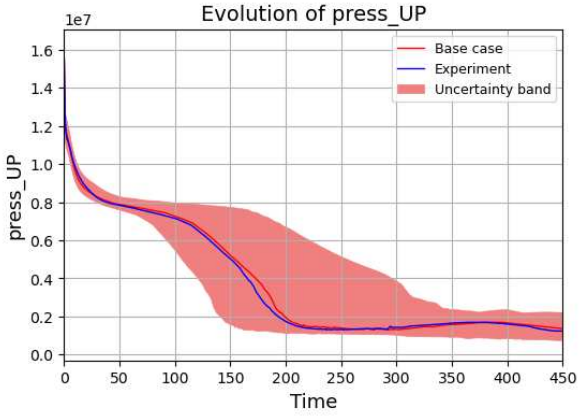

(u) Upper Plenum Pressure

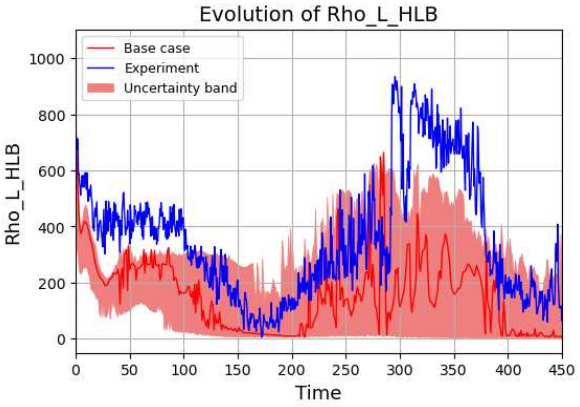

(v) Hot Leg B liquid Density

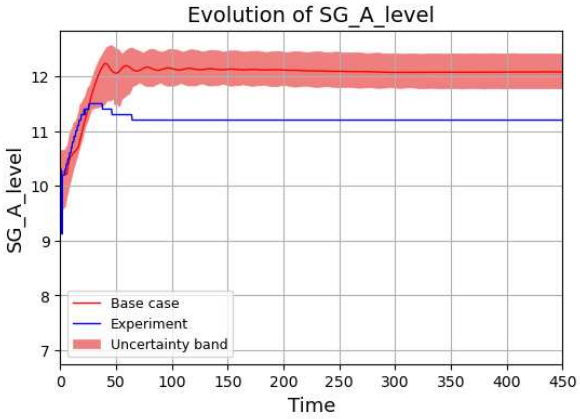

(w) SG A Level

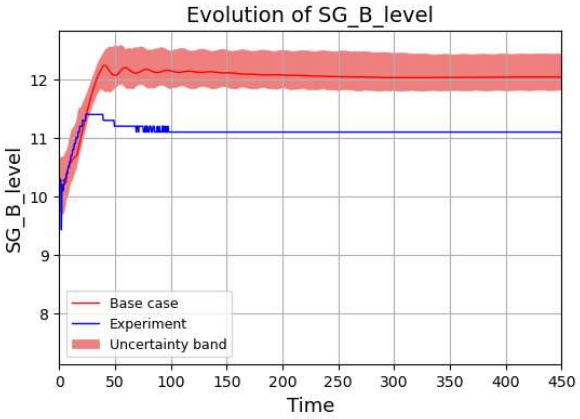

(x) SG B Level

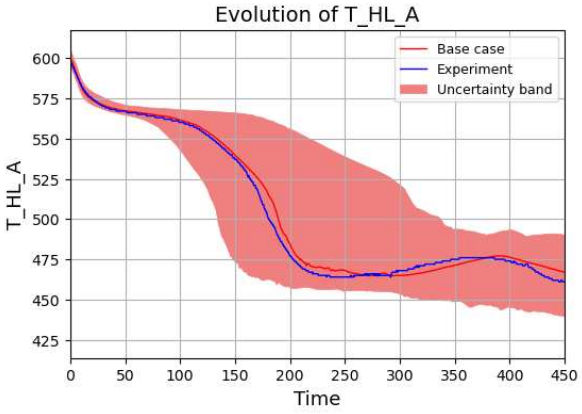

(y) Hot Leg A Temperature

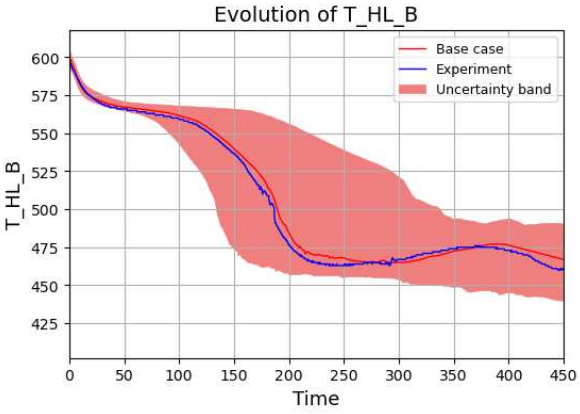

(z) Hot Leg B Temperature

Figure B.4: Time evolution plots with uncertainty bands